

# Sheffield Hallam University

*Stirring patterns in foaming oxygen steel making slags.*

SINGH, S.

Available from the Sheffield Hallam University Research Archive (SHURA) at:

<http://shura.shu.ac.uk/20367/>

## A Sheffield Hallam University thesis

This thesis is protected by copyright which belongs to the author.

The content must not be changed in any way or sold commercially in any format or medium without the formal permission of the author.

When referring to this work, full bibliographic details including the author, title, awarding institution and date of the thesis must be given.

Please visit <http://shura.shu.ac.uk/20367/> and <http://shura.shu.ac.uk/information.html> for further details about copyright and re-use permissions.

6965

7801959019



**Sheffield City Polytechnic  
Eric Mensforth Library**

**REFERENCE ONLY**

This book must not be taken from the Library

PL/26

R5193

ProQuest Number: 10701013

All rights reserved

INFORMATION TO ALL USERS

The quality of this reproduction is dependent upon the quality of the copy submitted.

In the unlikely event that the author did not send a complete manuscript and there are missing pages, these will be noted. Also, if material had to be removed, a note will indicate the deletion.



ProQuest 10701013

Published by ProQuest LLC (2017). Copyright of the Dissertation is held by the Author.

All rights reserved.

This work is protected against unauthorized copying under Title 17, United States Code  
Microform Edition © ProQuest LLC.

ProQuest LLC.  
789 East Eisenhower Parkway  
P.O. Box 1346  
Ann Arbor, MI 48106 – 1346

STIRRING PATTERNS

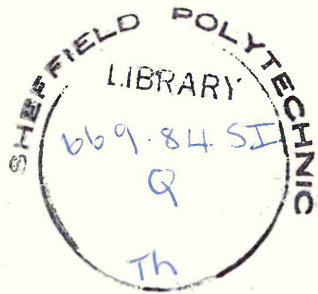
IN FOAMING OXYGEN STEEL MAKING SLAGS

by

S. Singh

July 1978

Department of Metallurgy  
Sheffield City Polytechnic



78-01959-01

## PREFACE

This thesis is submitted for the degree of Doctor of Philosophy of the Council for National Academic Awards, the research work described having been carried out in the Metallurgy Department of Sheffield City Polytechnic. No part of the work described has ever been submitted for the award of any other degree.

In addition to the research, the following courses were attended:

- 1 Process Metallurgy
- 2 Advanced Thermodynamics
- 3 Numerical Methods and Programming

The author is indebted to Dr. A.W.D. Hills for his supervision and for arranging the financial support. Sincere thanks to Dr. R.J. Hawkins of the British Steel Corporation for his valuable discussion from time to time. The personal recommendation and friendly advice of Dr. S.L. Malhotra are also gratefully acknowledged.

From time to time the author received a great deal of support, both technical and personal from his research colleagues and from Technical officers of the Polytechnic. It is not possible to list all the names but sincere thanks are expressed to each of them especially to Dr. R. Acheson for checking the typed script, and to Mr.D. Latimer and Mr. P. Fisher for their ever ready support.

Finally thanks go to the British Steel Corporation for their financial assistance in support of this work.

S. Singh

## SYNOPSIS

A slice reactor has been constructed to study stirring patterns in jetted liquid/liquid reaction systems of the type found in top blown oxygen steel making processes. The two liquids used in the study have been mercury and highly viscous glycerol water mixture. The reaction has involved the oxidation of metallic sodium dissolved in the mercury by hydrochloric acid produced in the glycerol water mixture by jetting the liquids with a nitrogen hydrogen chloride gas mixture. The reaction takes place between droplets of the mercury amalgam and the acidified glycerol water solution, this reaction modelling the reaction that takes place in top blown steel making processes between droplets of iron carbon alloy and the oxidising slag. Gaseous hydrogen is produced by the reaction that has been studied, and it is bubbles of hydrogen that produce and maintain the foam within the slice reactor. The slice reactor has been constructed to represent a vertical section cut across the diameter of a centrally jetted axi-symmetric reactor of the BOS type, so that the jet is provided by a slit nozzle set at right angles to the sides of the reactor. The symmetry of gas and liquid flow patterns in the slice reactor is thus essentially two dimensional as opposed to the axi-symmetric flow patterns that exist in actual BOS reactors.

The interactions between the two dimensional jet and the liquids have been studied in the absence of any reaction in order to establish the extent to which the two dimensional system behaves in the same way as the axi-symmetrical system. Particular attention was paid in this study to the depth of the depression produced in the liquid surface by the impact of the jet and the conditions under which liquid was splashed out from the impact region. These studies showed that the characteristics of the two dimensional jetting system are very similar to those of the axi-symmetric systems that have been extensively studied previously.

The behaviour of the slice reactor in the presence of the reaction that produces and sustains the foaming slag has been studied by injecting a colour tracer into the foam and studying its

movement. Two distinct flow zones have been observed in the foam, and the effect of changes in operating variables, such as lance height and gas flow rate, on these two flow zones has been studied.

The presence of the tracer has allowed the metal droplets sprayed out from the jet impact region to be visible during their path through the foam. The size, velocity and spatial distribution of these droplets have been studied and their response to changes in the operating variables ascertained.

As well as studying the behaviour of the reactor with a vertical jet produced from a single slit nozzle, a series of experiments have been carried out with two slit nozzles in which two jets of gas are produced at different angles of divergence. The behaviour of the system with these two slit nozzles has been compared with its behaviour with the single slit nozzle.

The results of the investigation have been discussed in relation to the operation of industrial oxygen steel making processes.

## CONTENTS

List of Tables

List of Figures

List of Photographs

Symbols and Subscripts

	Page
1. INTRODUCTION	1
2. LITERATURE REVIEW	
2.1 Flow Through Oxygen Steelmaking Nozzles	3
2.2 Oxygen Jet	5
2.3 Interaction of a Gas Jet with a Liquid Bath	8
2.4 Splashing	10
2.5 Bath Circulation	12
2.6 BOS Slags	13
2.7 Decarburisation	15
2.8 Foams and Emulsions	19
3. EXPERIMENTAL APPARATUS	22
3.1 Construction	22
3.1.1 Reactor	22
3.1.2 Slit Nozzles	23
3.1.3 Frame Assembly	24
3.1.4 Tank	24
3.1.5 Overall Apparatus	25
3.1.6 Amalgam Cell	25
3.1.7 Mercury Purifying Unit	26
3.2 Major Factors Considered in the Design of the Reactor	26
3.2.1 Reactor	26
3.2.2 Slit Nozzles	28
3.2.3 Frame Assembly	28
3.2.4 Tank	28
3.2.5 Ancillary Apparatus	28

	Page
4. EXPERIMENTAL PROCEDURE	30
4.1 Measurement of the Depth of Depression	30
4.2 Preparing Sodium Amalgam	31
4.3 Blowing onto Sodium Amalgam	31
4.4 Processing the Mercury	32
4.5 Safety	32
4.6 Development of the Technique for Examining Motion in the Foam	33
4.7 Cine Photography	35
4.8 Temperature Measurement	36
5. RESULTS	37
5.1 Depth of Depression Measurements	37
5.2 Shape of the Depression Formed by Two Slit Nozzles	42
5.3 Model Study	42
5.3.1 Visual Observations	42
5.3.2 Performance of Investigated Tracer Materials	44
5.3.3 Different Flow Zones in the Model Foam	44
5.3.4 Time for Tracing the Path	46
5.3.5 Time for Complete Mixing	48
5.3.6 Trajectory of the Droplets	48
5.3.7 Distribution of Droplets in the Foam	49
5.3.8 Size Distribution of the Droplets	50
5.3.9 Temperature Measurement	50
6. DISCUSSION	60
6.1 Depth of Depression	60
6.2 Shape of the Depression Formed by Two Slit Nozzle	64
6.3 Studies on Reacting Model	65
6.3.1 Flow Zones in the Model Foam	65
6.3.2 The Size and Shape of the Reverse Flow Zone	70
6.3.3 Time for Tracing the Path	72
6.3.4 Time for Complete Mixing	75
6.3.5 Trajectory of the Droplets	76
6.3.6 Number of Droplets in the Foam	78

	Page
6.3.7 Distribution of Droplets in the Foam	78
6.3.8 The Size Distribution of Droplets	79
6.3.9 Temperature Measurement	80
6.4 Application to Basic Oxygen Steelmaking	80
6.4.1 Flow Patterns in the Foaming Steelmaking Slags	80
6.4.2 The Reaction Systems	82
7. CONCLUSIONS	87
References	89
Appendices	
Figures	
Plates	

LIST OF TABLES

Table Number	Description	Page Number
1	Depth of Depression Measurements in Nitrogen Water System. Single Slit Nozzle	38
2	Depth of Depression Measurements in Mercury system. Single Slit Nozzle	39
3	Depth of Depression Measurements in Nitrogen Water system. Two Slit 20° Nozzle	40
4	Effect of Experimental Variables on Amount and Movement of the Foam. Single Slit 1 mm Nozzle	41
5	The Effect of Variables on the Time for Path Tracing and the Time for Total Mixing of the Tracer	47
6 to 9	Analysis of Droplets Velocity	51 to 54
10	The Effect of Droplet Size on their Velocity of Descent	55
11	The Number of Droplets per Frame (Averaged over 12 frames)	56
12	Mean of Horizontal Distribution ( $\bar{x}$ ) and Mean of Vertical Distribution ( $\bar{y}$ ) with 95% Confidence Limits	57
13	Mean Diameter of Droplets with 95% Confidence Limits	58
14	The Effect of Nozzle Height on Maximum Temperature of the Foam. Single Slit Nozzle, Flow Rate 76.6 litres/min.	59
15	Calculation of Down Stream Distance from the Imaginary Nozzle to the Boundary between the two Flow Zones and Comparison with the Length of the Supersonic Core Predicted from the results of Anderson and Johns	73

LIST OF FIGURES

Figure Number	Description
1	The Structure of a Subsonic Jet
2	The Structure of a Supersonic Jet
3	The Flow Pattern Produced by a Gas Jet Impinging onto a Water Bath Covered by a Layer of Oil
4	Typical Slag Formation Paths
5	The Variation in Decarburisation Rate Throughout a typical BOS Blow
6	The Reactor Assembly
7	The Reactor Construction
8	The Gas Outlet Connection (A) and the Slit Nozzle Assembly (B) of the Reactor
9	The Top Cover (A) and Bottom (B) of the Reactor
10	The Two Slit Nozzle
11	The Frame for supporting the Reactor
12	The Perspex Blocks (A) and the U shaped Rod (B) for Adjusting the Bottom of the Reactor
13	Schematic Diagram of the Reactor and other Ancillary Equipment
14	The Amalgam Cell
15	(A) The Stirrer used in the Amalgam Cell (B) the Mercury Purifying Unit
16	The Arrangement for Injecting the Tracer adjacent to the Jet Exit
17	The Arrangement for Injecting the Tracer through the Outlets
18	The Effect of Jet Momentum on the Depth of Depression in the Nitrogen Water System
19	The Effect of Jet Momentum on the Depth of Depression in the Nitrogen Mercury System
20	The Effect of Nozzle Type on the Depth of Depression in the Nitrogen Water System
21	A Plot of Dimensionless Jet Momentum $\left( \frac{\dot{M}}{\rho_L g h^3} \right)$ versus Dimensionless Depth of Depression $\left( \frac{n_o}{h} \right)$
22	A Plot of Dimensionless Groups $\left( \frac{\dot{M}}{\rho_L g n_o b_o L} \right)$ versus $\left( \frac{h+n_o}{b_o} \right)$

- 23 A Schematic Diagram of the Stirring Pattern in the Model Reactor
- 24 The Effect of Flow Rate on the Size and Shape of the Reverse Flow Zone:- Single Slit Nozzle,  $h = 0.2$  cm
- 25 The Effect of Flow Rate on the Size and Shape of the Reverse Flow Zone:- Two Slit Nozzle,  $h = 0.2$  cm
- 26 The Effect of Nozzle Height on the Size and Shape of the Reverse Flow Zone:- Single Slit Nozzle, Gas Flow Rate - 76.6 litres/min.
- 27 The Effect of Nozzle Height on the Size and Shape of the Reverse Flow Zone:- Two Slit Nozzle, Gas Flow Rate - 76.6 litres/min.
- 28 and 29 The Effect of Nozzle Type on the Size and Shape of the Reverse Flow Zone:-  $h = 0.2$  cm, Gas Flow Rate 76.6 litres/min.
- 30 and 31 The Paths of the Droplets falling through the foam
- 32 The Velocity of the Droplets falling through the foam
- 33 to 35 The Distribution of Droplets in the Foam
- 36 The Distribution of Droplets with Horizontal Distance from the Nozzle Centre Line:- Single Slit Nozzle
- 37 The Distribution of Droplets with Horizontal Distance from the Nozzle Centre Line:- Two Slit Nozzle
- 38 The Vertical Distribution of Droplets for the Single Slit Nozzle
- 39 The Vertical Distribution of Droplets for the Two Slit Nozzle
- 40 The Size Distribution of Droplets with Distance from the Nozzle Centre Line.
- 41 The Frequency Distribution of Droplets Sizes for the Single Slit Nozzle
- 42 The Frequency Distribution of Droplets Sizes for the Two Slit Nozzle
- 43 The Effect of Nozzle Height on the Temperature of the Model Foam for the Single Slit Nozzle at a Flow Rate of 76.6 lit./min.
- 44 The Comparison Between the Single Slit and the Two Slit Nozzle Treating the latter as Two Single Jets
- 45 A Schematic diagram showing Analysis of the Stirring Pattern in the Model Foam
- 46 A Schematic Diagram Showing the Position of the Imaginary Nozzle
- 47 A Schematic Diagram of the Cross Flow Reaction Region

LIST OF PHOTOGRAPHS

Plate Number	Description
1	The Slice Reactor and Ancillary Equipment
2	The Amalgam Cell
3	A Photograph of the Model Foam before injecting the Tracer
4	The Effect of Jet Momentum on the Shape of the Depression Formed by the Jet from the Two Slit Nozzle
5	(a) The Flow Zones using Ink as the Tracer (b) The Flow Zones using Universal Indicator as Tracer
6 and 7	Photographs showing the way Mixing Proceeds
8	Drops Formed from the Waves Generated from the Depression
9	Droplets in the Foam

## SYMBOLS

A	Area of cross section
b	Width of the nozzle
c	Velocity of Sound
d	Nozzle diameter
g	Acceleration due to gravity
H	Height
h	Nozzle height, lance height
K	Constant
L	Length of the supersonic core, length of the nozzle
M	Mach number
$\dot{M}$	Jet momentum (dynes)
$\dot{m}$	Mass flow rate
$n_o$	Depth of depression
P	Gas pressure
R	Gas constant
r	Radial distance
T	Absolute temperature
V	Velocity
x	Axial length
$\beta$	Constant, compressibility
$\gamma$	Ratio of specific heats of gas
$\theta$	Angle between the two slit
$\rho$	Density

## Subscripts

a	Ambient medium
ads	Adsorbed
c	Centre line
e	Exit
f	Foam
g	Gas
L	Liquid
O	Initial value
r	Reverse flow zone
s	Supersonic core
t	Throat

1.        INTRODUCTION

The invention of the L.D. process was probably the greatest recent event in the field of steel making. Many improvements have taken place in this process making it almost universally acceptable for converting hot metal into steel.

The full form of the name 'L.D.' appears to be controversial. According to one opinion, which is the more common, the name originated from two Austrian cities Linz and Donawitz. The first production plant went into operation at Linz in November 1952 and the second at Donawitz in May 1953. According to another opinion, which appears to be more appealing, the name originated from 'Linzer Dusemuerfahren' i.e. Linz Jet Process.<sup>75</sup> With improvements and modifications in the process, terms like L.D.-A.C, O.L.P, B.O.F, B.O.P. were evolved. For the sake of uniformity and convenience, the term BOS (Basic Oxygen Steelmaking) will be used to include all these terms.

The steel maker, like his counterpart in other industries, has always sought to produce at faster and faster rates from the same facilities because faster production rates mean greater profitability. Attempts to drive the BOS process harder than the current limit result in slopping caused by excessive foaming.

It is very strange that our understanding of most of the activities going on inside the BOS furnace is not well established. Old concepts have gone, or are under challenge.

Foaming depends on properties of the slag, operating parameters and is the result of the oxidation products of carbon finding difficulty in escaping through slag, making it foam and thus expand in volume.

Acheson and Hills<sup>76</sup> developed a room temperature model using sodium in an amalgam to represent carbon in the pig iron and blowing a nitrogen and hydrogen chloride gas mixture on to a water/glycerol mixture to simulate the reaction of oxygen on the slag in steel making. The product gas in the model is hydrogen which simulates the carbon monoxide produced by oxidising carbon in the actual process. The model has been studied in detail and appears to be suitable for studying foam formation and behaviour in BOS process.

The object of the present study is to observe some of the phenomena occurring in BOS, with special reference to the stirring patterns in foaming BOS slags.

The gas nozzle in this 'slice reactor' is in the form of a narrow slit so that a two-dimensional flow field is set up. In order to relate these two-dimensional flow fields to the axi-symmetrical flow fields existing in BOS vessels and in virtually all other experimental investigations into the BOS process, this work has started with a study of the depression caused by the two dimensional jet and by the onset of splashing from the edges of the two dimensional depressions.

## 2. LITERATURE REVIEW

### 2.1 Flow Through Oxygen Steelmaking Nozzles

The oxygen jet velocity is supersonic at the exit plane of the nozzle. This high velocity enables the jet to penetrate the slag and impinge strongly on the molten metal. A great deal of fundamental work has been done on the subject of supersonic flow in connection with research on jet propulsion. The application of the results of this fundamental work to the Basic Oxygen Steelmaking process is discussed below.

Sonic velocity may not be exceeded in a pipe of constant cross sections <sup>1</sup>. The effect of change in the cross sectional area on the velocity is given by the following equation <sup>2</sup>:

$$\frac{dA}{dV} = \frac{A}{V} (M^2 - 1) \quad \text{_____} \quad (1)$$

Re-arranging gives:

$$\frac{dA}{A} = \frac{dV}{V} (M^2 - 1) \quad \text{_____} \quad (2)$$

The velocity of oxygen is expressed in terms of its Mach number M which is the ratio of the local flow velocity to the local speed of sound in the fluid. Oxygen enters a nozzle at a subsonic velocity (M less than unity). As the area of cross section is decreased, the velocity increases up to the sonic velocity (M = 1) and any further reduction in area would give rise to an increase in density but no increase in velocity. If now, the cross section area were to increase, M could become greater than 1 so that the sign of  $\frac{dV}{V}$  would reverse. The gas flow velocity would thus increase with the diverging cross-sectional area of the nozzle. Thus in actual practice a convergent-divergent nozzle is used in oxygen steelmaking, sonic velocity being attained at the throat.

The effect of Mach number on temperature, pressure and density of the gas is given by the following equations: <sup>2-4</sup>

$$\frac{T_0}{T} = 1 + \left(\frac{\gamma - 1}{2}\right) M^2 \quad \text{_____} \quad (3)$$

$$\frac{P_0}{P} = \left[ 1 + \left(\frac{\gamma - 1}{2}\right) M^2 \right]^{\frac{\gamma}{\gamma - 1}} \quad \text{_____} \quad (4)$$

$$\frac{\rho_0}{\rho} = \left[ 1 + \left(\frac{\gamma - 1}{2}\right) M^2 \right]^{\frac{1}{\gamma - 1}} \quad \text{_____} \quad (5)$$

The above equations show that as the gas accelerates during its flow through the convergent-divergent nozzle, its temperature, pressure and density decreases.

The pressure at the nozzle exit should be equal to the pressure of the surrounding atmosphere. Any difference in the pressure cannot be communicated to the upstream of the nozzle because the velocity of communication (sonic) is less than the velocity of the oxygen (supersonic). This lack of communication results in the generation of shock waves, the thickness of the shock wave region being a few thousandth of an inch.<sup>3</sup> The presence of shock waves is undesirable due to resulting loss of the kinetic energy of the jet.<sup>5</sup> For a given Mach number and pressure in the surrounding atmosphere, the upstream pressure in the nozzle can be calculated from equation 4.

The effect of temperature on the velocity of sound at any position in the nozzle is given by the following equation:<sup>4</sup>

$$c = \sqrt{\gamma RT} \quad \text{_____} \quad (6)$$

The above equation shows that, as the temperature decreases, the velocity of sound decreases. Thus with the same velocity, the flow may be subsonic or supersonic depending on its temperature.

The area of cross section, Mach number and pressure at any point are interrelated (equation 2 and 4). This means, for a fixed Mach number and pressure at the exit of the nozzle, there should be some fixed area at the exit of the nozzle. This area is related to the throat area by the following equation:

$$\frac{A}{A_t} = \frac{1}{M} \left[ \frac{1 + \left(\frac{\gamma - 1}{2}\right) M^2}{\frac{\gamma + 1}{2}} \right]^{\frac{\gamma + 1}{2(\gamma - 1)}} \quad \text{_____} \quad (7)$$

For a given nozzle, the area and pressure at the exit are fixed. This means, the blowing rate is fixed. Any deviation from the designed flow rate will result in loss of kinetic energy due to the formation of shock waves. For blowing rates within  $\pm 20\%$  of the design flow rate, the efficiency of pressure conversion to kinetic energy is not reduced appreciably.

The nozzle is made of copper and is water cooled so that its dimensions do not change due to softening and mechanical wear.

## 2.2 Oxygen Jet

The oxygen jet issuing from the mouth of the nozzle is supersonic in nature, but most of the information available in the literature about the behaviour of jets has been obtained from studies of subsonic jets. This is probably because, due to the generation of shock wave, one nozzle is suitable only for one supersonic flow rate. Therefore studies on subsonic jets will also be discussed.

Figure 1 shows different regions in a subsonic jet. A subsonic jet may be a submerged jet or free jet depending on whether the surrounding medium is liquid or gas. A gas jet (subsonic or supersonic) when discharged into another medium (gas or liquid) exerts a tangential shear force along the boundary between the jet and the surrounding medium. As a result of this interaction along the boundary, the moving fluid is slowed down, whereas the stationary fluid starts moving. The mixing is turbulent in nature. With the increase in distance from the nozzle, the slowing down of the jet shifts towards the centre. After some distance from the jet exit, the centre line velocity starts decreasing. The region of the jet corresponding to the unaffected centre line velocity is called the potential core<sup>5,7</sup> or initial flow region<sup>1</sup> or zone of flow establishment.<sup>8</sup> Beyond the potential core, the region corresponding to decreasing centre line velocity is known as the region of fully developed flow<sup>1,5</sup> or zone of established flow. Since the change from one region to the other is not sharp due to the statistical nature of the mixing process, there is a zone between the two, known as the transition region.

The structure of a supersonic jet is similar to the structure of a subsonic jet. Figure 2 shows the different regions in a supersonic jet. The major difference is due to the supersonic axial velocity.

As in subsonic jets, the region close to the nozzle is known as the potential core. In this region, the centre line velocity is equal to the exit velocity. Beyond the potential core, the centre line velocity is less than the exit velocity but is greater than the velocity of sound. The entire region (including the potential core) over which the centre line velocity is greater than the velocity of sound is known as the supersonic core. Beyond the supersonic core, the centre line velocity is subsonic and thus the region is known as the subsonic region.

The jet momentum is conserved. The mass flow rate is increased with the increase in distance from the nozzle exit. Ricou and Spalding<sup>9</sup> have shown that the rate of entrainment for subsonic jets is given by the following equation:

$$\frac{\dot{m}}{\dot{m}_0} = 0.32 \frac{x}{d_0} \left( \frac{\rho}{\rho_0} \right)^{\frac{1}{2}} \quad \text{-----(8)}$$

The equation shows that the rate of entrainment increases with increase in density of the surrounding medium or decrease in the density of the jet medium.

Kapnar et al<sup>14</sup> exhausting a supersonic air jet into a hot medium of air have observed that the rate of entrainment decreases with increase in temperature difference between the surrounding medium and the jet. This agrees with equation 8 on the basis of change in the densities with temperature. The same study also shows that the rate of entrainment decreases with increase in the Mach number of the jet.

Chatterjee<sup>5</sup> has reviewed that the rate of entrainment is much lower in the supersonic portions of the jet than in the subsonic portions.

The lengths of the potential and the supersonic cores depend upon the entrainment rate. Taylor et al<sup>7</sup> have reported the length of the potential core to be 3.5 nozzle diameters while Donald and Singer<sup>10</sup> reported it to be 13 nozzle diameters. This discrepancy might be due to large differences in the kinematic viscosity, because the lower value obtained by Taylor et al is for an air jet discharging in air while the higher value reported by Donald and Singer is for a water jet discharging in water.

The results of Kapnar reviewed by Chatterjee <sup>5</sup> show that the length of potential core increases from 4.5 nozzle diameters to 9 nozzle diameters with increase in the Mach number from 1 to 1.8. The same work also shows that increase in temperature of the surrounding atmosphere increases the length of the potential core.

In order to determine the length of the supersonic core, Shirie and Seubold <sup>11</sup> using data from 25 investigations developed a correlation. They plotted  $Pe/Pa$  against  $\frac{x_s}{d_e} e^{-0.11 \gamma_e M_e^2}$  and found good agreement. Unfortunately the few points showing maximum departure are for shock free jets. The relationship is thus not so suitable for shock free supersonic jets.

Anderson and Johns <sup>12</sup> using heated air jets investigated the length of the supersonic core. The results show that the length of supersonic core increases with the Mach number and to a lesser degree with decrease in the temperature of the jet.

As a result of entrainment the jet velocity decreases. In the supersonic region, investigation of the decay in the jet velocity is complicated by shock waves. <sup>12</sup> In subsonic regions of the jet, the axial decay in velocity is given by the following equation: <sup>13</sup>

$$\frac{V_c}{V_o} = K \frac{d_o}{x} \quad \text{-----(9)}$$

The value of K varies with Reynolds number and distance from the nozzle exit. K is higher at higher Reynolds number and lower distances from the nozzle exit.

The radial velocity distribution has been shown to be of the following form: <sup>13</sup>

$$\frac{V}{V_o} = \exp. -\beta \left| \frac{r}{x} \right|^2 \quad \text{-----(10)}$$

Kapnar etal <sup>14</sup> have shown that the velocity profiles also depend upon the density of the jet as well as the density of the surrounding medium. The same study shows that the axial decay of velocity decreases as the Mach number or the temperature difference between the surroundings and the jet increases.

The angle of spread\* of the subsonic jet increases with increase in Kinematic viscosity or decrease in Reynold number. <sup>10</sup> The supersonic portion of a jet will have a lower angle of spread than the

\* whole angle

Entrainment, length of the potential core and the supersonic core, velocity profiles and angle of spread are all linked together both in subsonic and supersonic jets. As a generalisation, an increase in the entrainment rate decreases the length of the potential and supersonic cores but increases the angle of spread and the rate at which velocity decays. An increase in the entrainment rate is brought about by decreasing the jet velocity or the density of the jet medium or increasing the density of the surrounding medium.

The angle of spread of an air jet in the subsonic regions is about 20 degrees.<sup>6,10</sup> In the type of multi-hole nozzles used in BOS, the fields of entrainment from adjacent jets can interact. Smith<sup>6</sup> using a Mach 2 oxygen jet observed that when the angle of inclination of jets in a multi-hole nozzle is 5 degrees, the flow fields intersect each other, whereas at 10 degrees inclination the flow fields do not intersect each other. The angle of spread is higher in subsonic regions as compared to supersonic regions of a jet.<sup>10,78</sup> Thus with the decrease in the angle of inclination of the jets in a multi-hole nozzle the flow fields will first intersect in the subsonic regions. This is also clear from the work of Smith.<sup>6</sup>

### 2.3 Interaction of a Gas Jet with a Liquid Bath

The length of the supersonic core of a BOS jet is about 15 nozzle diameters. The lance height is about 40 nozzle diameters. The jet is therefore subsonic before it impinges onto the bath. Thus for the purpose of discussing the interaction of the oxygen jet with the bath, there is no need to make any distinction between the subsonic jet and the supersonic jet.

When a gas jet impinges on a liquid surface, it forms a depression at the area of impact. With increase in the intensity of blowing, the depth of depression increases. When the depression is relatively large, a raised up portion of liquid is formed all around it. This raised portion is known as a lip. With further increase in the intensity of blowing, the depression oscillates vertically as well as horizontally. As the intensity of blowing is further increased, liquid droplets are splashed out from the region of the depression. The depth of depression corresponding to the commencement of splashing is called the critical depth of depression.

Flinn et al<sup>15</sup> using an oxygen-molten pig iron system developed

the following empirical relationship:

$$n_o = \frac{1.1 P_o d_t}{h} + 38.1 *$$

The above relationship has the drawback that it indicates that a positive depth of depression would exist when the blowing pressure at the entrance to the nozzle is equal to zero (i.e. no gas being blown). This study, however, makes a significant contribution to the study of the depth of depression because it has been done on the oxygen-molten pig iron system that exists in the actual practice of the Basic Oxygen Steelmaking Process.

At the surface of the depression, the downwards force due to the change in the momentum of the jet gases is balanced by the total upwards force exerted by the liquid over the entire surface of the depression. This upwards force is equal to the weight of liquid displaced in forming the depression. The magnitude of the downwards force will vary from  $\dot{M}$  to  $2\dot{M}$  depending on the average vertical component of the gas velocity after it leaves the depression. Maatsch<sup>17</sup> observed that the weight of liquid displaced is 1.3 times the jet momentum. Coheur and Decker<sup>18</sup> reported that the weight of liquid displaced varies between  $\dot{M}$  and  $1.3 \dot{M}$ , while Dennis<sup>19</sup> reported the weight of liquid displaced varying between  $\dot{M}$  and  $1.4 \dot{M}$ .

At the centre of the depression the dynamic pressure due to the centre line velocity is converted to static pressure. This is counterbalanced by the pressure in the liquid. Mathematically:

$$n_o \rho_L g = \frac{1}{2} \rho_g v_c^2 \quad \text{-----} \quad (11)$$

Substituting the value of  $v_c$  from equation 9:

$$n_o \rho_L g = \frac{1}{2} \rho_g \left( \frac{K v_o d_o}{h} \right)^2 \quad \text{-----} \quad (12)$$

But the momentum through the nozzle is:-

$$\dot{M} = \frac{\pi}{4} d_o^2 v_o^2 \rho_g$$

So that:-

$$d_o^2 v_o^2 = \frac{4}{\pi} \frac{\dot{M}}{\rho_g} \quad \text{-----} \quad (13)$$

---

\* As given in reference 16.  $n_o$ ,  $d_t$ ,  $h$  in mm and  $P_o$  in  $\text{KN/m}^2$ .  
Original formula is in Imperial units.

Substituting the value of  $d_o^2 v_o^2$  from equation 13 in equation 12:-

$$\frac{n_o}{h} = \frac{2 K^2}{\pi} \frac{\dot{M}}{\rho_L g h^3} \quad \text{-----(14)}$$

For deep cavities h is replaced by  $(h + n_o)$  in equation 14 to yield:-

$$\frac{n_o}{h} \left( 1 + \frac{n_o}{h} \right)^2 = \frac{2 K^2}{\pi} \frac{\dot{M}}{\rho_L g h^3} \quad \text{-----(15)}$$

The above procedure has been adopted by Cheslak et al.<sup>20</sup>

Similar expressions have been obtained by Banks and Chandrasekhara<sup>21</sup> and also by Wakelin.<sup>22</sup>

Dimensional analysis has been used by a number of investigators to interpret measurements of the depth of depression.<sup>13,21,23,25-28</sup> Each group of investigators made their own choice of dimensionless groups. The best treatment available so far is probably that of Bradshaw<sup>24,25</sup> because it includes the effect of surface tension and viscosity of the liquid on the critical depth of depression. Chatterjee and Bradshaw<sup>25,28</sup> have shown that the critical depth of depression is nearly independent of the lance height, although a close examination of the results show that the critical depth of depression increases systematically but slowly, with decreasing lance height. The difference between the minimum and the maximum depth of depression covered in their results is as high as thirty percent.

Shrivastava et al.<sup>26</sup> have shown that the critical lance height is a better criteria than the critical depth of depression for the onset of splashing. This approach appears to be more useful for a BOS operator because lance height is an operating variable used during a BOS blow.

Different approaches for estimating the depth of depression in the BOS have been reviewed by Chatterjee<sup>5</sup>. The estimates vary from 40 cm to 135 cm.

Figure 21 shows the results of Chatterjee and Bradshaw on depth of depression measurements.

#### 2.4 Splashing

The literature on splashing in the BOS is inadequate. The aims have been different for different workers and the experimental

techniques used were unsatisfactory.

Kunli <sup>29</sup> used a room temperature model to study splashing during oxygen lancing in the open hearth furnace. In this study the impressions of droplets were obtained by placing a filter paper over the mouth of the model box for a period of one minute. With this technique the droplets splashing to a height less than the height of the filter paper from the bath, will not be included. It is not possible to find any specific trend from this study.

In another investigation carried out by Chedialle and Harvais <sup>30</sup> the total quantity of water splashed from the mouth of a model converter was collected. The study was undertaken with a view to minimising the undesirable effects of splashing, such as the clogging of the lance, fume hood, converter mouth and the decrease in metallic yield through mechanical losses. The study concludes that the quantity of liquid splashed out of the converter passes through a maximum value with the variation in each of the operating variables:- gas flow rate, lance height, bath depth. In a similar investigation carried out at Swinden Laboratories, <sup>31,32</sup> the same technique has been used to study splashing in a model converter. The results are summarised below:

1. For the single hole lance, the splashing rate increased with increase of the lance height, whereas for the three hole lance the splashing rate was nearly independent of the lance height.
2. The three hole lance gave much less splashing than the single hole lance.

Chatterjee and Bradshaw <sup>25</sup> collected the splashed water in a tray fitted just above the surface of the water in a model converter. The tray covered one ninth of the total liquid surface. They concluded from their results that increasing the jet momentum or decreasing the lance height caused the amount of splashing to rise to a maximum value. Beyond this further changes caused a decrease in the volume of liquid splashed.

Molloy <sup>33</sup> has described a change over that occurs with increasing flow rate or decreasing lance height from the splash mode of behaviour of the jet to a penetration mode. This change over is accompanied by a decrease in the rate of splashing. A part of the splashed liquid, entrained by the jet is fed back to the depression resulting in a

decrease in the amount of liquid splashed out of the depression.

## 2.5 Bath Circulation

The initial concept of circulation in the metal bath was that metal flows downwards along the jet axis and upwards along the vessel walls. This concept resulted from the following arguments:

1. The force of the jet at the point of impact pushes the metal downwards along the jet axis.
2. The specific gravity of refined metal is higher (7.2) than that of unrefined metal (6.8). The refined metal in the neighbourhood of the depression will therefore move downwards along the jet axis.

Model studies have been carried out to investigate the circulation of metal and slag in the BOS. Wakelin<sup>22</sup> using the carbon dioxide water system observed that the liquid moves upwards along the jet axis, away from the depression on the liquid surface and downwards along the walls of the vessel. Similar observations have been reported by Holden and Hogg.<sup>34</sup> This type of flow pattern is explained on the basis of the shear force between the deflected gas jet and the liquid.

Turkdogan<sup>36</sup> studied the flow patterns using two immiscible liquids (oil and water) representing the slag and the metal. The gas used was argon. The flow patterns observed are reproduced in Figure 3. The flow of the oil phase at the surface of the depression is outwards. This is similar to the flow pattern observed by Wakelin<sup>22</sup> in the carbon dioxide water system. As the flow rate is increased, a dome is formed in the lower liquid (water) due to negative pressure in the upper liquid (oil). This negative pressure in the oil phase just below the depression is created as a result of the oil being dragged away by the jet. With further increase in the flow rate, the jet makes contact with the lower liquid (water). The flow of water is upwards along the axis of the jet.

It has been pointed that the flow pattern might be reversed if the gas forming the jet is highly soluble in the liquid.<sup>37</sup> Maatsch<sup>35</sup> is of the opinion that with thirty to fifty percent of the total gas absorbed by the bath, the flow pattern is reversed. Sheridan<sup>37</sup> reported that the flow pattern obtained by an insoluble gas jet was reversed in the case of the carbondioxide - aqueous sodium hydroxide solution system.

However, Chatterjee<sup>20</sup>, using the sulphur dioxide-water system, observed that the flow pattern is not reversed if the gas jet is soluble in a liquid. E. Prott, quoted by Chatterjee<sup>28</sup>, showed by choosing different gas - liquid systems that the nature of the flow pattern depends on changes in the surface tension of the liquid. If the surface tension of the liquid is lowered as a result of the gas absorbed, the flow of the liquid surface will be outwards from the depression. The reverse is true when there is an increase in the surface tension of liquid.

Observations made on the experimental converters show that the flow of the metal is upwards along the jet axis, away from the depression on the slag - metal surface and downwards along the vessel wall.

The overall rate of reaction in a high temperature system like the BOS process is controlled by the rate of mass transfer. The rate of mass transfer is improved by decreasing the concentration gradient. A bath free from concentration gradients is said to be a homogeneous bath. The kinetic energy in the jet transferred to the bath is utilised in stirring the bath and thus minimising the concentration gradient. The kinetic energy in the jet decreases with decrease in the flow rate and increase in the lance height. Wakelin<sup>22</sup> observed that in the carbon dioxide - water system there is better transfer of kinetic energy from the gas to the liquid bath at higher lance heights than lower lance heights. Results on experimental converters however, show that the bath is insufficiently well stirred to be homogeneous in composition and temperature<sup>38,39</sup>. The same view is supported by the observation of Wakelin<sup>22</sup> on the oxygen-silver system. Simultaneous bottom blowing has been found to give a homogeneous bath<sup>38</sup>.

## 2.6 BOS Slags

In the field of steelmaking there is a quotation, 'take care of the slag, the slag will take care of the steel.' The slag is a source of oxygen supply, a medium of refining and a receptacle for the reaction products. In order to discharge these functions the chemical and physical properties of the slag are very important for good steelmaking practice. Since the process is very fast, the slag should be formed in the shortest possible time.

Figure 4 reproduced from the British Steel Corporation research

report<sup>40</sup> shows the types of variation in slag composition that occur in the BOS. Just before the start of a blow, there is practically no slag. Lime charged is present in the solid state. Immediately after the start of the blow, silicon and iron begin to oxidise. The amount of iron oxidised depends upon the lance position. Initially the vessel is blown at higher lance heights in order to increase the amount of iron oxide in the slag, since this increases the rate at which the lime dissolves.

Once sufficient iron oxide is present in the slag the lance height is decreased in order to increase the decarburisation rate. This in turn decreases the amount of iron oxide in the slag. Towards the end of the blow as the decarburisation rate decreases, the amount of iron oxide in the slag once again increases. These variations are shown by the paths across the ternary diagram shown in Figure 4.

Slags which move into region B on the diagram are low in iron oxide and low in volume, and they have reduced basicity resulting in poor dephosphorisation. Slag which enter region A are high in iron oxide, far from equilibrium with the metal and have a marked tendency to cause unstable blowing and slopping<sup>40</sup>.

The initial slag formed is rich in silica. The precipitation of calcium orthosilicate around lime particles in the form of an impervious shell inhibits further dissolution of the lime<sup>42</sup>. The precipitation of calcium orthosilicate is undesirable because it increases the viscosity of the slag and slows the rate at which lime dissolves in the slag. The dissolution of lime in the slag is further influenced by the quality of the lime and by the slag composition.

The ability of lime to go into solution to form slags is represented by its reactivity. There are different tests used by suppliers and purchasers to measure the reactivity<sup>42</sup>. The rate of dissolution depends upon the surface area per unit mass which in turn depends on the particle size and the interparticle spacing. Hard burnt lime has less surface area per unit mass due to sintering, but is free from hydration. Chemically, lime should have the minimum of silica and sulphur.

In practice iron oxide (ore, mill scale or flue dust), magnesia, manganese ore, alumina, or fluorspar are added for the purpose of slag control. These additions affect the slag in one or more of the following ways<sup>42-44</sup>.

1. Alter the di-calcium silicate saturation range.
2. Alter the structure of di-calcium silicate shells.
3. Lower the melting point of the slag or its viscosity at any given temperature.

Lime premixed with such additions may be an attractive proposition in the future.

As with the precipitation of di-calcium silicate in the refining of low phosphorus pig iron, the precipitation of calcium silico phosphate can cause a problem in the refining of high phosphorus pig iron<sup>44</sup>. Like refining of low phosphorus pig iron, the liquidus temperature of the slag is lowered by the addition of iron oxide, magnesia, alumina or manganese oxide in the refining of high phosphorus pig iron.

From the chemistry point of view, the BOS slag should have a good ability to dephosphorise the metal. Not only in industry but also according to thermodynamics it is said that dephosphorisation requires a highly oxidising basic slag. With increase in the amount of lime in the slag, dephosphorisation first increases, passes through a maximum and then again decreases<sup>45</sup>.

## 2.7 Decarburisation

The first theory of decarburisation in the BOS process was proposed by Hauttmann. According to this theory, the jet penetrates like a solid body<sup>46</sup>. The oxygen reacts with the iron at the point of impact to form ferrous oxide<sup>47</sup>. This ferrous oxide is then circulated through the bulk of the bath, reacting with the carbon in the iron. The circulating currents caused by the difference in density of the refined and unrefined metal, and by the action of the jet, bring fresh metal to the slag - metal interface where removal of metalloids takes place.

Hammer<sup>48</sup> after carrying out experiments on models and large scale units proposed a different theory. According to this theory, deep penetration inside the metal by the jet is not expected. With increase in the intensity of blowing beyond a certain limit, small droplets of metal are formed. These small droplets are carried by the deflected jet. The droplets are oxidised during their flight. As the droplets fall back, oxygen is transferred to the bath.

The common features of these theories are that ferrous oxide acts as a carrier of oxygen and that no refining takes place within the slag phase.

Meyer et al <sup>49,51</sup> and Kozakevitch<sup>50</sup> have shown that decarburisation occurs mainly in the slag phase. The terms 'foams' and 'emulsions' were introduced <sup>50,52</sup>. An emulsion is defined as a system in which the distance between the droplets of liquid or gas bubbles dispersed in another liquid is sufficiently great to permit, in principle, an independent 'free' movement of each droplet or bubble. If the volume of liquid is much less than the volume of gas, the bubbles cannot move freely and the whole system is then called a foam. Meyer and his co-workers collected the ejected material through the tap hole of a basic oxygen vessel on a sample collecting pan. The metal particles were then liberated from the slag. From their examination of these particles, Meyer and his co-workers concluded:

1. The mean residence time for the metallic droplets in the slag is about three minutes.
2. The surface area for the carbon-oxygen reaction is very large and may reach as high as 2000 sq. ft. per ton (183 sq. meters per tonnes).
3. The quantity of metal in the gas - slag - metal emulsion may reach as high as 30 percent of the metal charged to the vessel.
4. The metal in the emulsion has a substantially lower carbon concentration than the average metal within the vessel.
5. The major part of the decarburisation process occurs in the emulsion. At the height of refining, most of the decarburisation occurs within the emulsion. On an average 70% of the decarburisation occurs from metal emulsified in the slag.
6. Carbon diffusion is the rate controlling mechanism only when the bulk carbon concentration is below 0.35 percent.
7. The existence of relatively stable slag-metal emulsions is a key technical factor in the commercial success of the BOS process.

Meyer and his co-workers<sup>49</sup> have proposed the following mechanism of decarburisation in BOS:

1. Metal droplets are ejected from the bulk metal into the slag phase due to a combination of:

- (a) The action of the impinging oxygen jet.
  - (b) The action of carbon monoxide bubbles rising out of the metal into the slag.
  - (c) The resultant turbulence on the surface of the bulk metal; where two 'waves' meet each other droplets of metal will be thrown upwards into the slag phase.
2. The ejected metal droplets are completely surrounded by slag, and oxygen is transferred to them from the slag by unsteady state diffusion. Since the metal droplets can exist surrounded by slag for a period of time without 'seeing' any carbon monoxide gas bubbles, a high degree of supersaturation can be achieved with respect to the decarburisation reaction.
  3. In time, the oxygen saturated metal droplets may come into close contact with carbon monoxide bubbles rising through the slag. At this stage, carbon monoxide evolution from the droplets will proceed extremely rapidly. Alternatively, solid lime particles might provide nucleation sites for carbon monoxide gas.
  4. Oxygen supersaturation within the emulsion metal droplets could become so high as to allow nucleation of carbon monoxide bubbles within the droplet itself.

Chernyatevich et al <sup>53</sup> have observed that there is a considerable decrease in the level of the upper surface of the metal during a BOS blow. This observation supports Meyer's view that a large part of the metal is present in the slag phase.

The experimental technique used by Meyer et al is likely to introduce error in the results. A part of carbon in the droplets might have oxidised in air before the droplets were cooled. Price <sup>54</sup> investigated decarburisation in the BOS using an in-blow bomb sampling device. He has estimated that approximately thirty five percent of the carbon was removed through the emulsified metal droplets.

Chatterjee et al <sup>38,55</sup> have estimated that thirty five to forty percent of the total decarburisation occurs via the oxidation of droplets dispersed above the bath. They have also observed that equally good decarburisation can be achieved by exposing the droplets to an oxidising atmosphere above the bath.

Estimates about the percentage of carbon removed via the slag-metal emulsion may vary for different investigations or practices. It

appears to be a generally accepted fact that the gas - slag - metal emulsion plays an important role in the refining of pig iron in the BOS.

Figure 5 shows a typical decarburisation rate curve in a BOS blow. The rate increases during the early stages with the increase in the amount of slag formed. The rate of decarburisation then becomes practically constant. During the peak decarburisation period, extended to the major part of the blow, the rate of decarburisation is controlled by the rate of carbon monoxide removal<sup>56</sup>. Towards the end of the blow the rate of decarburisation decreases with the decrease in carbon content of the bath.

In view of the importance of refining in the slag phase, the reaction between single iron carbon droplets and slag has been studied.<sup>57-59</sup> The droplets are surrounded by the product gas. The droplets may rise or sink depending upon their size and the amount of gas attached to them. The movement of the droplets is along a preferred path created by the movement of the foam that forms as a result of the escape of the product gas carbon monoxide. Sometimes the droplet breaks into two or three smaller droplets. The rate of decarburisation is retarded by the presence of silicon, manganese, phosphorus and sulphur.

Davis et al<sup>57</sup> have reported that the droplets are surrounded by gas phase, called a halo, and suggest that the reaction takes place via a CO/CO<sub>2</sub> gas mixture in this gas. Hills<sup>60</sup>, is of the opinion that the presence of such an additional step in the transport chain, could not explain the high reaction rates.

Acheson and Hills<sup>73,76</sup> have studied the reaction between single droplets of sodium amalgam and acidified water glycerol mixture. The photographs of falling droplets show clearly that the product gas hydrogen is evolved at the back of the droplet and there is no evolution of gas at the front of the droplet. On the strength of this study, they proposed that a part of an iron droplet will be in contact with the slag where iron ions will accept electrons forming iron atoms. Electrons for this reaction will be provided by combination of oxygen ions with the carbon producing carbon monoxide.

Ojeda<sup>81</sup> is of the opinion that as the gas is detached from the surface of the droplet, vacuum is created followed by short lived contact between the droplet and the slag. This process repeats at so high a frequency that under normal observing conditions, it

is not visible. This mechanism is that of nucleate boiling. In nucleate boiling as the bubbles rapidly form and detach, fresh liquid rushes to the former bubble site. The process of bubble formation and detachment repeats again and again. The net result is that all the bubble sites act as micro-pumps and increase the heat transfer coefficient <sup>79,80</sup> in boiling, or the mass transfer coefficients in the slag/metal decarburisation process.

For a long time, it was believed that the heterogeneous nucleation of carbon monoxide was not possible. Ward <sup>62</sup> estimated that a bubble nucleus of molecular dimensions of the order of  $6A^{\circ}$  radius requires an internal pressure of  $5 \times 10^4$  atmospheres to sustain it. The attainment of so large a pressure requires impossibly large supersaturations of carbon and oxygen.

Meyer et al <sup>49</sup> suggested that homogeneous nucleation of carbon monoxide is possible. Davis et al <sup>57</sup> and Ojeda <sup>59</sup>, refining iron carbon droplets in slag, observed that homogeneous nucleation does occur. Richardson <sup>63</sup> explained this on the basis of slag entrapment leading to heterogeneous nucleation. Baker et al <sup>64</sup> proposed that metal from the surface of the droplet saturated with oxygen is migrated by eddy diffusion inside the droplet, resulting in supersaturation with respect to carbon monoxide. Ward and Nakao <sup>65</sup> proposed that the process of transport is by molecular diffusion instead of eddy diffusion. At high flow velocities, the static pressure in a liquid may fall below its vapour pressure <sup>80</sup>. Under these conditions bubbles can form with virtually no super saturation at all. Intense surface turbulence can lead to the nucleation of bubbles inside eddies due to the large negative pressure that can exist at the centre of eddies <sup>83</sup>. Robertson and Jenkins <sup>81</sup> have observed intense surface turbulence in levitated drops decarburised with oxygen. Robertson and Jenkins are of the opinion that there will be intense surface turbulence even in the absence of an electromagnetic field. Whatever may be the explanation, homogeneous nucleation of carbon monoxide does occur in BOS. The calculated partial pressure of carbon monoxide in equilibrium with carbon and oxygen varies from 10 to 60 atmospheres <sup>64-66</sup>.

## 2.8 Foams and Emulsions

BOS foam is dynamic in nature. It is caused by the gas liberation <sup>53</sup>.

The foaming reaction takes place within the slag phase<sup>69</sup>. The physical properties of the slag are thus of secondary importance.

It is a general observation that towards the end of a BOS blow, the foam tends to subside because the decarburisation rate decreases. The rate of decarburisation and thus the amount of gas produced within the slag phase depends on the rate at which metal droplets are ejected from the depression and on the activity of iron oxide in the slag. The product gas tries to escape through the slag phase. The slag phase offers resistance to the escape of gas, producing the foam.

Acheson and Hills<sup>76</sup> using a room temperature model have suggested that the removal of carbon monoxide bubbles from the reacting foaming slag plays a major role in controlling the decarburisation rates in the BOS process. On the basis of this study they have also predicted the decarburisation rates in industrial and pilot scale converters with a high degree of accuracy.

Urquhart and Davenport<sup>70</sup> have used low temperature emulsion concepts to describe mechanisms in slag metal emulsions. The low temperature system chosen is water-oil. In BOS during refining, for most of the time the metal droplets are surrounded by the product gas. The contact between the slag and metal droplets is for a short duration as observed by Mulholland et al<sup>58</sup>. The droplets stay in the gas - slag - metal emulsion only as long as there is evolution of gas due to carbon removal. The major role in floating the droplet in the foam is thus played by the surrounding product gas and not by the bonding between the slag and metal as proposed by Urquhart and Davenport.

The low surface tension of slags favours foaming. Silica, phosphorus penta oxide, titania and iron oxide lower the surface tension of BOS slags<sup>50,68</sup>.

High viscosity retards the drainage and thus contributes to foaming. Cooper and Kitchener<sup>68</sup> have observed that in a slag containing silica, lime and phosphorus pent-oxide, the foam stability increases with increase in the silica content from 50 to 63 percent. They have also observed an increase in foam stability with decrease in the temperature of the slag. These observations are in agreement with the effect of increase in silica content and decrease in temperature on slag viscosity. The presence of solid particles increases the viscosity. Examples are undissolved lime,

precipitates of di-calcium silicate, calcium silico phosphate and chromium oxide.

Increase in the temperature decreases the viscosity, but increases the rate of decarburisation. Thus the increase in temperature may increase or decrease the foaming depending upon the dominating factor.

It has been observed that with increase in lance height together with increase in flow rate of oxygen, the volume of foam increases <sup>69,71</sup>.

It is a general observation that good dephosphorisation is associated with a foamy slag. The Phosphorus removal reaction is a slag - metal reaction. High rates of decarburisation can be achieved even in the absence of a foam. Excessive foaming can cause overflow of slag from the mouth of the vessel and decrease in the metallic yield. A limited and controlled foaming is thus desirable for good dephosphorisation and smooth operation.

### 3.1 Construction

#### 3.1.1 Reactor

The reactor assembly is shown in Figure 6. The important features of the reactor are its adjustable bottom and the slit nozzle covering the entire width. The main body and the bottom of the reactor were made from transparent Perspex. Quickfit glass joints were used for the gas inlet and outlets. The inside dimensions of the reactor were 25 cm height, 10.5 cm width and 2.0 cm thickness. Perspex dissolved in chloroform was used as glue for getting a homogeneous bond.

The body of the reactor was constructed by first fixing two Perspex sheets of 10.5 X 1.0 cm on either end of a 0.3 cm thick, 35.0 X 12.5 cm sheet to serve as guides for controlling the width of the reactor (Figure 7a). Two sheets of 35.0 X 2.0 X 1.0 cm were then joined forming two sides of the reactor (Figure 7b). Precision in the 2.0 cm dimension was achieved by grinding on a hand facer and measuring with a micrometer. A 0.3 cm thick 35.0 X 12.5 cm sheet was then joined to the two side sheets, completing the four sides. Both ends of the reactor were then cropped in order to remove the two sheets used as guides (Figure 7c).

A central slot of 0.6 cm width was then cut through the upper half of the front and back faces of the reactor to act as a guide for the slit nozzle (Figure 7d). It was then sealed with 0.3 cm thick, 1.6 cm wide sheet on both the faces. The top cover of the reactor was made out of 0.5 cm thick sheet (Figure 9a). It was provided with two circular openings for attaching outlet connections and a slot for insertion of the nozzle. The purpose of the top cover was to attach the outlet connections and the slit nozzle to the reactor in a way that permitted replacement. Twelve holes were made for attaching the outlet connections and the slit nozzle assembly. The cover was then fixed on the top of the reactor.

The two outlet connections consisted of Quickfit 19/26 cones which were attached separately to two 0.5 cm thick 5.0 X 5.0 cm Perspex sheets using Araldite as adhesive (Figure 8a). These were then bolted to the top cover to provide the outlets.

The bottom of the reactor was milled from a solid Perspex block.

The upper face of the bottom was shaped of curved surface of radius 13.0 cm (Figure 9b). A 0.5 X 1.0 cm groove was cut in all four vertical faces, to be filled with silicon rubber, allowing a portion to project above the groove. The silicon rubber seal was polished on a polishing wheel so as to fit tight inside the reactor. Two stainless steel hooks were fixed to the lower face of the bottom for pulling it out of the reactor. Hooks were fixed to both ends of a 0.2cm diameter stainless steel rod, which was then bent in the form of a U for withdrawing the bottom (Figure 12b).

Perspex blocks of cross section corresponding to the reactor were made for pushing the bottom inside the reactor (Figure 12a). The blocks had varying thickness so that a combination of one or more allowed the bottom to be pushed up to the desired height.

### 3.1.2 Slit Nozzles

Two types of slit nozzles were used. The first type was a single slit producing a single jet of gas flowing vertically downwards. The second type of nozzle produced two jets flowing downwards at specific angles on either side of the vertical axis. The first single slit nozzle was 0.1 cm in width and was made using a method similar to that used for the body of the reactor (Figure 8b). Two thin spacer trips 2.0 cm in length were fixed on either end of 2.6 cm wide Perspex sheet. Two long spacer strips of 0.3 cm width and 0.16 cm thickness were then fixed, maintaining an exact distance of 2.0 cm using strips already fixed as guides. The two ends were then cropped to get the required length. The width of the slot was reduced to 0.1 cm by polishing the spacer strips on a polishing wheel and measuring with a micrometer. Another sheet 2.6 cm in width and 0.3 cm in thickness was fixed completing the four sides of the slit nozzle. One end of the slit nozzle was joined to a 4.0 X 6.0 cm Perspex sheet of 0.3 cm thickness. Another such sheet was joined to the cone of a 19/26 Quickfit joint. The two sheets were then joined together completing the slit nozzle assembly (Figure 8b). The tip of the nozzle was faced on the polishing wheel. The nozzle was then inserted through the top cover and bolted in place.

At a later stage it was felt that the width of the slit nozzle should be reduced from 0.1 cm to 0.05 cm in order to increase the

momentum of the jet without increasing the gas flow rate. A 0.05 cm deep, 2.0 cm wide slot was cut in a Perspex sheet 0.3 cm in thickness and 2.6 cm in width. Another Perspex sheet 0.3 cm in thickness and 2.6 cm in width was joined to cover the slot. The assembly of two sheets forming the slit nozzle was connected to the cone of a 19/26 Quickfit joint as described for the 0.1 cm nozzle. The length of the nozzle was adjusted to fit the entire length of the slot of the reactor by cutting the excess length from the lower end.

The construction of the two slit nozzles is shown in Figure 10. For making a two slit nozzle, two Perspex sheets 0.5 cm in thickness, 2.6 cm in width and 14 cm long were cut. One end of both the sheets was tapered from one face at the required half angle between the two slits. A groove 0.025 cm in depth and 2.0 cm wide was cut along the length of both the sheets. The two sheets were then joined together using chloroform as binder. A wedge was inserted into the tapered portion of the two sheets assembly as shown in Figure 10. The two slit nozzle thus fabricated was joined to the cone of a 19/26 Quickfit joint as described above for the single slit nozzles. Since the outer width of the two slit nozzles was greater than that of the single slit nozzles, a second reactor was constructed to fit the two slit nozzle. The second reactor was otherwise identical to the original reactor.

### 3.1.3 Frame Assembly

The frame assembly was constructed in order to clamp the reactor and the moveable bottom. Four sockets were welded on four corners of 0.6 cm thick 23 X 12 cm stainless steel sheet (Figure 11). Four 44 cm long, 1.2 cm diameter stainless steel rods were then screwed into the sockets and two aluminium frames clamped to the four rods using 0.6 cm screws. Each frame was provided with six 0.8 cm clamping screws. 0.1 cm thick Teflon sheets were fixed on the front faces of the clamping pads.

### 3.1.4 Tank

The reactor was immersed in a tank of water. The inside dimensions of the tank were 40 X 50 cm cross section and 37 cm height. 0.6 cm thick Perspex sheet was used for its construction. The corners were reinforced with aluminium angle using brass screws for fixing. Silicon

rubber was used as sealing material between the aluminium angle and the Perspex sheet.

### 3.1.5 Overall Apparatus

The overall apparatus used for the present work is shown schematically in Figure 13. Plate 1 shows a photograph of the overall apparatus. Gas from a nitrogen cylinder regulated by a single stage regulator flowed through a Metric 10 G type Rotameter. Hydrogen Chloride gas from a cylinder regulated by a needle valve flowed through a Metric 7 G type Rotameter. The float of the Rotameter used for the hydrogen chloride gas was made of Korannite. Both the gases had a common mercury manometer for the measurement of their total pressure and separate thermometers for the measurement of their temperature prior to entering the Rotameters. On leaving the Rotameters, the two gases were mixed in a mixing vessel (a one litre capacity conical flask). Gas from the mixing vessel passed to the reactor through the 19/26 Quickfit joint. The reactor (Figure 6) was clamped in the frame (Figure 11) and was placed in the tank filled with water. The two outlets of the reactor were connected to two 1.5 cm diameter plastic tubes through 19/26 Quickfit joints. The exit gas streams were connected to two, one litre capacity, conical flasks used as mercury traps. The two streams were then connected together by a 'Y' joint. The outgoing gas stream was then connected to a gas cleaner (a 40 litres capacity aspirator) filled with water. The gas, now free from hydrochloric acid and mercury was passed to the exhaust system.

### 3.1.6 Amalgam Cell

Sodium amalgam was made in an amalgam cell. A rectangular box of inside dimensions 15 X 15 X 15 cm open at the top, was made out of 0.6 cm thick Perspex sheet (Figure 14). An L shaped 1.5 cm wide, 0.1 cm thick stainless steel strip was fixed with Araldite along the centre of the bottom and back face of the box to serve as the cathode. Along the back face, the cathode was covered with a Perspex channel using Araldite as the adhesive. The anode made of platinum gauze was supported in the centre by another Perspex strip. The Perspex strip was supported on the two sides of the cell.

A tap hole was drilled in the front face, and a 0.4 cm internal diameter Perspex tube connected to it.

The Perspex tube was connected to a glass capillary. A pinch cock was used to regulate the flow of amalgam from the cell.

A stirrer motor was provided for the cell by mounting it on a stand. The motor operated at 220 volts A.C. Its stirrer was made by fitting a Perspex blade on a Perspex tube of 0.6 cm outside diameter (Figure 15a). A 2 cm long stainless steel rod was connected to the top end of the stirrer for tightening it in the chuck.

The power supply to the cell was provided by a Farnell stabilised power supply unit type TSV 70 MK 2. Using a selection switch it was possible to connect one of the following output settings:-

1. 0 to 10 amperes, 0 to 35 volts.
2. 0 to 5 amperes, 0 to 70 volts.

The amalgam cell with its stirrer is shown in Plate 2.

### 3.1.7 Mercury Purifying Unit

A 50 cm<sup>3</sup>, 1.2 cm diameter glass tube was attached to the top of a 12 cm high, 2 cm diameter glass tube by means of a bung (Figure 15b). The lower end of the glass tube was attached to a swan neck capillary tube forming a siphon system for tapping the mercury collected in the glass tube. A capillary tube was attached to a funnel for purging mercury. A small quantity of pure mercury was initially poured into the unit to balance the height of the 5 percent solution of nitric acid that was subsequently poured in.

## 3.2 Major Factors Considered in the Design of the Reactor

The construction of the reactor and of the ancillary equipment has already been described in the previous section. The purpose of this section is to explain the reasoning behind this construction and alterations that were subsequently made.

### 3.2.1 Reactor

If a thin vertical section passing through the centre of a BOS vessel during a blow is imagined, the view will be two dimensional and the entire thickness of the centre of the section will be occupied by the lance. In order to simulate this situation it was decided to use a two dimensional slice reactor and cover the entire width with a slit nozzle. Since it is extremely difficult to construct a

moveable slit nozzle to cover the entire width of the reactor it was decided to construct a moveable bottom to the reactor in order to vary the nozzle height.

If the thickness of the reactor had been too small, the front and back faces would have exerted in undue influence on the flow patterns within it. On the other hand, the greater the width the greater the consumption of gas during an experiment. A compromise was arrived at by choosing 2.0 cm as the reactor thickness.

The width of the reactor was chosen to be nearly equal to the diameter of the axi-symmetrical model reactor used by Acheson<sup>73</sup>. The height of a BOS converter is approximately twice its diameter. Thus the height of the slice reactor has been fixed at about 2.5 times its diameter in order to accommodate the thick bottom and to allow for its vertical movement. In industry the vessel volume is about six times the metal volume. If a BOS converter is considered as a cylinder, the molten metal will occupy one sixth of its total height; equivalent to one third of its diameter. In the slice reactor the depth of the metal was therefore arranged to be one third of the diameter of the reactor. This gave a 3.5 cm depth of metal corresponding approximately to 70 cm<sup>3</sup> of amalgam. The depth of slag in a BOS vessel is approximately half the depth of metal. Thus the depth of the simulated slag in the slice reactor was kept at about 2.0 cm. The top of the vessel was arranged to be 10 cm above the tip of the nozzle so that the slag could expand up to at least five times its original volume before it overflowed.

The split of the vessel's height is thus as follows:-

Above the tip of the nozzle	= 10.0 cm
Maximum distance from the nozzle tip to the slag surface	= 5.0 cm
Height of the slag	= 2.0 cm
Height of the metal	= 3.5 cm
Height of the bottom	= 4.5 cm
Total	= 25.0 cm

The front and back walls of the reactor were made out of 0.3 cm thick sheet, a compromise between elasticity and strength. Elasticity is needed for making a good seal with the bottom when the sides were pressed by the clamping screws attached to the frame assembly. Thick side walls gave large surface area of contact for the joints, allowing clean, leakproof joints to be made. Another advantage of the thick side wall was that they could be joined easily to the front and back

walls exactly at right angles. The 0.5 cm thickness of the top cover and the outlets was sufficient to avoid gas leaks due to bending the sheet when the outlet and slit nozzle assemblies were bolted into place.

Two outlets were needed because the slit nozzle divided the upper portion of the reactor into two halves so that the exit gas could not pass from one half to another. The total area of the two outlets was greater than the area of the single outlet used by Acheson<sup>73</sup>.

### 3.2.2 Slit Nozzles

The slit nozzle width was initially formed at 0.1 cm a compromise between gas consumption and dimensional accuracy. Later another nozzle of 0.05 cm width was constructed so that the jet momentum could be increased without increasing the total gas consumption.

In a multi-hole lance, the individual jets should be inclined at an angle of at least 10 degrees to the vertical in order to ensure the existence of separate jet impact areas<sup>6</sup>. The minimum angle between the two slits was therefore chosen to be 20 degrees. The other two angles chosen were 40 degrees and 60 degrees for studying the effect of the angle of inclination. The distance between the two slits at the exit end was 0.5 cm in all three cases. The construction of the slit nozzle assembly was such that it could be replaced by another one without making major changes in the reactor construction.

### 3.2.3 Frame Assembly

The purpose of the frame assembly was to maintain the leak proof joint between the body and the bottom and also to support the reactor. Plain carbon steel was not used due to the problem of rusting. Telfon sheets on the front face of the clamping pads avoid scratching the surface of the reactor.

### 3.2.4 Tank

The reaction inside the reactor is exothermic. The working temperature for Perspex should be well below 80°C, so that the water tank was needed to cool the reactor and act as a safety precaution against failure of the reactor during a run. Aluminium angles and brass screws were used to avoid leakage of water due to corrosion.

### 3.2.5 Ancillary Apparatus

The polythene pipe used for making the gas connections was of

sufficiently large size (cross section) to allow the gases to flow freely. Two mercury traps connected in parallel were used to ensure that the outgoing gas was reasonably free from mercury.

The entire assembly was arranged on a working bench and was covered by a Perspex roof and plastic curtains on four sides (Plate 1). This helped to keep any small amount of leaked gas restricted in a limited space. The Perspex roof was connected by two exhaust pipes into the fume ducting system.

4.1 Measurement of the Depth of Depression

For the experiments in which the depth of the depression was to be measured, the bottom of the reactor was adjusted to allow for a bath depth of at least 5.0 cms with the bath surface at the predetermined height below the tip of the nozzle. The reactor was clamped vertically in the frame assembly and it was then placed in the tank. Liquid (water or mercury) was transferred into the reactor through one of the two outlets. A cathetometer (telescope travelling along the vertical axis) was used for measuring the depth of depression. The cathetometer used for the present work was mounted on a vertical graduated rod to allow for, and measure its vertical movement. The cathetometer was placed in front of the reactor, The level of the cathetometer was adjusted and it was focused on the meniscus of the liquid. The height between the nozzle and the bath surface was adjusted to the desired value by adding small amounts of liquid and checking the cathetometer reading. The nitrogen gas supply was then turned on at the predetermined value and after allowing about two minutes for the depression to become stable, its position was measured with the cathetometer. The temperature and pressure of the gas were recorded prior to entering the Rotameter. At higher flow rates the depression was observed to be oscillating. For measuring the depth of an oscillating depression, the maximum and minimum depth were recorded and the average of these two values was taken to represent the depth of depression.

In the case of the nitrogen-water system, distilled water was used as the liquid. The depression was observed under transmitted light by arranging a table lamp on the other side of the reactor. The shade of the lamp was covered with green paper to minimise eyestrain and this resulted in better observation.

Initially the reference level was observed to change continuously during experiments with this system and the surface to nozzle height increased gradually. An experimental investigation established that this loss was due to evaporation. Details of the investigation are given in Appendix 1. In order to overcome this problem the blow was quickly stopped after each measurement of the depth of the depression and the

reference level of the bath re-measured with the cathetometer. Small amounts of water were then added to make up the evaporation loss, thus allowing the next blow to be started with the bath surface at the original reference level.

In the case of the nitrogen mercury system triple distilled mercury was used. Reflected light was used for observing the depression. The mercury was replaced when a layer of oxide was observed on the surface. The fume ducting system was used for keeping the working place free from mercury vapour.

#### 4.2 Preparing Sodium Amalgam

Solutions of sodium hydroxide containing 150 grams per litre were prepared by dissolving sodium hydroxide pellets in distilled water. The solution was stored in a five litre capacity bottle. About 250 cm<sup>3</sup> of mercury was transferred into the amalgam cell producing a mercury bath, something over one centimetre in depth. The sodium hydroxide solution was added to the cell so that the anode was fully immersed in it. The rotor of the stirrer was adjusted so that its blade was also immersed in the mercury. The stirrer was turned on at slow speed. A 5 amp D.C. current was supplied to the cell from the power supply unit at a potential of 5 volts. As the concentration of sodium in the amalgam increased, its viscosity increased. The power supply and the stirrer were switched off just before the amalgam was too thick to flow. Before this occurred, however, the evolution of hydrogen gas would be observed from time to time at the cathode when the concentration of sodium hydroxide in the electrolyte had become insufficient. The deficiency of sodium hydroxide was made up by the addition of fresh sodium hydroxide solution. The amalgam was tapped from the cell into 100 cm<sup>3</sup> bottles and stored under alcohol.

#### 4.3 Blowing onto Sodium Amalgam

For the experiment in which the sodium amalgam was to be reacted with simulated slag, the outer safety tank was filled with water containing a small amount of sodium nitrite, the sodium nitrite being added to prevent corrosion of the frame assembly. This water was changed periodically after a few runs.

Before each run, the bottom of the reactor was adjusted with the help of the Perspex blocks and the U-shaped rod, and the reactor was clamped vertically into the frame. About seventy cm<sup>3</sup> of the amalgam was transferred into the reactor. Forty cm<sup>3</sup> of glycerol water (60% glycerol) mixture was then transferred into the reactor. The nozzle height was adjusted to its predetermined value by adding small amounts of the amalgam and observing the level of the amalgam through the cathetometer. The reactor and its frame were then transferred in to the tank.

A high-speed camera has been used in this investigation for studying the stirring patterns in the foam. The necessary details about the camera are given in section 4.7. The high-speed camera and the necessary lighting equipment were set up in front of the reactor. The inlet and outlet Quickfit joints were then connected to the reactor. After the operator had donned a respirator, the fume extraction system was switched on and the nitrogen and hydrogen chloride supplies were turned on at their predetermined rates. The run was photographed with the high-speed camera. Temperature and pressure of both the gas supplies were recorded by mercury thermometers and manometer prior to entering the Rotameters. The blow was terminated by first turning off the hydrogen chloride gas followed by the nitrogen gas. The Quickfit joints were disconnected. After allowing half an hour to purge the atmosphere of the working area, the fume ducting system was turned off. The reactor frame assembly was taken out of the tank and the contents of the reactor were transferred to a beaker. The reactor was washed with distilled water and then inverted for drainage.

#### 4.4 Processing the Mercury

The contents of the reactor collected in the beaker were decanted. The impure mercury containing residual sodium and mercury oxide was passed through the mercury purifying unit. The process was repeated to obtain clean mercury free from oxide.

#### 4.5 Safety

Hydrogen chloride gas and mercury are dangerous for health. The maximum allowable concentration of mercury in air is 0.01 p.p.m.

(0.1 m.g.m.<sup>-3</sup>).<sup>77</sup> The following steps were taken in order to ensure safe working conditions.

1. Trays were used during pouring mercury or amalgam so that if there was any spilt, it was retained in the tray.
2. Spilt mercury was first collected and then the traces of mercury left were made harmless by dusting with sulphur.
3. All mercury containers were either kept closed with a stopper or the mercury surface was covered with water.
4. The fume ducting system was used during and up to half an hour after each run.
5. Mercury was always handled and the amalgam prepared under the exhaust hood.
6. The working and experimental areas were periodically checked with a mercury detector.
7. Water used in the washing of the reactor and the amalgam cell was subsequently collected in a container for safe disposal.
8. Respirators were worn by the operators during each run.
9. The investigator, and others associated with the work were required to undergo periodic blood and urine tests.

#### 4.6 Development of the Technique for Examining Motion in the Foam

The main purpose of the investigations was the study of velocities and stirring patterns in the foam. In a number of experiments it was established that the movement of the foam could not be ascertained by simple visual observation of the foaming slag, nor from cine film, whatever the intensity of blowing or the speed of filming (over the range from 16 to 500 frames per second). In experiments using a low proportion of hydrogen chloride gas in the jet, no foam was produced but movement was visible. It was decided that the motion of the foam could not be seen because of its opacity which was due to the scattering of light from the surfaces of the multitudes of minute bubbles contained in the foam (Plate 3). It was therefore decided that some type of tracer technique was needed to observe the foam movement.

Bubbles of nitrogen gas were therefore initially introduced into the foam at very slow speeds through a glass capillary. This was done on the assumption that the movement of individual nitrogen bubbles would follow that of the foam and their large size would allow this motion to be observed. However, the tracer bubbles grew in size at the expense of the foam

bubbles, increasing the buoyancy force acting upon them and thus locally distorting the movement of the foam. The attempt to use nitrogen gas bubbles as a tracer was therefore discontinued.

It was then decided to try injecting a colour tracer into the foam in order to make its motion visible. Potassium permanganate, litmus solution, methyl orange and organic dyes for anodising were all tried in turn. The performance of these tracers is given in section 5.3.2. Blue-black Parker Quink was then tried and proved to be an excellent tracer, providing a strong contrast and retaining its colour throughout each entire experiment. The liquid tracer was injected through 'T' - shaped three way Quickfit joints connected to the two outlets of the reactor as shown in Figure 17. The stem of each 'T' was horizontal and connected to the exhaust system. The opening on one side of the cross of the 'T' was connected to the outlet of the reactor and the other side vertically above the outlet was used for injecting the tracer. A rubber bung through which a hypodermic needle had been passed was fitted into this opening. One  $\text{cm}^3$  of the tracer was sucked into a syringe and the syringe then connected to the hypodermic needle. The same procedure was followed for the other outlet. The tracer was injected into the foam at the appropriate time during a run by pressing the plunger into the syringe.

This technique allowed the movement of the foam to be seen when the Parker Quink was used as the tracer, but the technique was crude. The tracer entered the foam as a series of drops, each drop falling at a different location on the surface of the foam. An improved technique was therefore developed to allow the tracer to be injected at specific points within the foam. Long thin stainless steel tubes were purchased and mounted in the rubber bungs in place of the hypodermic needles. The tubes were positioned with their exits close to the slag-metal interface and to the side and front walls. The tracer could thus be injected at two points equally remote from the depression and close to the front face of the reactor. This technique allowed the movement of the foam to be determined and disclosed the type of flow patterns formed, but it did not allow the mixing of jet material into the foam to be studied. This was because the tracer took a considerable time to be entrained into the jet region, and even then entered at very low

concentrations.

Attempts were therefore made to inject the tracer through the slit nozzle itself. A three way joint together with a hypodermic needle was used for injecting the tracer in the manner previously described. The slit was temporarily blocked by the injected tracer and the sudden rise in the back pressure of the gas blew the mercury out of the total pressure manometer. A relief valve was therefore connected to the nitrogen stream before the mixing vessel, allowing some gas to be discharged to the atmosphere as soon as the gas pressure exceeded a certain critical limit. However, with this modification the tracer did not flow rapidly through the slit because of the reduction of the driving pressure allowed by the pressure limit valve.

It was therefore decided to abandon the idea of injecting the tracer through the jet itself, but to inject it at points adjacent to the jet exit. The arrangement for injecting the tracer at a point adjacent to the jet exit is shown in Figure 16. Two hypodermic needles were connected to two long stainless steel tubes. Two holes were drilled along the inlet and two stainless steel tubes were permanently fixed so that the tips of the tubes were close to the slit nozzle and front wall. The tubes were extended up to the lower end of the slit nozzle. The technique worked successfully and was also extended to the two slit nozzles.

#### 4.7 Cine Photography

It was anticipated that the foam velocity would be too high to be observed at the normal speed of sixteen pictures per second. It was therefore decided to use a high speed cine camera. A John Hodland Hyspeed camera was used with Ektachrome commercial type 7252 film. The camera was positioned in front of the reactor at a distance of 1.5 metres from the reactor. Four lamps, each of 750 watts power were used for illuminating the cell. The lamps were fixed on two stands (two lamps on each stand) in the same horizontal plane as the reactor but inclined at an angle of 45 degrees to its front face, and approximately 30 centimetres away from it. The aperture used was f 16. The exposure is related to the film speed (number of pictures per second). For 54 pictures per second the speed employed for the present investigations the exposure was  $6.25 \times 10^{-3}$  seconds. In the initial stage of the project some still photographs were also taken in order to standard-

ise the procedure for high speed photography.

Movement of the tracer suggested that the foam moved at comparatively slow speed. Trial experiments were performed using speeds of 16 and 64 pictures per second. It was decided that the 64 pictures per second speed of the film was suitable for the investigation.

The runs were filmed for about half a minute starting after the flow rates of the gases had been stabilised so that the experiments could be terminated before the precipitation of salt. The precipitation of salt is described in greater detail in section 5.3.1. About three runs were filmed on a film of 200 feet length. The film was then sent for 'rush' printing.

The films were analysed with the help of a frame by frame analyser. A 60 X 40 cm graph paper was fixed with cellulose tape on a portable screen. The distance between the screen and the projector was adjusted to magnify the object five times. The following information was plotted:-

- (a) The path of the tracer.
- (b) The path of the droplets falling through the foam.
- (c) Location of the total number of droplets in the foam at any moment of time.

The number of frames, and thus the time required, for the foam to trace its complete path and for the complete mixing of the tracer were also recorded.

#### 4.8 Temperature Measurement

A chromel-alumel thermocouple protected by a stainless steel sheath was used for measuring the temperature of the foam. The thermocouple was inserted into the reactor through one of the two exhausts using a three way Quick-fit joint, as described in section 4.7 for inserting the stainless steel tubes. The tip of the thermocouple was positioned in such a way that it was in the centre of the foam in the right half of the reactor. The thermocouple was connected to an Oxford 3000 recorder. The chart speed was maintained at 5 cm per minute and the span was 10 millivolts.

## 5. RESULTS

### 5.1 Depth of Depression Measurements

Depth of depression measurements in the nitrogen water system were made at different flow rates of gas for  $h = 1, 2, 3, 4, 5$  and 8 centimetres. The single slit nozzle of one millimetre width was used. The data is shown in Table 1. The effect of jet momentum on the depth of depression for different values of  $h$  is shown graphically in Figure 18. The jet momentum was calculated from the Rotameter reading and the pressure of the gas measured where it entered the Rotameter. Details of the calculations are shown in appendix 2.

Depth of depression measurements in the nitrogen mercury system were made at different flow rates of gas for  $h = 0.5$  and 2.0 centimetres. The single slit nozzle of one millimetre width was used. The data is shown in Table 2. The effect of jet momentum on the depth of depression for the two values of  $h$  is shown graphically in Figure 19.

In order to compare the depth of depression produced by a single hole lance with the depth of depression produced by a multi-hole lance, the two slit,  $20^\circ$  nozzle was used to measure the depth of depression in the nitrogen water system. The data is shown in Table 3. The effect of the nozzle type on the depth of depression is shown in Figure 20.

A convenient way of plotting the data obtained for different liquids and different nozzle heights in the form of a single curve is to plot dimensionless depth of depression against dimensionless jet momentum. The results of present investigation have been plotted in this form in Figure 21. For the sake of comparison, the results of Chatterjee and Bradshaw<sup>25</sup> have also been plotted.

The results of Chatterjee and Bradshaw were obtained on an axisymmetric jet while the present work is for a plane jet. The different geometries could be expected to produce slightly different correlations. Banks and Bhavamai<sup>23</sup> have carried out depth of depression measurements for a plane jet, and the results of the present investigation have been compared with their results in Figure 22. The dimensionless groups used in Figure 22 are one of the many forms used by Banks and Bhavamai in plotting their results.

Table 1

Depth of depression measurements in nitrogen water system.  
Single slit nozzle.

S. No.	Pressure (cm Hg)	Rotameter reading (cm)	Volume (lit./min.)	Momentum (dynes)	Depth of depression (cm) for h					
					1 cm	2 cm	3 cm	4 cm	5 cm	8 cm
1	0.3	1.0	11.50	218.2	0.19	0.18	0.12	0.09	0.06	0.05
2	0.4	2.0	14.50	347.3	0.40	0.30	0.22	0.18	0.14	0.11
3	0.5	3.0	17.50	506.3	0.58	0.38	0.32	0.26	0.23	0.17
4	0.6	4.0	20.50	695.4	0.74	0.55	0.43	0.34	0.32	0.19
5	0.7	5.0	23.50	914.7	0.86	0.71	0.55	0.41	0.36	0.22
6	0.8	5.5	25.05	1040.3	0.91	0.77	0.65	0.45	0.36	0.25
7	1.0	6.0	26.60	1175.2	1.01	0.84	0.62	0.47	0.40	0.28
8	1.1	6.5	28.15	1317.4	1.08*	0.86	0.64	0.52	0.44	0.30
9	1.2	7.0	29.70	1467.8	1.15	0.90	0.68	0.53	0.47	0.32
10	1.3	7.5	31.25	1626.5	1.21	0.96	0.73	0.58	0.49	0.36
11	1.5	8.0	32.80	1795.2	1.28	1.04*	0.83	0.61	0.57	0.43
12	1.6	8.5	34.35	1970.7	1.37	1.15	0.93*	0.68	0.61	0.47
13	1.8	9.0	35.90	2156.5	1.46	1.20	1.03	0.76	0.68	0.52
14	1.9	9.5	37.45	2348.9	1.56	1.25	1.08	0.87*	0.73	0.56
15	2.0	10.0	39.00	2549.7	1.58	1.34	1.14	0.96	0.79	0.64
16	2.2	10.5	40.55	2761.4	-	1.38	1.23	1.04	0.86*	0.72
17	2.3	11.0	42.10	2979.3	-	1.43	1.27	1.12	0.88	0.78*
18	2.5	11.5	43.65	3208.5	-	-	-	-	0.97	0.80
19	2.7	12.0	45.20	3446.7	-	-	-	-	1.09	0.83

\* Commencement of splashing

Table 2

Depth of depression measurements in nitrogen mercury system.  
Single slit nozzle.

S. No.	Pressure (cm Hg)	Rotameter reading (cm)	Volume (lit./min.)	Momentum (dynes)	Depth (cm) for h	
					0.5 cm	2 cm
1	0.6	4.0	20.5	695.4	0.07	0.03
2	1.0	6.0	26.6	1175.2	0.12	0.06
3	1.5	8.0	32.8	1795.2	0.19	0.10
4	2.0	10.0	39.0	2549.7	0.29	0.14
5	2.7	12.0	45.2	3446.7	0.34	0.18
6	3.7	14.0	52.0	4603.1	0.39	0.21
7	4.7	16.0	59.0	5978.8	0.44	0.26
8	5.8	18.0	66.5	7669.3	0.49*	0.28
9	7.0	20.0	74.0	9596.1	0.56	0.31
10	8.6	22.0	82.0	11944.9	0.65	0.31*

\* Commencement of splashing

Table 3

Depth of depression measurements in nitrogen water system.  
Two slit, 20° nozzle.

S. No.	Pressure (cm Hg)	Rotameter reading	Volume (lit./min.)	Momentum (dynes)	Depth (cm) for h	
					1 cm	5 cm
1	2.0	2.0	14.5	704.9	0.39	0.18
2	3.6	4.0	20.5	1429.5	0.85	0.34
3	5.4	6.0	26.6	2445.6	1.14*	0.53
4	7.4	8.0	32.8	3783.5	1.46	0.76
5	9.6	10.0	39.0	5449.5	1.76	1.01*
6	11.8	12.0	45.2	7453.8	2.12	1.22
7	14.4	14.0	52.0	10073.0		1.63

\* Commencement of splashing

Table 4

Effect of experimental variables on amount and movement of the foam.

Single slit, 1mm nozzle.

S. No.	h cm	HCl (lit./min.)	N <sub>2</sub> (lit./min.)	Glycerol (% V/V)	Amount/height of foam	Movement of foam
1	1.0	2.0	78.0	50	Insufficient	not visible
2	0.5	4.0	90.0	50	Insufficient	visible
3	1.0	8.2	82.0	60	Sufficient	not visible
4	0.2	5.6	52.0	60	Insufficient	visible
5	0.2	7.0	80.0	60	Sufficient	not visible
6	0.2	6.5	90.0	60	3.9 cm	not visible
7	0.2	6.5	90.0	70	3.9 cm	not visible
8	0.2	6.5	90.0	80	3.9 cm	not visible
9	0.1	7.0	70.0	60	3.9 cm	not visible

## 5.2 Shape of the Depression Formed by Two Slit Nozzles

In the literature on BOS it has been argued that at a low angle of inclination with the vertical axis, the boundaries of the jets issuing from a multi-hole lance can intersect each other.<sup>6,85</sup> There is no reference about the shape of the depression formed by a multi-hole lance. In the model studies using two slit nozzles, it was observed that in most of the cases the two jets produced one single depression (Figures 25,27,28,29). In order to study this aspect in greater detail, nitrogen gas was blown through the two slit, 20° nozzle onto the surface of water. The nozzle height was maintained at 1 centimetre, which is equivalent to 40 nozzle diameters in an actual BOS vessel. It was observed that at low jet momentum (less than 1000 dynes) the two jets formed two separate depressions. As the jet momentum was increased further, the two depressions merged into one as shown in Plate 4. At the nozzle height of 5 centimetres, only one depression was formed by the two slit 20° nozzle throughout the entire range of jet momentums.

## 5.3 Model Study

### 5.3.1 Visual Observations

Initial experiments were performed in order to ascertain the experimental conditions under which the foaming reaction would occur and the foam movement would be visible. These experiments are summarised in Table 4. From these experiments it was established that about 7 percent hydrogen chloride gas in the gas mixture was sufficient to produce the foam. In subsequent experiments the amount of hydrogen chloride gas was fixed at 10 percent of the nitrogen gas (about 9 per cent in the gas mixture). The volume of foam was about twice the volume of the model slag. Some experiments were performed to increase the volume of the foam by increasing the amount of glycerol in the model slag (Table 4). It was observed that there was no increase in the amount of foam and precipitation of salt was accelerated. The precipitation of salt during the model blow is described below.

After about one and a half minutes of blowing the precipitation of a grey substance started. In the presence of this precipitate the model slag took on the appearance of a colloidal solution. As the blow progress-

ed the amount of precipitate increased, increasing the viscosity of the model slag. In an attempt to analyse the precipitate, the model slag was collected from a large number of experiments performed for long blowing time. The entire model slag thus collected was filtered through a filter paper. The amount of residue (precipitate) left on the filter paper was extremely small. On washing the residue with distilled water, practically nothing was left on the filter paper. A major portion of the precipitate was thus water soluble and sample of precipitate could not be obtained for chemical analysis.

Sodium chloride is white in colour, the solubility of sodium chloride in water is 25 percent at room temperature. In the presence of hydrochloric acid, the solubility of sodium chloride will be decreased. If the entire amount of sodium in the amalgam reacted during the model runs, the concentration of sodium chloride in the water of the model slag phase would be 6.68 percent. Mercury oxide is black in colour. The grey precipitate thus appears to be a combination of sodium chloride and mercury oxide.

In order to increase the amount of foam and reduce the salt precipitation, the possibility of replacing sodium in the amalgam with some other alkali metal was explored. The solubility (atomic percent) of metals in mercury and metal chlorides in water decreases with increase in atomic mass.<sup>24</sup> The idea of replacing sodium with some other alkali metal was therefore abandoned.

An examination of the foam volumes obtained by Acheson<sup>73</sup> revealed that in most of the experiments the foam volume was 2.6 times the volume of glycerol water mixture. No further efforts were therefore felt necessary to try to increase the volume of foam. In order to avoid the effect of the precipitation of salt, all the runs were filmed for about half a minute and were terminated well before the precipitation of salt.

In order to observe the movement of the foam, it was decided to increase the jet momentum without increasing the flow rate of gases by replacing the 1 millimetre wide nozzle with 0.5 millimetre wide nozzle. A starting point for fixing the flow rate and the nozzle height was obtained from the last experiment of Table 4. The flow rate was fixed at 76.6 litres/minute and the nozzle height was fixed at 0.2 centimetres. The maximum height at the flow rate of 76.6 litres/minute and the minimum flow rate at the nozzle height of 0.2 centimetres were determined by

blowing nitrogen gas on the surface of mercury covered by the model slag. The maximum nozzle height and the minimum flow rate were indicated by the splashing of metal. Any further increase in the nozzle height or decrease in the flow rate was marked by the absence of splashing. The maximum nozzle height and the minimum flow rate were further confirmed by blowing the mixture of hydrogen chloride and nitrogen gas onto the amalgam covered with the model slag. When the flow rate was 76.6 litres/minute the maximum height was observed to be 1.2 centimetres for the single slit nozzle and 0.8 centimetres for the two slit nozzle. Similarly the minimum flow rate at 0.2 centimetres nozzle height was observed to be 47.6 litres/minute.

### 5.3.2 Performance of Investigated Tracer Materials

The movement of the foam was not directly visible so various tracers were used in attempts to allow the foam stirring to be studied. The first tracer used was nitrogen gas introduced into the foam through a small bore glass tube. The nitrogen gas bubbles increased in size during their flow through the foam and produced their own movement instead of following the movement of the foam.

Potassium permanganate lost its colour through reduction almost immediately after it was introduced into the foam. Litmus solution produced a pink colour in the acid medium but this was too light to produce a visible contrast. Methyl orange produced better contrast but still not sufficiently strong to be used as a tracer for the model foam. Various organic dyes used in anodising were tried but were observed to lose most of their colour in an alkaline medium in the presence of glycerol. Since the hydrogen ion concentration varies throughout the foam in an unknown way, it was essential that the material selected as tracer should not change its colour with change in hydrogen ion concentration in the bath. Blue black Parker Quink was found to produce good contrast of colour and the colour produced was observed to be independent of hydrogen ion concentration in the foam. It was therefore chosen as the tracer material,

### 5.3.3 Different Flow Zones in the Model Foam

The movement within the foam has been studied by projecting the cine films. The colour tracer injected close to the slag metal interface and

the side and front walls moved inwards for some distance along the slag metal interface. The tracer was then lifted upwards while moving towards the centre (Plate 5a). When the tracer approached the region in which the gases travel upwards after deflection from the depression in the surface of the mercury bath, the tracer was carried upwards in the gas/foam mixture until it reached the upper surface of the foam. On the upper surface some of the tracer moved away from the centre and then downwards near the side walls of the reactor. Some was sprayed up into the gas above the foam to fall back onto the foam surface where it rejoined the general circulation of the remainder.

The movement of the tracer showed two flow zones in the model foam. The general location of the two flow zones and the directions of flow are shown in Figure 23. The lower zone is called the reverse flow zone because its direction of movement opposes the flow of the jet gases reflected upwards from the surface of the mercury bath. The upper zone is called normal flow zone because its direction of flow is the same as that of the reflected gases.

The presence of two types of flow zones was also confirmed by adding Universal pH Indicator solution prior to blowing. The two types of flow zones show different pH values as shown in Plate 5b. The pH of the normal flow zone is 5 and that of the reverse flow zone is 6. In three cases the size and shape of the reverse flow zone indicated by the universal indicator were compared with the size and shape of the reverse flow zone indicated by the injected tracer. These comparisons showed that the height of the reverse flow zone indicated by both techniques was the same but that the width of the reverse flow zone as indicated by the injected tracer was roughly 75 percent of that indicated by the universal indicator. A comparison of the two techniques is shown in Plate 5. The colour contrast produced by the injected tracer is many times greater than that produced by the universal indicator. The universal indicator method was therefore only used to show the variation of hydrogen ion concentration in the foam, detailed study of the flow patterns being carried out using the injected tracer.

The path initially followed by the tracer was marked on a large graph paper (60 cm X 40 cm) which was attached to a projector screen. The path of the tracer in the foam could not be defined precisely because of diffusion of the tracer and because of oscillations of the

foam resulting from wave motions at the metal surface. The reverse flow zone was marked as soon as it was traced by the tracer. By visual approximations, the frame showing the mean location of the path was selected for tracing. The diagrams were reduced to suitable size by photography and retraced from the photographs. With the help of these diagrams the effect of flow rate, nozzle height and nozzle type on the size and shape of the reverse flow zone are shown in Figures 24 to 29.

A schematic diagram of the stirring patterns in the model foam is shown in Figure 23. The initial path was most clearly defined as the tracer moved initially towards the jet region. The lower limit of this path marked the upper boundary of the reverse flow zone. In the neighbourhood of the jet region the tracer was carried upwards at higher velocity indicating that the foam moved upwards at fairly high velocity within the jet region. In the upper region of the normal flow zone, the colour tracer showed the flow velocity to be intermediate. The tracer was transported very slowly into the region just above its initial entry (between the reverse flow zone and the side walls) indicating that the foam in this region moved at very slow velocity.

#### 5.3.4 Time for Tracing the Path

Due to the oscillation of the foam and the diffusion of the tracer, it was not possible to observe a well defined tracer path. Measurement of the foam velocity was thus not possible. It was therefore decided to observe the time taken for the tracer to trace the entire path in the foam in those experiments in which the tracer was injected close to the nozzle. The number of frames required for the tracer to complete the loop from its initial appearance near the nozzle to its rejoining this initial path were counted by the counter attached to the projector. From the number of frames and the film speed, the time required for tracing the path was calculated. Table 5 shows the effect of nozzle height, flow rate and nozzle type on the time required for tracing the path.

The reflected jet carried the tracer from the depression to the upper surface of the foam in about 0.06 seconds (4 frames). From this data the average velocity of the foam in contact with the reflected jet can be estimated to be about 6 metres per second. Above the top surface of the foam, the tracer with the entrained foam separated from the return-

Table 5

The effect of variables on the time for path tracing and the time for total mixing of the tracer.

(a) The effect of nozzle height:

flow rate = 76.6 litres/minute

S. No.	nozzle type and nozzle height	Time for tracing the path (seconds)	Time for complete mixing (seconds)
1	Single slit, h = 0.2 cm	2.55	8.41
2	Single slit, h = 1.2 cm	1.70	4.61
3	Two slit, h = 0.2 cm	1.87	5.50
4	Two slit, h = 0.8 cm	1.53	3.91

(b) The effect of flow rate:

nozzle height = 0.2 cm

S. No.	nozzle type and nozzle height	Time for tracing the path (seconds)	Time for complete mixing (seconds)
1	Single slit, 76.6 lit./min.	2.55	8.41
2	Single slit, 47.6 lit./min.	2.73	5.23
3	Two slit 20°, 76.6 lit./min.	1.87	5.50
4	Two slit 20°, 47.6 lit./min.	1.79	4.80

(c) The effect of nozzle type:

h = 0.2 cm

flow rate 76.6 litres/minute

S. No.	nozzle type	Time for tracing the path (seconds)	Time for complete mixing (seconds)
1	Single slit	2.55	8.41
2	Two slit 20°	1.87	5.50
3	Two slit 40°	1.42	4.69
4	Two slit 60°	1.05	2.61

ing jet. From the upper surface of the foam the average distance travelled by the tracer in completing the path was estimated to be 3.5 centimetres. The average time for tracing this distance was about 1.8 seconds (Table 5). The circulating velocity in the model foam is thus estimated to be about 2 centimetres per second.

#### 5.3.5 Time for Complete Mixing

The time for tracing the principle circulation path gives some idea of the velocity in the normal flow zone but does not represent the whole bath, particularly when there are two flow zones. The portion of the bath between the reverse flow zone and the side walls mixes very slowly with the remainder of the foam. In order to get an idea about the time taken for the slag phase to homogenise in a BOS vessel, it was decided to observe the time taken for the tracer to spread through the entire foam phase. For this purpose the tracer was injected near the nozzle exit. The number of frames required for the tracer to be distributed uniformly throughout the entire foam phase was observed, thus allowing the time for total mixing to be calculated. The effects of nozzle height, flow rate and nozzle type on the time for complete mixing are shown in Table 5. The mixing of the tracer within the model foam is shown in Plates 6 and 7.

#### 5.3.6 Trajectory of the Droplets

While carrying out still photography for the purpose of standardising the conditions for cine photography it was observed that the droplets were formed from the crest of waves on the mercury surface as these travelled away from the depression. This mechanism of droplet formation is shown in Plate 8.

In the absence of the tracer, the droplets were not visible in the foam (Plate 3), the product gas surrounding the droplets making them invisible. In the presence of the tracer, however, the foam was coloured while the droplets and the surrounding product gas were unaffected by the tracer. The droplets were thus visible during the downwards part of their trajectory, especially once the tracer was uniformly mixed into the foam as a whole (Plate 9). The droplets were not visible during their upwards flight.

The paths of the falling droplets were plotted on a large graph

paper (40 cm X 60 cm) attached as before to the projector screen. The locations of individual droplets were marked frame by frame. Most of the droplets were visible for only a short section of their path. Droplets visible for relatively long distances during their descent were selected for plotting. Figures 30 and 31 show the paths of droplets through the foam. It was observed that the velocities of droplets vary a great deal during their fall through the foam. Twenty droplets from each experiment were selected for velocity measurements. Their diameter, average velocity for the entire path, maximum velocity, minimum velocity and the sequence of fast and slow velocities are shown in Tables 6 to 9. The tables also show the mean average velocity in each case. The mean velocity is nearly independent of the operating variables.

In order to study the effect of size on the falling velocity of droplets, the mean velocity of each size was calculated from the information given in Tables 6 to 9 and is shown in Table 10. The data from Table 10 has been plotted in Figure 32 together with data of Crimes et al for mercury droplets falling through water that has been cited by Richardson<sup>74</sup>. It is clear from Figure 32 that the velocity of the droplets falling through the model foam is much slower than the velocity of mercury droplets falling through water.

#### 5.3.7 Distribution of Droplets in the Foam

In order to get an idea of the distribution of droplets in the foam at any moment of time, all the droplets visible on one frame were plotted on a large sheet of graph paper (40 cm X 60 cm) attached to the screen. Droplets from six separate frames were plotted together on each sheet, the separate frames being chosen at twenty frame intervals during the run. The plotting was done in duplicate. Typical droplet distributions in the single slit nozzle and the two slit, 20° nozzle experiments are shown in Figures 33 to 35. The effect of flow rate and nozzle height on the number of droplets per frame is given in Table 11.

The droplets thus plotted were analysed statistically for their horizontal and vertical distribution. Figures 36 to 39 show the horizontal and the vertical distribution of droplets produced by the single and the two slit, 20° nozzle. The distribution looks like a normal distribution skewed towards the right hand side. Statistical means of the horizontal distance of the droplets from the jet axis and their

vertical distances above the metal/foam interface are given in Table 12.

#### 5.3.8 Size Distribution of the Droplets

The size distributions of the droplets were studied in order to see if there is any preference for smaller or larger droplets to be located near or away from the nozzle. For this purpose the diameters of the droplets plotted on the large sheets of graph paper used for studying the distribution of droplets in the foam (Section 5.3.7) were measured and classified into six size fractions. The mean diameter of droplets over a distance of 1 cm (on the large sheets) was calculated. The process of measurement was repeated until all droplets were measured. Figure 40 shows the mean diameter of droplets at different distances from the slit nozzle. It is observed from Figure 40 that the mean diameter of the droplets was independent of the distance from the nozzle. It also indicates that the size of droplets depended upon the experimental conditions. In order to study the effect of experimental variables on the size of droplets, the size distribution of droplets has been plotted in Figures 41 and 42. The mean diameter of droplets under different experimental conditions is shown in Table 13.

#### 5.3.9 Temperature Measurement

Continuous temperature measurement was carried for a limited number of runs in order to study the effect of nozzle height on the temperature of the model foam. The traces of temperature measurement are shown in Figure 43. The maximum temperature attained in each experiment is shown in Table 14.

Table 6

Analysis of droplets velocity.

h = 0.2 cm

Single slit nozzle

76.6 litres/minute

S. No.	Diameter (mm)	Velocity over the entire path. (cm/sec.)	Max. Velocity (cm/sec.)	Min. Velocity (cm/sec.)	Sequence
1	0.7	6.9	11.5	4.2	F-S-F
2	0.8	6.7	12.0	2.2	F-S-F-S-F-S-F
3	0.8	11.5	17.9	3.4	F-S-F
4	1.0	9.1	16.8	5.1	F-S
5	0.8	9.7	12.8	3.2	F-S-F
6	0.7	10.1	13.4	5.1	F-S-F
7	0.8	10.4	18.3	7.7	S-F
8	0.8	6.6	-	-	-
9	0.9	8.8	-	-	-
10	0.9	9.2	12.8	6.1	F-S
11	0.8	10.1	19.2	4.8	S-F-S-F
12	1.2	19.5	-	-	-
13	1.0	31.4	-	-	-
14	0.9	8.5	13.6	5.8	S-F
15	1.3	12.8	16.6	8.4	F-S-F
16	1.2	26.0	-	-	-
17	0.9	6.0	-	-	-
18	1.2	14.4	23.0	8.5	S-F
19	0.9	16.5	23.0	10.9	F-S-F-S
20	1.0	7.7	13.9	3.2	S-F-S-F-S

Mean velocity over the entire path = 12.1 cm/sec.

F = Fast

S = Slow

Table 7

Analysis of droplets velocity.

h = 0.2 cm      Single slit nozzle      47.6 litres/minute

S. No.	Diameter (mm)	Velocity over the entire path (cm/sec.)	Max. Velocity (cm/sec.)	Min. Velocity (cm/sec.)	Sequence
21	1.1	26.3	-	-	-
22	1.2	41.9	-	-	-
23	1.0	14.0	21.3	7.0	S-F-S
24	1.0	14.6	23.5	8.4	S-F
25	1.0	13.5	15.5	8.0	F-S
26	0.9	17.7	-	-	-
27	1.2	19.9	26.2	16.0	S-F
28	0.8	14.2	-	-	-
29	0.9	9.3	11.5	6.4	S-F
30	0.8	10.9	16.0	8.4	F-S
31	0.7	6.5	9.0	4.4	S-F
32	0.8	10.8	14.4	5.8	S-F-S-F
33	0.8	14.7	15.0	12.2	S-F
34	1.1	15.5	20.2	12.8	S-F
35	1.0	10.7	12.8	8.8	F-S-F
36	1.0	13.9	16.0	11.5	S-F
37	1.0	9.6	12.8	7.4	S-F-S
38	0.8	5.7	7.7	3.5	S-F-S-F
39	1.0	11.5	-	-	-
40	1.0	12.8	-	-	-

Mean velocity over the entire path = 14.7 cm/sec.

F = Fast      S = Slow

Table 8

Analysis of droplets velocity.

h = 1.2 cm      Single slit nozzle      76.6 litres/minute

S. No.	Diameter (mm)	Velocity over the entire path (cm/sec)	Max. Velocity (cm/sec)	Min. Velocity (cm/sec)	Sequence
41	0.7	5.0	10.4	3.8	F-S
42	0.6	3.4	4.9	2.8	F-S
43	0.6	4.1	-	-	-
44	0.9	9.7	17.5	5.6	S-F
45	1.0	32.9	-	-	-
46	0.8	12.8	16.1	10.2	F-S-F-S
47	1.0	13.3	18.3	10.7	S-F
48	1.3	30.6	-	-	-
49	1.1	9.1	10.6	7.4	S-F
50	1.0	14.8	-	-	-
51	1.2	10.3	13.0	6.7	F-S
52	1.1	13.2	-	-	-
53	1.0	10.3	15.7	7.5	S-F
54	1.2	21.6	27.3	16.6	S-F
55	1.3	30.7	-	-	-
56	1.2	23.5	27.8	19.2	S-F
57	1.0	11.8	17.3	7.4	F-S-F
58	1.0	20.6	-	-	-
59	0.8	9.8	14.4	7.0	S-F-S-F
60	1.4	16.4	23.7	9.6	S-F

Mean velocity over the entire path = 15.2 cm/sec.

F - Fast      S - Slow

Table 2

Analysis of droplets velocity.

h = 0.2 cm      Two slit 20° nozzle      76.6 litres/minute

S. No.	Diameter (mm)	Velocity over the entire path (cm/sec)	Max. Velocity (cm/sec)	Min. Velocity (cm/sec)	Sequence
61	1.0	9.8	16.9	5.8	F-S-F-S
62	0.9	9.6	14.3	5.1	S-F-S
63	1.0	24.3	-	-	-
64	1.2	19.5	25.6	13.3	S-F
65	1.0	11.7	17.3	8.6	S-F-S
66	1.1	20.3	25.3	18.6	S-F
67	0.9	21.6	25.6	20.2	F-S
68	1.2	8.5	11.5	6.4	F-S-F-S
69	1.2	29.9	-	-	-
70	0.8	20.5	-	-	-
71	1.1	12.5	14.4	9.6	F-S-F
72	0.9	7.7	-	-	-
73	0.9	9.4	-	-	-
74	0.8	13.4	23.7	6.4	F-S
75	1.0	6.3	9.6	2.7	S-F
76	1.0	21.8	-	-	-
77	1.1	12.2	15.9	8.7	F-S-F
78	0.6	10.9	13.4	8.6	F-S-F
79	0.9	7.6	10.2	6.4	S-F
80	0.9	7.4	10.2	3.7	F-S-F-S

Mean velocity over the entire path = 14.2 cm/sec.

F--Fast      S--Slow

Table 10

The effect of droplet size on their velocity of descent.

S. No.	Diameter (mm)	Mean Velocity of droplets (cm/sec.)		
		Velocity over the entire path	Maximum Velocity	Minimum Velocity
1	0.6	6.1	9.2	5.7
2	0.7	7.1	11.0	4.4
3	0.8	11.2	15.6	6.2
4	0.9	10.6	16.1	8.3
5	1.0	14.8	16.3	7.3
6	1.1	15.6	17.3	11.4
7	1.2	21.4	22.1	12.4
8	1.3	24.7	16.6	8.4
9	1.4	16.4	23.7	9.6

Table 11

The number of droplets per frame. (Averaged over 12 frames)

(a) Single slit nozzle

<u>S. No.</u>	<u>Variables</u>	<u>No. of droplets/frame</u>
1	h = 0.2 cm, 47.6 lit/min	19.2
2	h = 0.2 cm, 76.6 lit/min	30.9
3	h = 1.2 cm, 76.6 lit/min	45.7

(b) Two slit 20° nozzle

<u>S. No.</u>	<u>Variables</u>	<u>No. of droplets/frame</u>
1	h = 0.2 cm, 47.6 lit/min	16.6
2	h = 0.2 cm, 76.6 lit/min	35.9
3	h = 0.8 cm, 76.6 lit/min	34.5

Table 12

Mean of horizontal distribution ( $\bar{X}$ ) and mean of vertical distribution ( $\bar{Y}$ ) with 95 percent confidence limits.

(a) Single slit nozzle.

S. No.	Variables	$\bar{X}$			$\bar{Y}$	
		Absolute value (cm)	Fraction of half reactor width	Absolute value (cm)	Fraction of foam height	
1	$h = 0.2$ cm 47.6 lit./min.	$1.42 \pm 0.13$	$0.273 \pm 0.024$	$2.84 \pm 0.19$	$0.709 \pm 0.047$	
2	$h = 0.2$ cm 76.6 lit./min.	$1.51 \pm 0.09$	$0.290 \pm 0.017$	$2.72 \pm 0.17$	$0.685 \pm 0.042$	
3	$h = 1.2$ cm 76.6 lit./min.	$1.91 \pm 0.09$	$0.367 \pm 0.017$	$3.11 \pm 0.15$	$0.776 \pm 0.038$	

(b) Two slit nozzle

S. No.	Variables	$\bar{X}$			$\bar{Y}$	
		Absolute value (cm)	Fraction of half reactor width	Absolute value (cm)	Fraction of foam height	
1	$h = 0.2$ cm 47.6 lit./min.	$1.63 \pm 0.12$	$0.313 \pm 0.023$	$3.31 \pm 0.26$	$0.827 \pm 0.066$	
2	$h = 0.2$ cm 76.6 lit./min.	$1.56 \pm 0.08$	$0.301 \pm 0.015$	$3.11 \pm 0.14$	$0.777 \pm 0.035$	
3	$h = 0.8$ cm 76.6 lit./min.	$1.48 \pm 0.06$	$0.284 \pm 0.012$	$2.72 \pm 0.14$	$0.680 \pm 0.034$	

Table 13

Mean diameter of droplets with 95 percent confidence limits.

(a) Single slit nozzle

S. No.	Variables	Mean diameter (mm)
1	h = 0.2 cm, 47.6 lit/min.	0.761 ± 0.025
2	h = 0.2 cm, 76.6 lit/min.	0.820 ± 0.017
3	h = 1.2 cm, 76.6 lit/min.	0.746 ± 0.015

(b) Two slit 20° nozzle

S. No.	Variables	Mean diameter (mm)
1	h = 0.2 cm, 47.6 lit/min.	0.751 ± 0.024
2	0.2 cm, 76.6 lit/min.	0.836 ± 0.020
3	0.8 cm, 76.6 lit/min.	0.635 ± 0.020

Table 14

The effect of nozzle height on maximum temperature of the foam.  
Single slit nozzle 76.6 litres/minute

S. No	Nozzle Height (cm)	Temperature (°C)
1	0.2	33
2	0.8	36
3	1.2	40
4	1.6	39

6.1 Depth of Depression

Figure 18 shows that as the jet momentum is increased, the depth of depression increases. It also shows that for the same jet momentum, the depth of depression decreases with increase in the nozzle height. This is because the centre line velocity decreases with increase in the distance from the nozzle exit. For  $h = 2$  cm the curve has an unexpected concave portion for the jet momentums from about 1200 to 2500 dynes. The same effect is observed for all curves except  $h = 1$  cm. As  $h$  increases, the concavity becomes less pronounced but extends over a large range of jet momentum.

The concave portion of the curves was observed to coincide with the formation of a single standing wave on the surface of the water halfway between the depression and each side wall of the reactor. It was concluded that the concave portion of the curves was due to a resonance effect dependent on the width of the reactor, and not, therefore of general relevance. It is, moreover, likely that conditions for constructive interference would be far less favourable in a circular reactor, further reducing the significance of the concave portions of the curves observed in this work. However, Turkdogan<sup>36</sup> observed similar concavity in experiments on a circular jet which he attributed to the transition from a parallel jet to a normal expanding jet as the flow rate of the gas increased. The concavity observed by Turkdogan corresponds to a jet momentum of 114 dynes where as in the present investigation the concavity starts forming at 1000 dynes. This large difference between the jet momentums at which the concavity is observed under the two sets of experimental conditions tends to confirm that the concavity is due to the nature of the vessel rather than due to characteristics of the jet, such as the transition from a parallel to a normal expanding jet.

The effect of jet momentum on the depth of depression in the nitrogen mercury system is shown in Figure 19. The curves are similar to those for the nitrogen water system shown in Figure 18, although the concave portions are absent. This is probably because

mercury having a higher inertia due to its high specific gravity gives rise to different surface resonance characteristics in the reactor. The absence of the concave portion from the curves for the nitrogen mercury system tends to confirm that its presence in the nitrogen water system is due to surface resonance effects and not jet characteristics.

Figure 20 shows a comparison between the depth of depression measured for the two slit and the single slit nozzles. For the same jet momentum the single slit nozzle gives a much greater depth of depression. This is because its area of impact is less than that of the two slit nozzle. The weight of the liquid displaced in forming the depression in the surface is reported to vary between  $\dot{M}$  and  $1.4 \dot{M}$ ,<sup>18,19</sup>  $\dot{M}$  being the jet momentum. This means that for a given jet momentum and for a given liquid, the volume of the depression will be very nearly constant. If the width of depression increases due to an increase in the area of impact of the jet, the depth of the depression will decrease so that the volume of depression may remain unchanged.

The lower depth of depression produced by the two slit nozzle is also due to the faster rate at which the centre line velocities decay. The width of the individual slits of the two slit nozzle is half that of the single slit nozzle resulting in faster rate of decay of the absolute value of the axial velocities. Thus, for the same nozzle height and total jet momentum, the centre line velocity at the point of impact is lower for the two slit nozzle than it is for the single slit nozzle resulting in a lower depth of depression.

However, it is possible to analyse the depth of depression produced by the two slit nozzle in terms of results obtained for the single slit nozzle. The 20° two slit nozzle can be treated as a source of two independent jets, each carrying half the total jet momentum. Depth of depression measured for the two slit nozzle are replotted in Figure 44 against the momentum for each separate slit together with the data obtained for the single slit nozzle. It can be observed from this figure that the depths of depression produced by each separate jet of the two slit nozzle are almost identical to those produced by the single jets, showing that a multi jet nozzle can be analysed as so many single jets.

Figure 21 shows a comparison between the results of the present investigation and the results obtained by Chatterjee and Bradshaw.<sup>25</sup> The two sets of results show similar trend, except that the curve for the nitrogen mercury system is below that for the nitrogen water system. This is because mercury being opaque, could not be observed at the centre of the depression. Instead, the depth of the depression was observed at locations adjacent to the front face of the vessel where the depth was slightly less than at the centre due to the slight effect that the reactor walls have on the velocities in the gas jet.

The data of the present work (Figure 21) shows some kind of height dependance. The agreement with the data obtained by Chatterjee and Bradshaw is as good as could be expected when it is remembered that the present system with two dimensional symmetry is being compared with the axi-symmetrical system used by Chatterjee and Bradshaw. It has already been shown by stagnation pressure analysis (Equation 14) that for an axi-symmetrical jet the dimensionless depth of depression and the dimensionless jet momentum are related by the following equation:-

$$\frac{n_o}{h} = \frac{2 K^2}{\pi} \frac{\dot{M}}{\rho_L g h^3}$$

Using the same procedure Banks and Chandrasekhara<sup>21</sup> have derived the following equation for a two dimensional jet:-

$$\frac{\dot{M}}{\rho_L g L n_o h} = \frac{2}{K_1^2} \quad \text{-----} \quad (16)$$

Rearranging

$$\frac{n_o}{h} = \frac{K_1^2}{2} \frac{\dot{M}}{\rho_L g L h^2} \quad \text{-----} \quad (17)$$

Equation 17 is similar to equation 14 but differs in the following two respects:-

- 1 In the denominator of the dimensionless momentum one power of h is replaced by L.

2 The constant term is different.

Comparison of equation 14 and 17 explains why the results of the present investigation differ from those of Chatterjee and Bradshaw (Figure 21).

For deep cavities, substituting  $h+n_0$  for  $h$  in equation 16, rearranging and dividing both sides by  $b_0$  gives:-

$$\frac{h + n_0}{b_0} = \frac{K_1^2}{2} \frac{M}{\rho_L g n_0 b_0 L} \quad \text{--- (18)}$$

On the basis of equation 18 the present work has been compared with the data obtained by Banks and Bhavamai<sup>23</sup> in Figure 22. The figure shows that Equation 18 applies, although with considerable scatter to the present data as to the data obtained by Banks and Bhavamai. The scatter shown in the figure also tends to confirm the observation made by Banks and Bhavamai that data obtained with two-dimensional jets tends to be more scattered than that obtained with axi-symmetrical jets. This is again due to wall effect.

From the slope of the data for the nitrogen water system, the value of  $K_1$  for the present work is estimated to be 2.9. This compared well with the value of 3.17 reported by Banks and Bhavamai<sup>23</sup> for an air water system. The value of  $K_1$  obtained by other investigators, and reported by Banks and Chandrasekhara, are 2.20 (Albertson et al), 2.63 (Miller and Commings), 2.4 (Reichardt), so that the data obtained in the present work lies well within the range of data previously described.

Figures 18, 19 and 20 show clear distinction between a splashing region and a non splashing region similar to that reported in Chatterjee's work. This latter work shows that the depth of depression corresponding to the commencement of splashing, and known as the critical depth of depression, is nearly independent of the distance between tip of the nozzle and bath surface. Strictly speaking the critical depth of depression decreases slightly with an increase in the height that the tip of the nozzle is above the liquid surface. The present work is in agreement with Chatterjee's work except that the height dependance found is more pronounced and the numerical value of the critical depth of depression is considerably different. Banks and Chandrasekhara<sup>21</sup> obtained lower critical depths

of depression in their two-dimensional system than in their three-dimensional system. From the present work and that of Chatterjee and of Banks and Chandrasekhara, it appears that the critical depth of a two-dimensional depression for splashing to occur is smaller than the critical depth of a three dimensional depression. This is no doubt partly due to differences in the stabilities of the depressions due to their different geometries. However, the fact that the critical depth of the two dimensional depression is found in this work to vary more strongly with nozzle height than in Chatterjee's work suggests that the depth of depression is not the sole criteria for the onset of splashing. It is possible that the velocity field in the gas in the vicinity of the lip will also have a part to play. Once again, the velocity field would be affected by the geometry, and this is most possibly why the variation found in this work is greater than that found by Chatterjee.

However, comparison between the results for depths of depression and splashing characteristics obtained in this work for the two-dimensional jet and the results obtained in previous studies on axisymmetrical jets shows that the two types of jets behave in very similar fashion. The similarity in their behaviour is certainly sufficient to conclude that the two types of jet will play very similar roles in sustaining the foaming reactions occurring in the normal axisymmetric reactor and the two-dimensional reactor used in this work. The two types of reactor are, therefore, likely to demonstrate initially identical reaction characteristics.

## 6.2 Shape of the Depression Formed by Two Slit Nozzle

Plate 4 shows that the two depressions formed by the 20° two slit nozzle at low momentums merge into one depression at higher jet momentums. The merger of the two depressions into one depression is not due to the spread of the jet because:-

- 1 The angle of spread decreases with increasing flow rate.
- 2 If the merger of the two depressions into one were caused by the spread of the jet, the line joining the centre of the depression and the centre of the slit nozzle in plate 4b would form a rough boundary of the jet and the angle of spread would be about 40 degrees - a figure too high to be accepted.

The two depressions merge into one depression as the jet momentum is increased because the increasing jet momentum increases the amount of liquid accelerated outwards from the depression region due to the drag force of the jet gases, reducing the liquid pressure between the two jets. Turkdogan<sup>36</sup> also observed in a water bath covered by a layer of oil, that the level of water layer immediately below the depression was raised due to this reduction in pressure. This observation of Turkdogan is shown in Figure 3.

### 6.3 Studies on Reacting Model

#### 6.3.1 Flow Zones in the Model Foam

The motion of the tracer indicates that there are two distinct flow zones in the foam. Tracer injected close to the outer walls, does not move straight along the surface of the metal bath into the jet impact region but moves upwards joining the reflected jet gases at an intermediate height within the foam. The tracer is then swept upwards, some of it moving outwards along the upper surface of the foam, and some being swept into the gas space above the foam subsequently to fall back on to the upper surface of the foam. The motion of this indicator is then downwards through the foam close to the wall whence it repeats its circulation path. This flow zone, indicated in Figure 23, is termed the normal flow zone. In addition, a reverse flow zone exists below the normal flow zone. Foam in this reverse flow zone moves downwards in the centre against the jet gases and then outwards along the surface of the metal bath until it meets the inward flow of the normal flow zone. Foam in the reverse flow zone then moves upwards and back towards the jet region whence it moves downwards against the jet gases again continuing its circulation path. The motion in the two zones is indicated in Figure 23 and in Plates 6 and 7.

Universal indicator was dissolved in the foam for some runs and the resulting colour distribution is shown in Plate 5. This plate confirms the existence of the two zones and shows that the pH in the normal flow zone is about 5 whereas it is about 6 in the reverse flow zone. Thus foam in the normal flow zone is more acidic than foam in the reverse flow zone. The normal flow zone is most strongly influenced by the jet gases - acidic in the model reactor, whereas the reverse flow zone is more strongly influenced by the metal-alkali in

the model reactor due to the presence of sodium. The relative strengths of these two influences will be discussed later.

The direction of movement in the normal flow zone is in agreement with that observed by Turkdogan<sup>36</sup> and by Holdan and Hogg<sup>47</sup> obtained in oil water systems. No previous evidence has been advanced, however, for the existence of the reverse flow zone.

The reason why the two different flow zones exist can be seen from Figure 45 (a). The body of foam between the jet impact region and the outer walls of the reactor is subjected to two principal shears. In the first place, jet gases reflected upward from the jet impact zone will provide a central upward shear as shown by the central upward arrow in Figure 45 (a). The jet gas, flowing upwards and outwards within the depression in the surface of the metal bath, however will cause liquid metal to flow outwards along the surface of the bath underneath the foam. This motion will provide the outward horizontal shear indicated by the corresponding arrow shown in Figure 45 (a). In the absence of any other effects, these two shears would produce the two symmetrical flow zones as shown in the two diagonal halves of Figure 45 (a).

There are, however, two other effects. In the first place slag is continually flowing through the body of foam as shown in Figure 45 (b). This flow is produced by droplets of slag which enter the upward flowing jet gases in the central region and are then swept into the gas space above the foam. When these slag droplets fall back upon the upper surface of the foam, they produce the slow circulating flow through the foam as shown in Figure 45 (b). This flow is in the opposite sense to that in the lower of the two symmetrical flow zones shown in Figure 45 (a). It thus opposes the flow in the lower zone, particularly the upward flow against the outer wall and enhances the flow in the upper zone. The type of flow field that would result from the combination of these two flows is shown in Figure 45 (c).

However, the flow pattern shown in Figure 45 (c) does not represent the actual flow pattern that was observed. The reason for this arises from the nature of entrainment flows into freely discharging jets. The central upward shear shown in Figure 45 (a) is due to entrainment of the foam into the upward flowing jet produced

by the reflection of the jet gases from the surface of the metal bath. These gases contain a high density of suspended liquid drops and it is not possible to draw a precise boundary between the foam and the jet gases. Thus the central upward shear is due to entrainment into a freely discharging jet within a continuous two phase region. The two phases are the slag or model slag and the gases from the jet and the refining reaction.

The entrainment behaviour of supersonic jets is significantly different from that of subsonic jets. Thus it is necessary to determine the velocity of sound in the foaming slag in order to understand the nature of the entrainment process that gives rise to the central upward shear shown in Figures 45 (a) and 45 (c).

The velocity of sound in any medium is that of a weak pressure wave. By carrying out a momentum balance on a weak pressure wave front, the velocity can be determined as:-

$$c = \sqrt{\frac{dp}{d\rho}} \quad \text{—————} \quad (19)$$

For any medium, this expression can be related to the compressibility and density of the medium. If we define the compressibility as:-

$$\beta = \frac{1}{v} \frac{dv}{dp} \quad \text{—————} \quad (20)$$

equation 19 becomes

$$c = \sqrt{\frac{-1}{\rho\beta}} \quad \text{—————} \quad (21)$$

The compressibility of a foam is that of the gas that it contains so that, for the foam

$$\beta_f = \frac{-1}{\gamma P} \quad \text{—————} \quad (22)$$

and we can write

$$c_f = \sqrt{\frac{\gamma P}{\rho_f}} \quad \text{—————} \quad (23)$$

The glycerol water mixture has a density of 1.17 grams per cm<sup>3</sup> and the model slag normally expands to twice its original volume, so that  $\rho_f = 0.505$  gram per cm<sup>3</sup> which with P = 1 atmosphere gives:

$$c_f = 15.4 \text{ metres per second} \quad \text{—————} \quad (24)$$

The calculated velocity of the gases leaving the actual nozzle varies between 79 to 128 metres per second, but the gas jet that stirs the foam is provided by the gases reflected from the surface of the metal bath. Some idea of the velocity of these gases can be obtained by considering that they behave as if they originated from an imaginary nozzle pointing upwards and immersed in the metal bath, the momentum flow through this imaginary nozzle being equal to the momentum reflected back from the surface of the metal bath. The weight of the liquid displaced by the jet gases has been reported to vary between  $\dot{M}$  and  $1.4 \dot{M}$ <sup>17 - 19</sup>, so that the momentum flow of the reflected jet gases will vary from zero to some 40 percent of the momentum flow through the actual jet. Remembering that the momentum flow is proportional to the square of the fluid velocity and taking an intermediate value for the reflected momentum suggests that the reflected gases will behave as if they left the imaginary nozzle at velocities between 35 and 60 metres per second. Thus, as far as stirring the foam is concerned, the jet gases will behave as if they come from a supersonic jet.

The rate of entrainment into supersonic jets is much slower than into subsonic jets.<sup>5</sup> Close to the nozzle where the central jet gases are still flowing at supersonic speeds, and are thus surrounded by a field of shock waves, the rate of entrainment is effectively zero and the jet is hardly interacting with its surroundings at all. Thus when the reflected jet gases first enter the foam, they will have very little effect on the foam, being effectively surrounded by a system of shock waves in the foam. It is not until they have slowed down sufficiently to be subsonic within the foam that they will start to exert a stirring effect on the foam. This is indicated by the shaded barrier in Figure 45 (d) to show that vertical upwards shear is only exerted on the upper part of the foam body.

Thus the lower reverse flow zone shown in Figure 45 (c) can expand in the central region allowing the foam to flow vertically downwards in the centre opposing the upward flow of jet gases, but protected from this upward flow by the system of shock waves that surrounds the jet gases. The dominating effect on the foam in the reverse flow zone is thus that provided by the liquid metal bath. The velocities in the liquid metal bath are, of course, much lower than

those in the jet region and will be subsonic from the outset. No impediment will thus exist to the transfer of momentum, or indeed mass, from the liquid metal bath to the slag in the reversal flow zone. That this is so is born out by the distribution of pH shown in Plate 5 indicating that the chemical conditions in the reverse flow zone are closer to those in the liquid bath than they are to conditions in the jet region. On the other hand, chemical conditions in the normal flow region are closer to those in the jet region, as would be expected from the jet/foam interaction which produces the normal flow region.

Kluth and Maatsch<sup>86</sup> seem to be the only previous authors who have studied the effect of gas jets on foaming liquids. They observed that the amount of liquid entering the jet is negligible when the tip of the nozzle is above the surface of the foam but when the tip of the nozzle is inside the foam, large amount of liquid enters the jet. From this observation they suggested that, when the tip of the nozzle is above the foam, the foam moves away from the centre on its upper surface and downwards along the side walls. This is the direction of flow observed in the normal flow zone in this work, but when the nozzle is inside the foam, Kluth and Maatsch suggest that the flow direction is reversed. It is difficult to see how this could be so because of the influence of the jet gases reflected from the surface of the metal bath, a factor that Kluth and Maatsch do not appear to have considered. The foam cannot cross the reflected gases moving upwards and then be accelerated downwards by the central jet moving downwards and transfer this downward motion to the bulk of the foam body outside the jet region. It is possible that a small amount of foam is caught between the jet moving downwards and the reflected jet moving upwards but the movement in the body of foam between the central jet region and the vessel wall must be dominated by the influence of the reflected jet. Kluth and Maatsch used a single liquid system instead of a two liquid system and maintained their foam by passing a stream of gas bubbles through the bottom of their vessel. In these circumstances, it is most likely that the dominating effect that the reflected jet of gases has in the actual reacting system was not reproduced in the apparatus studied by Kluth and Maatsch.

The effect of experimental variables on the size and shape of the reverse flow zone is shown in Figures 24 to 29. There are only two flow zones in the foam so that the sizes of the normal and reverse flow zones do not require separate discussion, the normal flow zone occupying that part of the foam body that is not occupied by the reverse flow zone. It can also be observed from the Figures that the width of the reverse flow zone is practically constant. Thus the variations in the stirring patterns in the foam that are produced by variations in the operating variables can be fully described in terms of variations in the height of the reverse flow zone.

Figures 24 and 25 show that, as the flow rate of gases is decreased the height of the reverse flow zone is decreased. Figures 26 and 27 show that the height of the reverse flow zone is decreased with the increase in the nozzle height. Figure 28 shows that the height of the reverse flow zone is decreased when the single slit nozzle is replaced with the two slit nozzle. The height of the reverse flow zone is further decreased as the angle of inclination of the two slit nozzle is increased as shown in Figures 28 and 29. As an overall generalisation, then, it can be said that the height of the reverse flow zone decreases as the intensity of blowing is decreased.

The changes in the height of the reverse flow zone with these operating variables can be explained in terms of the different components that influence the flow pattern in the foam and are illustrated in Figure 45. In the first place, and simplest, Figure 45 (e) illustrates the way in which the angle of inclination of the two slit nozzle affects the height of the reverse flow zone. As the angle is increased, the direction at which the reflected jet gases leave the impact zone will become less and less vertical. In the schematic diagrams shown in Figure 45, this means that the central upward shear will become increasingly rotated in an anti-clockwise direction. As the Figure shows, this will tend to rotate the flow pattern decreasing the space occupied by the reverse flow zone, and increasing the space occupied by the normal flow zone. Thus the height of the reverse flow zone must be decreased as the angle between the two jets produced by the two slit nozzle is increased. The effect of nozzle height and gas flow rate on the height of the reverse flow zone can be explained in

terms of the length of the supersonic core of a supersonic jet. If we assume that the reflected jet gases behave as if they originated from the imaginary nozzle discussed in Section 6.3.1. we are picturing the behaviour of these gases in terms of the schematic diagram shown in Figure 46. The gases from the nozzle are reflected by the depression although not all the gases will travel to the bottom of the depression. On average, then, it is possible to imagine that the effective plane about which the jet is reflected is half the depth of the depression below the free surface of the liquid. Thus the imaginary nozzle will be at a distance  $h + n_0$  below the liquid surface (Figure 46). The analysis of the flow patterns in the foam presented in Section 4.3.1 would then suggest that the line of demarcation between the normal and reverse flow zones also marks the end of the supersonic core of the jet discharging from the imaginary nozzle. Anderson and Johns<sup>12</sup> have presented data to show how the length of the supersonic core of a supersonic jet varies with its Mach number. For Mach numbers greater than 1, their data falls on the following straight line relationship:-

$$\frac{L}{d_e} = 21.4 M - 31.4 \quad \text{--- (25)}$$

The Mach number of the imaginary jet can be calculated from the velocity of sound in the foam and the velocity with which the gases would have to leave the imaginary nozzle in order to provide an upward momentum flow equal to that provided by the actual reflected gases. Table 15 shows values of the Mach number calculated taking an intermediate value of 0.2 for the momentum reflection factor and the length of supersonic core calculated using equation 25 and the fact that the nozzle width is 0.5 mm. This length can then be compared with the distance from the imaginary nozzle to the top of the reverse flow zone. In making this comparison, however, it must be remembered that for much of the path from the imaginary nozzle to the end of the reverse flow zone the jet gases are not travelling within the foam. In so far as the path length from the imaginary nozzle to the surface of reflection mirrors the gas path within the central jet region, it takes place within the pure gas phase. Analysis of momentum transfer in freely discharging jet of any given fluid, shows that distance from the nozzle to the point at which the centre line velocity has decayed

to a given fraction of the nozzle velocity is inversely proportional to the square root of the density of the surrounding medium. Thus, as far as the decay of the jet velocity in the foam is concerned, the imaginary distance travelled between the imaginary nozzle and the surface of the liquid metal bath is much less effective than the distance travelled within the foam. If  $H_r$  is the height of the reverse flow zone above the surface of the liquid metal, the effective foam distance between the imaginary nozzle and the top of the reverse flow zone,  $L_r$ , is:-

$$L_r = (h + n_o) \sqrt{\frac{\rho_{air}}{\rho_{foam}}} + H_r \quad (26)$$

Table 15 shows values of  $H_r$  taken from Figures 24 to 29 for three sets of typical experimental conditions. It also shows values of  $n_o$  taken from Figure 24 for the first two cases and estimated from Figure 19 for the third case. The final column shows values of  $L_r$  calculated following equation 25. It can be seen that fairly good agreement is achieved for the first two cases between  $L_r$  and the length of the supersonic core of the imaginary jet,  $L_{sup}$ , tending to confirm the flow model discussed in Section 6.3.1.

The agreement achieved for the third case, when the nozzle height is 1.2 cm, is less good, at least when the momentum reflection factor is taken as 0.2. However, as the nozzle is raised, the depression in the surface of the liquid metal becomes flatter, suggesting that less of the momentum is reflected vertically upwards which would give rise to a lower value for the momentum reflection factor. If we assume this factor to be 0.15, the value of the imaginary Mach number becomes less and  $L_{sup}$  becomes 1.5, a value much closer to the calculated value for  $L_r$ .

Thus Table 15 shows that the size, as well as the shape and existence of the reverse flow zone can be explained in terms of the assumption that the jet gases reflected from the metal bath behave in the foam as if they were a freely discharging supersonic jet within the foam.

### 6.3.3 Time for Tracing the Path

Oscillations within the foam body produced by wave motions on the mercury surface meant that the tracer front moved somewhat erratically

Table 15

Calculation of down stream distance from the imaginary nozzle to the boundary between the two flow zones and comparison with the length of the supersonic core predicted from the results of Anderson and Johns.<sup>12</sup>

$h$ (cm)	gas flow (lit/ min)	$M$ (act.)	$r_f$	$M$ (imag.)	$L_{so}$ (cm.)	$\gamma_0$ (cm)	$H_y$ (cm)	$L_y$ (cm)
0.2	76.6	7.5	0.2	3.5	2.2	1.6	2	2.1
0.2	47.6	5	0.2	2.2	0.8	0.9	1	1.1
1.2	76.6	7.5	0.2	3.5	2.2	0.5(e)	1.3	1.4
1.2	76.6	7.5	0.15	2.4	1.5	0.5(e)	1.3	1.4

through the foam immediately after its injection. Thus the distance moved between frames in the movie films could not be used to determine local values of the velocity within the foam. Instead, it was decided to determine the time taken for the tracer front to trace the circular path from its point of injection, round through the foam and back again to its point of injection. This time gives an indication both of a mean value of local velocities within the foam and more importantly the speed with which the foam body as a whole is mixed by the stirring patterns produced by the jet.

Table 5 shows that the time for tracing the path decreases with an increase in the nozzle height for the single slit nozzle, but is nearly independent of the flow rate of gases through the nozzle.

This behaviour can be explained in terms of the analysis of the flow patterns presented in the previous section. The first two values in Table 15 show that, for any fixed nozzle height, the height of the reverse flow zone decreases as the flow rate is decreased, this decrease being due to the reduction in the length of the supersonic core that occurs as the Mach number of the imaginary jet is decreased. Thus, when the flow rate is reduced, the central vertical shear that gives rise to the circular motion in the normal flow zone is applied over a greater length. Thus, although the magnitude of the shear force is likely to be decreased due to the lower flow rate of gases, it will be applied to the foam body over a greater area. As far as the velocity with which the foam body circulates in the upper flow zone is concerned, then, these two effects will tend to compensate one for the other so that the velocity with which the foam circulates within the normal flow zone would tend to be independent of the flow rate of gases through the jet.

The reduction in the height of the reverse flow zone has very little effect on the total size of the reverse flow zone so that it is velocities within the normal flow zone that principally determine the time that it takes for the tracer to trace its path in the normal flow zone. Since these velocities, as discussed above, will tend to be independent of the flow rate of gases through the nozzle, we would expect the time for the tracer to trace its path in the foam to be independent of this flow rate also. As stated above, this is the effect that has been observed.

The effect of nozzle height can also be explained in terms of the flow pattern analysis. Increasing the nozzle height also reduces the height of the reverse flow zone, and thus increases the height over which the foam body is exposed to the central vertical shear that produces the recirculation in the normal flow zone. In this case, however, there is little or no reduction in the gas velocities so that the increased exposure to the central shear will tend to increase the velocities in the normal flow zone and thus reduce the time taken to trace the path - as has, in fact, been observed.

Table 5 also shows that the time for the tracer to trace its path in the foam decreases when the single slit nozzle is replaced by a two slit nozzle, or when the angle between the two slits is increased. As discussed in the previous section, these changes also reduced the height of the reverse flow zone and will thus increase velocities induced by shear in the reverse flow zone. In addition, however, it is likely that these changes will bring an increasing horizontal component to the shear force which will further increase velocities in the normal flow zone. Both these factors will tend to decrease the time taken for the tracer to trace its path, but Figures 28 and 29 indicate a further effect that may be relevant. As the single slit nozzle is replaced by the two slit nozzle, the central impact area is increased, thus tending to decrease the overall volume of the foam body, and further reducing the time that it takes the tracer to trace its path within the foam.

#### 6.3.4 Time for Complete Mixing

Table 5 shows that the time for the complete mixing of the foam decreases with an increase in the nozzle height and with a decrease in the flow rate of gases.

Since the time for the complete mixing of the foam depends upon the velocities with which the foam is stirred, we would expect the time for the complete mixing of the foam to be closely related to the time for the foam to trace its path. Thus the relationship that has been observed between the time for complete mixing and the nozzle height is totally consistent with the explanation advanced in Section 6.3.3 for the effect of nozzle height on the time for the tracer to trace its path.

However, the relationship between the time for complete mixing and the gas flow rate requires some further analysis. In fact, the time for complete mixing of the foam is not wholly determined by mixing velocities in the normal flow zone since the portion of the foam within the normal flow zone between the reverse flow zone and the side walls is very slow to mix - it is held back by the reverse flow zone (Plate 7). Thus, when the size of the reverse flow zone is decreased by a reduction in the gas velocity, the foam body can be mixed more rapidly because a greater proportion of it encompassed by the normal flow zone and because the dead portion of the normal flow zone between the reverse flow zone and the side walls is decreased in size. Thus, although recirculation times in the normal flow zone are unaffected by changes in the gas flow rate, the time for the complete mixing of the foam is decreased as the gas velocity is decreased. Table 5 also shows that the time for the complete mixing of the foam decreases when the single slit nozzle is replaced by the two slit nozzle, or when the angle of the two slit nozzle is increased. Once again, these observations are completely in keeping with the effects discussed in the previous section, that these changes have on stirring velocities in the normal flow zone.

#### 6.3.5 Trejectory of the Droplets

In the absence of a second liquid, droplets of metal are torn from the surface wave on the surface of the mercury as it travels away from the depression. This mechanism of droplet formation, observed while blowing nitrogen on the surface of mercury, is shown in Plate 8. It is in keeping with observations made by Davenport et al<sup>13</sup> who believe that the droplets are torn from the tip of the ripples. Chatterjee and Bradshaw<sup>16,25</sup> and Hammer and Kootz<sup>48</sup>, on the other hand, have reported that the droplets are torn from the lip of the depression. In the present investigation, when the sodium amalgam was blown with the nitrogen hydrogen chloride gas mixture using the glycerol water mixture as the model slag, it was observed that the droplets were torn from the depression. It appears that the model slag acts as cushion for the formation of droplets from the wave as it travels from the depression. In the neighbourhood of the depression, this cushion effect is absent and the droplets are torn from the lip of the depression to be accelerated by the jet gases reflected from the bath

surface.

Hammer and Kootz<sup>48</sup> in a model study observed that the droplets fall back into the bath following a parabolic path. Figures 30 and 31 of the present investigation show that the path of the falling droplets is not parabolic in shape. A parabolic path is to be expected when the droplets are falling under the influence of gravity alone. In the present investigation the path of the falling droplets is influenced by the presence and movement of the foam and by the cloud of product gas bubbles attached to droplet.

Initially the droplets descend vertically. Near the surface level of the foam, the droplets tend to move away from the centre of the reactor because, at this level, the foam separates from the gases and moves away from the central region. The change in the direction of the droplets is more pronounced the nearer they are to the nozzle because the amount of foam influencing the trajectory of the falling droplets, decreases with increasing horizontal distance from the nozzle. In the lower regions of the normal flow zone, the droplets tend to move towards the nozzle again because the foam in this region is flowing towards the nozzle.

Measured velocities of droplets falling through the foam are shown in Tables 6 to 9. There are large variations in velocities from droplet to droplet and also for the same droplet from time to time. These variations are due to changes in the amount of gas attached to the droplets and to variations in the local velocities in the foam. The mean velocity of twenty droplets studied under any given set of experimental conditions remains practically unchanged as changes are made in the operating variables. The mean velocity given in Table 6 might seem low when compared to those given in Tables 7 to 9 but a careful examination shows that, for the group as a whole, the droplets in Table 6 are of smaller size than the droplets in the other three tables.

Figure 32 shows that the velocity of droplets falling through the foam increases with an increase in their size. The velocity is much less than the velocity observed by Crimes et al, published by Richardson<sup>74</sup>, in spite of the fact that the density of the model foam is significantly less (0.6) than the density of the medium (water) used by Crimes et al in their work. Davies et al<sup>57</sup> observed that the

velocity of iron carbon droplets falling through steelmaking foams depends upon the degree of gas evolution, the evolved gases attaching themselves to the droplets and thus exerting a buoyancy force.

Kozakevitch<sup>57</sup> believes that this buoyancy force is produced by carbon monoxide bubbles when they adhere to the surface of the iron droplets.

#### 6.3.6 Number of Droplets in the Foam

Table 11 shows the effect of the operating variables on the number of droplets in the foam. As the flow rate is decreased, the number of droplets decreases. This observation is in agreement with the results of Chadialle and Harvais<sup>30</sup>, and Chatterjee and Bradshaw<sup>25</sup> obtained by blowing gas over a water bath. Table 11 shows that in the single slit nozzle experiments the number of droplets decreases with the decrease in the nozzle height. This observation is in agreement with the results of an investigation at the Swindon Laboratories<sup>31,32</sup>. Chadialle and Harvais<sup>30</sup>, and Chatterjee and Bradshaw<sup>25</sup> observed that with the decrease in the nozzle height, the amount of liquid splashed first increases, reaches a maximum level and then decreases. The present investigation does not show the variation in the number of droplets over the entire range of the nozzle height. It appears that the nozzle height of 0.2 cm is too low, splashing small number of droplets. Molloy<sup>33</sup> has described that when the nozzle height is too low, a part of the splashed liquid, entrained by the jet is fed back to the depression, resulting in a decrease in the amount of liquid splashed out of the depression.

For the two slit nozzle it appears from Table 11 that the number of droplets is nearly constant with variation in the nozzle height. This is in agreement with the investigation carried out at the Swindon Laboratories<sup>31,32</sup>. This is the only investigation reported in the literature on the splashing of liquid by multi hole lance.

The higher nozzle heights given in Table 11 are the highest possible values that can be investigated. As the nozzle height is increased further, the splashing practically stops very suddenly.

#### 6.3.7 Distribution of Droplets in the Foam

The distribution of droplets with horizontal distance from the nozzle centre is shown in Figures 36 and 37. The shapes of the curves are closely similar to those obtained by Chatterjee and Bradshaw<sup>25</sup>. For the single slit nozzle, with the increase in the nozzle height, the

location of the droplets shifts away from the nozzle axis (Figure 36 and Table 12). This observation is in agreement with the results obtained by Chatterjee and Bradshaw<sup>25</sup>. The effect of flow rate on the horizontal distribution of droplets for the single slit nozzle is not significant (Figure 36 and Table 12). This also agrees with the results of Chatterjee and Bradshaw<sup>25</sup> on the amount of liquid splashed from the jet impact region.

Chatterjee and Bradshaw<sup>25</sup> think that, with an increase in the nozzle height, the location of the droplets moves outwards away from the depression due to change in its shape. They have also shown that the gas flow rate has very small effect on the shape of the depression. Thus we would expect the horizontal distribution of droplets to be very nearly independent of the flow rate of gas.

For the two slit nozzle the effect of experimental variables on the horizontal distribution of droplets is not significant (Figure 37 and Table 12). The effect of nozzle height and flow rate on the shape of the depression formed by the two slit nozzle has not been studied so far. It appears from Figures 25 and 27 that the shape of the depression formed by the two slit nozzle is nearly independent of the nozzle height and the flow rate of gases. If this is so, it would explain why these variables appear to have no effect on the horizontal distribution of droplets.

Figures 38 and 39 show the vertical distribution of droplets. The shape of the curves is similar to the shape of the curves for the horizontal distribution. It was observed during analysing the films that all the droplets do not attain the same height, but that the maximum heights of their trajectories are distributed randomly.

The effect of flow rate on the vertical distribution of the droplets is insignificant both for the single slit and for the two slit 20° nozzle (Table 12). For the single slit nozzle, the mean height of the droplets above the bath level increases with increasing nozzle height whereas, for the two slit nozzle, the mean height of the droplets decreases with the increase in the nozzle height. No explanation can be advanced for these effects.

#### 6.3.8 The Size Distribution of Droplets

Figure 40 shows that the mean diameter of the droplets is nearly the same at any distance from the nozzle. There is no preference for

larger droplets to be confined to regions near the slit nozzle.

Figure 41 and 42 show respectively the size distribution of droplets in the single slit nozzle experiments and in the two slit 20° nozzle experiments. The mean diameter of droplets is given in Table 13. It is seen from Figures 41 and 42, and Table 13 that, for the single slit as well as the two slit 20° nozzle, the mean size of the droplets decreases with an increase in the nozzle height or a decrease in the flow rate. It appears that the shear force trying to break the liquid, decreases with an increase in the nozzle height and with a decrease in the flow rate. This reduced shear forces is not sufficient to break droplets of larger size away from the mercury surface.

#### 6.3.9 Temperature Measurement

Figure 43 shows that the foam temperature increases with time for about 1.25 minutes and then starts decreasing. This time corresponds to the precipitation of salt already discussed in Section 5.3.1. The fall in temperature indicates that the rate of sodium removal has retarded due to the precipitation of sodium chloride.

Table 14 shows the effect of nozzle height on the maximum temperature of foam. It is observed from Table 14 that the foam attains highest temperature when the nozzle height is 1.2 cm. This corresponds to good circulation of bath and the maximum number of droplets (Table 5 and 11).

The heat generated due to chemical reaction is transferred to the cooling water surrounding the reactor, the out going gases and the foam. The temperature rise in the initial stage corresponds to unsteady state heat transfer. Before a steady state is reached, at least for appreciable length of time, the precipitation of salt starts. Thus it is not possible to lay much emphasis on the temperature measurement.

### 6.4 Application to Basic Oxygen Steelmaking

#### 6.4.1 Flow Patterns in the Foaming Steelmaking Slags

No attempt has been made in this work to construct a model reactor that is similar in the formal sense to a top blown basic oxygen converter. Such an attempt would require either knowledge of the crucial physical and chemical phenomena that are important in such converters, or it would involve so many dimensional groups that complete similarity could not be achieved. In fact, this work has attempted to construct a reaction system that is likely to behave in the same way as the top blown converter in order to ascertain the type

of physical and chemical phenomena that are likely to be crucial to the operation of such converters. This step is one that must necessarily proceed the selection of a sufficiently restricted number of similarity criteria that a subsequent attempt could be made to construct a model that would be similar in a formal sense.

The work previously published by Acheson and Hills<sup>76</sup> has shown that an axi-symmetric model involving the reaction between sodium amalgam and an acidified water glycerol model slag has the same operating characteristics, when jetted with nitrogen hydrogen chloride gas mixtures, as a top blown oxygen steel making vessel. The present study has shown that two dimensional systems involving gas jets and liquids behave in the same way as axi-symmetric systems, so that it is virtually certain that the reaction system studied in this work will be very similar to that which exists in top blown converters.

The work of Flinn et al<sup>15</sup> has shown that the circulation patterns that exist in the metal bath in top blown steel making vessels involve the motion of molten metal outwards from the jet impact region immediately below the slag phase. Thus the horizontal shear, shown in Figure 45 (a), that produces the reverse flow zone in the slice reactor will certainly also exist in top blown steel making vessels.

The densities of steelmaking slags are about  $3 \text{ g cm}^{-3}$  and they expand some 5 or 6 times due to the foaming reaction that occurs during oxygen steel making. Thus the velocity of sound in these slag foams will be about 17.5 metres per second, whereas the velocity with which oxygen leaves a lance operating with an oxygen Mach number of 2 will be about 700 metres per second. Although a somewhat different reaction occurs between the metal and the jet gas, it is apparent that the upward jet produced by the reflected momentum of the oxygen gas will be supersonic as far as the foaming slag is concerned in the same way as the reflected gas jet in the slice reactor.

Thus the foaming slag close to the impact zone of the oxygen jet is likely to be protected by a similar shock wave system as the water glycerol foam is in the slice reactor. Unfortunately, it is not possible to estimate the likely extent of this shock system because the reflection factor for the jet momentum is not known in BOS. Neither is it possible to estimate the effect that the oxygen iron reaction

will have on the effective Mach number of the reflected jet. It is likely, however, that the effective foam Mach number will be somewhat larger in the BOS slag than it is in the slag foam in the slice reactor so that the structure of the reverse and normal flow zones that has been observed in the slice reactor will also exist in BOS vessel.

#### 6.4.2 The Reaction System

The type of reaction system that this work suggests might exist in BOS can be seen if the droplet distributions shown in Figures 33 to 35 are to be superimposed on the flow pattern model shown in Figure 23. Thus the principal region in which the metal droplets can react with the slag exists within the normal flow zone fairly close to the central jet region itself. The slag foam is moving radially through this region prior to being entrained upward in the reflected jet. The droplet paths determined in this work, and illustrated in Figures 30 and 31, show that the metal droplets move vertically downwards through this central reaction region so that a type of cross flow reactor is formed. This cross flow reaction region is illustrated in Figure 47.

The reaction that is occurring within this region is that between the metal drops and the slag, but this is only part of the reaction system. The other part of the reaction system involves the reaction between the jet and the slag and this occurs partly in the central impact zone, but principally in the region above the reverse flow zone where the normal flow zone interacts with the reflected jet gases. Indeed the analogy that exists between momentum and mass transfer suggests that the rate of entrainment, as evidenced by mean velocities induced in the normal flow zone, is a good measure of the rate of the slag/gas reaction.

The overall characteristic of the refining reactions in either the model or the actual BOS can thus be seen as a balance between these two reaction regions. Oxygen, or hydrogen chloride gas, is picked up by the slag foam where it reacts with the jet gases and is then removed from the slag foam by reaction with the metal droplets that are falling through the cross flow reaction region. In the steady state, of course, these two reaction rates must balance so that the concentration of the reactant species in the slag foam will remain constant. However, changes in the operating variables that affect the

kinetics of either reaction will cause changes in the steady state concentration of the reactant species. After any such change, of course, the concentration will tend to move towards its new steady state value, and it is this that constitutes the principle means for controlling the reactions.

If we consider the cross flow reaction region illustrated schematically in figure 47 we can see that the rate of the reaction between the metal and the slag will depend upon the total surface area of the metal droplets within the region and to a lesser extent, upon the mass flow rate of the slag and the metal flow through the region. Thus the extent of the cross flow region will play an important part in determining the rate of the slag metal reaction.

The reactant species is supplied to the slag foam where the latter is entrained into the reflected jet gases. The reactant species is then carried around the circular path in the normal flow zone to be supplied to the cross flow reaction region by the foam moving radially towards the centre of the reactor. The experiments in which universal indicator was injected into the foam have shown that chemical conditions in the reverse flow zone differ from those in the normal flow zone, being much closer to equilibrium with the metal phase than to the jet gases. This shows that the reactant species is transferred fairly slowly from the normal flow zone to the reverse flow zone and we would expect the rate of the slag metal reaction to be significantly slower in the reverse flow zone than in the normal flow zone. Thus the extent of the cross flow region will be closely related to the extent of the normal flow zone. Changes in operating variables that increase the extent of the reverse flow zone will obviously reduce the size of the cross flow reaction region and will thus reduce the slag metal reaction rate.

Thus we would expect that the rate of the slag metal reaction to increase with the number of metal droplets in the slag foam and with the mean size of these droplets, but to decrease with the height of the reverse flow zone. We would also expect the reaction rate to increase with the rate of circulation of slag foam in the normal flow zone, although this effect would be less marked. Furthermore, as we have already stated, we would expect the rate of entrainment of foam into the gas, and hence recirculation rates in

the foam, to give a very good indication of the rate of the gas foam reaction. Thus the observations made in this work can provide an explanation for the effect of changes in the operating conditions in BOS vessels.

The principal changes that can be made are changes in lance height and in gas flow rate. As section 6.32 has shown, an increase in the gas flow rate increases the height of the reverse flow zone and will thus decrease the extent of the cross flow reaction region. However, Figures 36 and 38 show that the number of droplets increases as the gas flow rate increases and Figure 40 shows that the mean radius of the droplets is more or less independent of gas flow rate. Thus the rate of the metal slag reaction in the normal flow zone will be affected relatively little by changes in the gas flow rate as long as the gas flow rate remains sufficient to maintain the splashing of metal droplets from the depression. In fact, since the more significant trend appears to be provided by the number of droplets. We would expect a slight increase to occur in the rate of the metal slag reaction as the gas flow rate is increased.

While discussing the time for the tracer to follow its path around within the normal flow zone, we showed that the entrainment of foam into the reflected jet gases tended to be independent of the gas flow rate. Thus we would expect the rate of the gas foam reaction to be more or less independent of the gas flow rate.

Inceases in the gas flow rate, then, slightly increase the rate of the foam metal reaction but do not affect the rate of the gas foam reaction. Thus, by considering the overall balance of reacting species within the foaming slag as a whole, we can see that an increase in the gas flow rate would tend to lead to a decrease in the concentration of the reacting species, although the effect would be small.

As the lance, or nozzle, height is increased, the height of the reverse flow zone decreases so that the extent of the cross flow reaction region will be increased. Figure 36 and 38 show that the number of droplets increases as the nozzle height is increased although the effect is not as great as it is with gas flow rate. Figure 40 shows that mean radius of droplets formed by the single slit nozzle

is more or less independent of lance height. Thus we would expect the rate of the metal slag reaction to increase with lance height although not very rapidly.

As was discussed in Section 6.3.3, the rate of entrainment from the reflected jet gases into the foam increases with the lance height, so we would expect the rate of the slag gas reaction to increase also. Thus we would expect that an increase in lance height would give a slow increase in the concentration of reactant species in the slag foam.

However, the range of lance heights that has been used in this work is not very great, owing to the necessity of sustaining the supply of splashed metal droplets in order to maintain the foaming reaction. As discussed in section 6.3.6, many workers have shown that number of droplets first increases as the lance height is increased, then passes through a maximum before decreasing fairly rapidly.

It is apparent that experiments have not been conducted in this work over the range of nozzle heights where the number of droplets is decreasing with the nozzle height. Once this range of nozzle heights has been reached, however the metal slag reaction rate will start to fall very rapidly as the nozzle height is further increased giving rise to a rapid rise in the concentration of the reactant species in the slag foam. However, whilst BOS converter is being operated at the lance height that corresponds to the splashing of the maximum number of droplets, the oxygen concentration in the slag can be increased by increasing the lance height.

The dissolution of lime sometimes causes problems in BOS vessels. The lime, either injected or added in powder or lump form, will find its way to the relatively quiescent reverse flow zone, and will dissolve fairly slowly there, more slowly than in the bulk of the slag. Another location of slow dissolution of lime is the portion of normal flow zone between the reverse flow zone and the vessel wall. It has been observed on experimental vessel that lime tends to solidify in this region.<sup>72</sup>

Multi hole lances give higher production rates than single hole lances. This increase has been explained on the basis of a higher

rate of oxygen input and greater area of contact between the bath and the jet.<sup>55</sup> Neither of these is really valid explanation. It is apparent that the BOS vessel can absorb all the oxygen that is blown into it, the only question being the space that is available. As Acheson and Hills<sup>73,76</sup> have shown, the main impediment to the reaction is the escape of the product gas, so that the main factors that determine the rate of operation of any one vessel are those that influence the effectiveness with which reaction space is used within the vessel. Examination of Figures 24 to 29 shows that the reverse flow zone is much smaller when the two slit nozzle is used than it is when the single slit nozzle is used. Thus the normal flow zone, and hence the cross flow reaction region, will occupy a larger proportion of the height of the foam when the two slit nozzle is used. Thus the metal slag reaction rate will be higher for the two slit nozzle because the space occupied by the slag foam is being used more effectively.

As discussed in Section 6.3.3 velocities in the foaming slag and hence, by analogy, mass transfer rates, are increased when the single slit nozzle is replaced by a two slit nozzle. Thus the rates of both, the slag metal and the slag gas reactions within a BOS vessel of a given size are likely to be increased by the change from a single hole to a multi hole lance. Also of interest in connection with such a change is the effect of lance height for a two slit nozzle upon the number of droplets splashed out from the impact region. Figures 36 and 39 show that the number of droplets splashed out from the impact zone varies much less with the height of a two slit nozzle than the height of a single slit nozzle. This observation is confirmed by work carried out at Swinden laboratories<sup>31,32</sup>, and means that changes in the height of a multi hole lance will have a more pronounced effect on the rate of the gas slag reaction than they do on the rate of the metal slag reaction. Thus an increase in the height of a multi hole lance will produce a more significant increase in the oxygen concentration in the slag than an increase in the height of a single hole lance. The process thus becomes more responsive to control, and it is this fact that is the principal advantage gained by changing from single hole lance practice to multi hole lance practice.

## 7. CONCLUSIONS

1. Gas jets with two dimensional symmetry behave in a similar manner to axi-symmetric gas jets in their interactions with liquid surfaces.
2. The depth of the depression created in a liquid surface by each individual gas jet from a multi holed nozzle is virtually identical to the depth of the depression created by a single nozzle of the same size through which gas is flowing at the same rate.
3. The velocity of sound in the type of reactive slag foams that exists in BOS vessels is very low - of the order of 10 to 20 metres/sec. As a consequence, circulation velocities induced in the foam by the action of the central jet are extremely low, some two orders of magnitude lower than the gas velocities in the jet.
4. Two distinct flow zones exist in the foam:- a normal flow zone produced by the direct interaction of the foam with the gas jet reflected from the metal bath, and a reverse flow zone produced by the interaction of the foam with the stirring patterns induced in the metal bath by the impact of the gas jet.
5. Somewhat different chemical conditions exist in the two flow zones, conditions in the normal flow zone being closer to equilibrium with the gas jet, and conditions in the reverse flow zone being closer to equilibrium with the liquid metal.
6. The height of the reverse flow zone varies with operating conditions such as the height of the lance, the total gas flow through the lance and the angle of separation between the different nozzles in a multi hole lance.
7. Velocities in the jet reflected from the surface of the metal bath are supersonic as far as the foaming slag is concerned.
8. The observed variations in the height of the reverse flow zone have been tentatively explained in terms of an imaginary jet pointing upwards within the liquid metal and producing a momentum flow identical to the reflected proportion of the momentum flow through the actual nozzle. In terms of this model, the reverse flow zone exists for that height of the imaginary

- reflected jet over which its rate of entrainment of the foam is very low because it behaves as a supersonic jet within the foam.
9. Recirculation velocities in the normal flow zone are nearly independent of the flow rate of gases through the jet but increase as the nozzle height is increased. Recirculation velocities produced by two slit nozzles are higher than those produced by single slit nozzle and increase with the angle between the jets.
  10. Mixing processes in the foam depend primarily on recirculation within the normal flow zone. The rate of mixing of the foam thus increases as velocities in the normal flow zone increase and as the size of the reverse flow zone decreases. As a generalisation, the rate of mixing of the slag foam increases as the blowing conditions become softer.
  11. Droplets of metal splashed out from the region where the gas jet impacts on the liquid surface do not follow parabolic paths through the foam but, once entering the foam, fall vertically downwards, their path being displaced from the vertical in certain regions by the recirculating motion of the foam.
  12. The velocity of fall of the droplets is about 25% of the velocity of fall of mercury droplets in water. This is due to the buoyancy force exerted on the droplets by the cloud of product gas bubbles which surrounds them.
  13. The mean diameter of the metal droplets increases with the intensity of blowing, and the velocity of fall of the droplets increases with the mean droplet diameter.
  14. For the single slit nozzle, the droplets tend to be concentrated in a band fairly close to the central jet region, although the centre line of this band tends to move outwards as the nozzle height increases, and the droplets tend to be thrown to a greater height.
  15. The bulk of the reaction between the metal droplets and the foaming slag takes place within this band, the droplets flow and the slag flow within this reaction region tending to be at right angles to one another.

## REFERENCES

1. Szekely, J. and Themelis, N.J., 'Rate Phenomena in Process Metallurgy', (Wiley-Interscience, 1971).
2. Streeter, V.L. and Wylie, E.B., 'Fluid Mechanics', (Mc Graw-Hill Book Co., 1976).
3. Gilbrech, D.A., 'Fluid Mechanics', (Wadsworth Publishing Co., 1965).
4. Hansen, A.G., 'Fluid Mechanics', (John Willey and Sons, 1967).
5. Chatterjee, A., 'Iron and Steel', 1973, 1, 627.
6. Smith, G.C., J. Met., 1966, 18, 846.
7. Taylor, J.F, Chem. Eng. Progress, 1951, 47, 175.
8. Albertson, M.L. et al, Trans American Soc. of Civil Engineers, 1950, 115, 639.
9. Ricou, F.B. and Spalding, D.B., J. Fluid Mechanics, 1961, 11, 21.
10. Donald, F.B., and Singer, H., Trans. Instn. Chem. Engrs., 1959, 37, 225.
11. Shirze, J.W. and Seubold, J.G., AIAA Journal, 1967, 5, 2062.
12. Anderson, A.R. and Johns, F.R., Jet Propulsion, 1955, 25, 13.
13. Davenport, W.G. et al, in 'Heat and Mass Transfer in Process Metallurgy', Hills, A.W.D. : Ed., (I.M.M., London, 1967), 207.
14. Kapnar, J.D. et al, Int. J. Heat Mass Transfer, 1970, 13, 932.
15. Flinn, R.A. et al, Trans. AlME, 1967, 232, 1776.
16. Chatterjee, A. and Bradshaw, A.V., Paper presented at the Kinetics of Metallurgical Processes in Steelmaking Conference, Aachen, 1970, 315.
17. Maatsch, J., Tech. Mitt. Krupp. Forschung, 1962, 20 (B.I.S.I. Translation 3696).
18. Coheur, P. and Decker, A., Paper presented at the International Congress on Oxygen Steel Plants, Le Touquet and Dunkirk, 1963, (B.I.S.I. Translation 3064).
19. Denis, E., Revue Universelle des Mines, 1963, Sept., 367, (B.I.S.I. Translation 3538).
20. Cheslak, F.R. et al, J. Fluid Mech., 1969, 36, 55.
21. Banks, R.B. and Chandrasekhara, D.V., J. Fluid Mechanics, 1963, 15, 13.
22. Wakelin, D.H., Ph.D. Thesis, University of London, 1966.
23. Banks, R.B. and Bhavamai, A., J. Fluid Mechanics 1965, 23, 229.
24. Sidgwick, N.V., 'Chemical Elements and their Compounds', Vol. 1, (Oxford University Press, 1951)

25. Chatterjee, A. and Bradshaw, A.V., J.I.S.I., 1972, 210, 179.
26. Srivastava, U.S. et al, Indian Journal of Technology, 1976, 14, 13.
27. Mathieu, F., Revue Universelle des Mines, 1962, 18, 482, (B.I.S.I. Translation 3639).
28. Chatterjee, A., Ph.D. Thesis, University of London, 1970.
29. Kunli, J.I.S.I., 1960, 196, 275.
30. Chedialle, J. and Harvais, M., C.D.S. Circ. Inf. Tech., 1962, 19, 361, (B.I.S.I. Translation 3057).
31. The United Steel Companies Limited Report no. F. & F.R. 5561/-/67.
32. Robertson, A.D. and Sheridan, A.T., J.I.S.I., 1970, 208, 625.
33. Molloy, N.A., J.I.S.I., 1970, 208, 943.
34. Holden, C. and Hogg, A.J., J.I.S.I., 1960, 196, 318.
35. Maatsch, J., Technische Mitt Krupp Forschung, 1963, 21, 1, (B.I.S.I. Translation 3696).
36. Turkdogan, E.T., Chem. Engg. Science, 1966, 21, 1133.
37. Discussion on reference 13, Participants Meyer, H.W., Richardson, F.D., Hills, A.W.D. and Sheridan, A.T.
38. Chatterjee, A. et al, Iron Making and Steel Making, 1976, 1, 21.
39. Rote, F.E. and Flinn, R.A., Met. Trans., 1972, 3, 1373.
40. British Steel Corporation Research Report No. CAPL/SM/A/31/74.
41. Bardenheuer, F. et al, Blast Furnace and Steel Plant, 1970, 58, 401.
42. Walker, R.D., and Anderson, D., Iron and Steel, 1972, 45, 403.
43. White, J., Iron Making and Steel Making, 1974, 1, 115.
44. Trentini, B., Trans. AIME, 1968, 242, 2377.
45. Walker, R.D. and Anderson, D., Iron and Steel, 1972, 45, 497.
46. Kootz, T., J.I.S.I., 1960, 196, 253.
47. Holdan, C. and Hogg, A.J., J.I.S.I., 1960, 196, 318.
48. Hammer, R. and Kootz, Th., Stahl und Eisen, 1957, 77, 1303, (B.I.S.I., Translation 733).
49. Meyer, H.W. et al, J. Met., 1960, 20, 35.
50. Kozakevitch, Paul, J. Met., 1969, 21, 57.
51. Meyer, H.W., J.I.S.I., 1969, 207, 781.
52. Kozakevitch, Paul, Paper presented at the Kinetics of Metallurgical Processes in Steelmaking Conference, Aachen, 1970, 513.

53. Chernyatevich, A.G. et al, Steel in the U.S.S.R., 1975, 5, 79.
54. Price, D.J., in 'Process Engineering of Pyrometallurgy',  
Jones, M.J. : Ed, (I.M.M., London, 1967), 8.
55. Chatterjee, A., T I S C O, 1973, 20, 35.
56. Hills, A.W.D., in 'Process Engineering of Pyrometallurgy',  
Jones, M.J. : Ed, (I.M.M., London, 1974), 81.
57. Davis, M.W. et al, in 'Richardson Conference', Jeffes, J.H. and  
Tait, R.J. : Ed, (I.M.M., London, 1973), 95.
58. Mulholland, E.W. et al, J.I.S.I., 1973, 211, 632.
59. Ojeda, O.M., Ph.D. Thesis, Sheffield City Polytechnic, 1977.
60. Discussions and Contributions, 'Process Engineering of  
Pyrometallurgy', Jones, M.J. : Ed, (I.M.M., London, 1974), 195.
61. Ojeda, O.M., Private discussion.
62. Ward, R.G., 'Physical Chemistry of Iron and Steelmaking',  
(Edward Arnold Ltd, London), 1962.
63. Richardson, F.D., in 'Chemical Metallurgy of Iron and Steel',  
(I.S.I., London, 1973), 82.
64. Baker, L.A. et al, Trans. AIME, 1967, 239, 857.
65. Baker, L.A. and Ward, R.G., J.I.S.I., 1967, 205, 714.
66. Distin, P.A. et al, J.I.S.I., 1968, 206, 821.
67. Kitchener, J.A. and Cooper, C.F., Quarterly Review of Chemical  
Society, 1959, 13, 71.
68. Cooper, C.F., Kitchener, J.A., J.I.S.I., 1959, 193, 48.
69. Bardenheur, F., B I S I T Translation 14161.
70. Urquhart, R.C. and Davenport, W.G., J. Met., 1970, 22, 36.
71. Jones, D.J. et al, J. Met., 1963, 15, 577.
72. Akira, Masui et al, in 'Iron and Steelmaking Symposium No. 4',  
Iu, W.K. : Ed., (Hamilton, Ont., Canada, 1976).
73. Acheson, R., Ph.D. Thesis, Sheffield City Polytechnic, 1976.
74. Richardson, F.D., Jernkont. Ann., 1969, 153, 359.
75. Brinn, D.G., British Steel Corporation Report No. SM/BIB/829.
76. Acheson, R. and Hills, A.W.D., in 'Physical Chemistry of Process  
Metallurgy - The Richardson Conference', Jeffes, J.H.E. and  
Tait, R.J. : Ed, (I.M.M., London, 1973), 95.
77. Bailer, J.C., 'Comprehensive Inorganic Chemistry', (Pergamon  
Press, 1973), Vol. 1.

78. Stevens, D.T., Technical Memo No 20, Richard Thomas and Baldwins Ltd., 1964.
79. Geiger, G.H. and Poirier, D.R., 'Transport Phenomena in Metallurgy', (Addison-Wesley Publishing Co, 1973).
80. Grassmann, 'Physical Principles of Chemical Engineering', (Pergamon Press, 1971).
81. Robertson, D.G.C. and Jenkins, A.E., in 'Heterogeneous Kinetics at Elevated Temperature', Belton, G.R. and Worrell, W.L. : Ed, (Plenum Press, New York, 1970), 393.
82. Sharma, S.K. et al, Paper presented at the 60th National Open Hearth and Basic Oxygen Steel Conference, Pittsburgh, 1977.
83. Dean, R.B., Journal of Applied Physics, 1944, 15, 446.
84. Bennett, C.O. and Myers, J.E., 'Momentum Heat and Mass Transfer', (Mc Graw-Hill Book Co, 1962).
85. Lee, C.K. et al, Ironmaking and Steelmaking, 1977, 4, 329.
86. Kluth, K.H. and Maatsch, J., Technische Mitt Krupp Forschung, 1964, 22, 93, (B.I.S.I. Translation 4242).
87. Schoop, J. et al, Ironmaking and Steelmaking, 1978, 5, 72.

## APPENDIX 1.

Loss of Water During Depth of DepressionMeasurements

Flow rate of the gas	=	18.9 litres/min at N.T.P.
Time of blowing	=	10 minutes
Volume of the gas used	=	189 litres
Decrease in the level of water	=	0.05 cm
Amount of water evaporated	=	$0.05 \times 10.5 \times 2 \text{ cm}^3$
Volume of water evaporated	=	$\frac{0.05 \times 10.5 \times 2 \times 22.4}{18}$ litres
	=	1.3 litres

Partial pressure of water

$$\begin{aligned} \text{vapours in the outgoing gases} &= \frac{1.3 \times 76}{189 + 1.3} \text{ cm of mercury} \\ &= 0.52 \text{ cm of mercury} \end{aligned}$$

The calculated vapour pressure of water (0.52 cm of mercury) is less than the saturation vapour pressure at 20°C and one atmosphere pressure (0.69 cm of mercury). The loss of water can therefore be attributed to evaporation and not to mechanical carry over.

## APPENDIX 2.

Calculation of the Jet Momentum

In a Rotameter the force balance on the stationary float leads to the following equation relating the bulk velocity around the annular ( $U_{br}$ ), volume of the float ( $V_f$ ), maximum cross sectional area of the float ( $A_f$ ), density of the float ( $\rho_f$ ) and density of the gas ( $\rho$ ):

$$U_{br} = C_r \sqrt{\frac{2 g V_f (\rho_f - \rho)}{A_f \rho}} \quad \text{-----} \quad (1)$$

The coefficient of discharge ( $C_r$ ) depends on the Reynolds number. The Reynolds number ( $R_e$ ) is defined as:

$$R_e = \frac{(D - D_f)}{\mu} U_{br} \rho \quad \text{-----} \quad (2)$$

Above Reynolds number = 10000  $C_r$  is constant. At Reynolds number below 10000 the chart given by Bennett and Myers<sup>84</sup> show that a two fold variation of the Reynolds number would increase the coefficient of discharge by about 4 percent. The change in the density of the gas due to changes in its temperature and pressure at the

Rotameter is very small. Moreover, since the gas velocity changes in the opposite way to the gas density, the product does not vary as much as each of the individual factors.<sup>80</sup> For the practical purpose of correcting the volumetric flow of gas flowing through the Rotameter, the coefficient of discharge can be treated as constant for the same setting of the float. It can thus be deduced from equation 1 that the volumetric flow rate of gas at the Rotameter under operating conditions ( $V_M$ ) is related to the density of gas at the Rotameter under operating conditions ( $\rho_M$ ), the volume ( $V$ ) and the density ( $\rho$ ) under standard conditions of calibration and at the same float position according to the following equation:

$$V_M = V \sqrt{\frac{\rho}{\rho_M}} \quad \text{-----} \quad (3)$$

From equation 3

$$\dot{m} = V \sqrt{\rho \rho_M} \quad \text{-----} \quad (4)$$

$\dot{m}$  = Mass flow rate of gas through the Rotameter

Assuming that the flow from the Rotameter to the nozzle and then through the nozzle in to the jet is adiabatic: We can write:

$$\frac{P}{(\rho)^\gamma} = \text{Constant}$$

$$\frac{P_J}{(\rho_J)^\gamma} = \frac{P_M}{(\rho_M)^\gamma}$$

$$\rho_J = \rho_M \left( \frac{P_J}{P_M} \right)^{1/\gamma} \quad \text{-----} \quad (5)$$

$P_J$  = Pressure of the jet (one atmosphere).

$P_M$  = Pressure of gas at the Rotameter.

$\rho_J$  = Density of the jet.

$\rho_M$  = Density of the gas at the Rotameter.

The jet momentum ( $\dot{M}$ ) is related to the mass flow rate of the gas ( $\dot{m}$ ), the area of the jet at the nozzle exit ( $A_J$ ) and the density of the jet ( $\rho_J$ ) according to the following equation:

$$\dot{M} = \frac{\dot{m}^2}{A_J \rho_J} \quad \text{_____} \quad (6)$$

Substituting the value of  $\dot{m}$  from equation 4 and the value of  $\rho_J$  from equation 5 gives:

$$M = \frac{V^2 \rho}{A_J} \left( \frac{P_M}{P_J} \right)^{\frac{1}{\gamma}} \quad \text{_____} \quad (7)$$

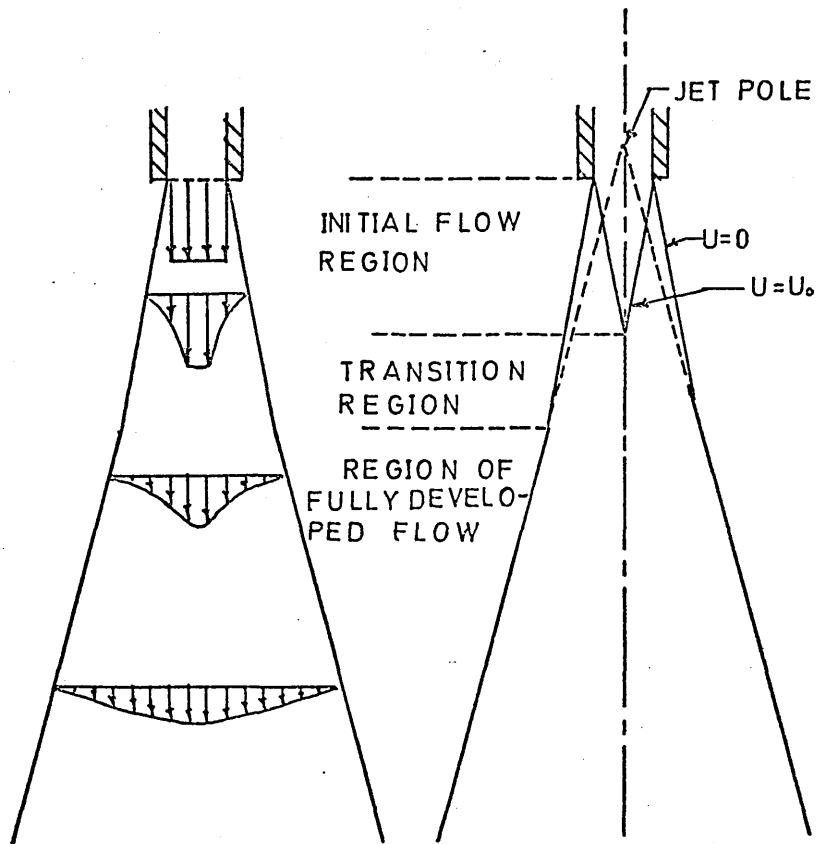


FIG.1 THE STRUCTURE OF A SUBSONIC JET [1]

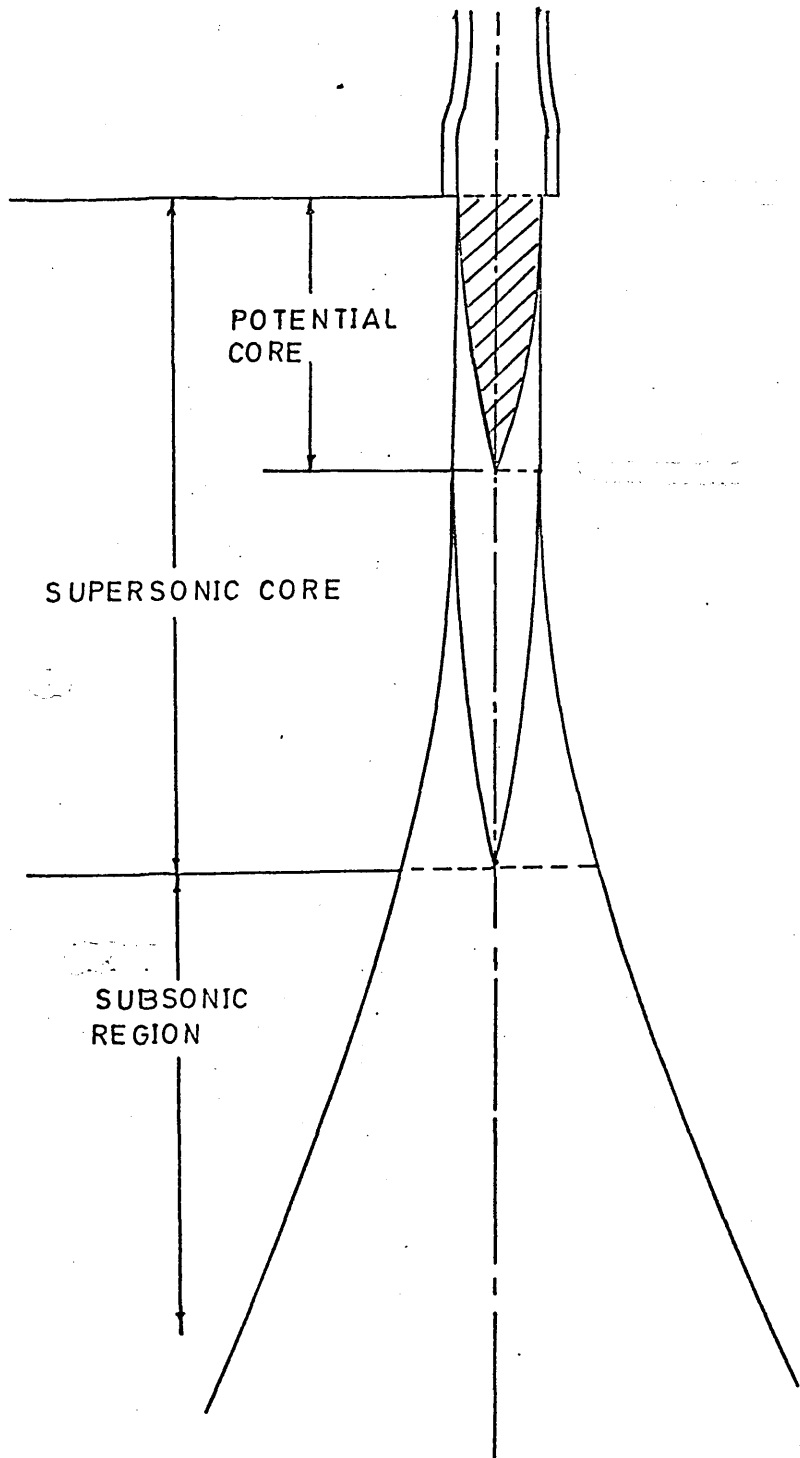


FIG.2 THE STRUCTURE OF A SUPERSONIC JET [5]

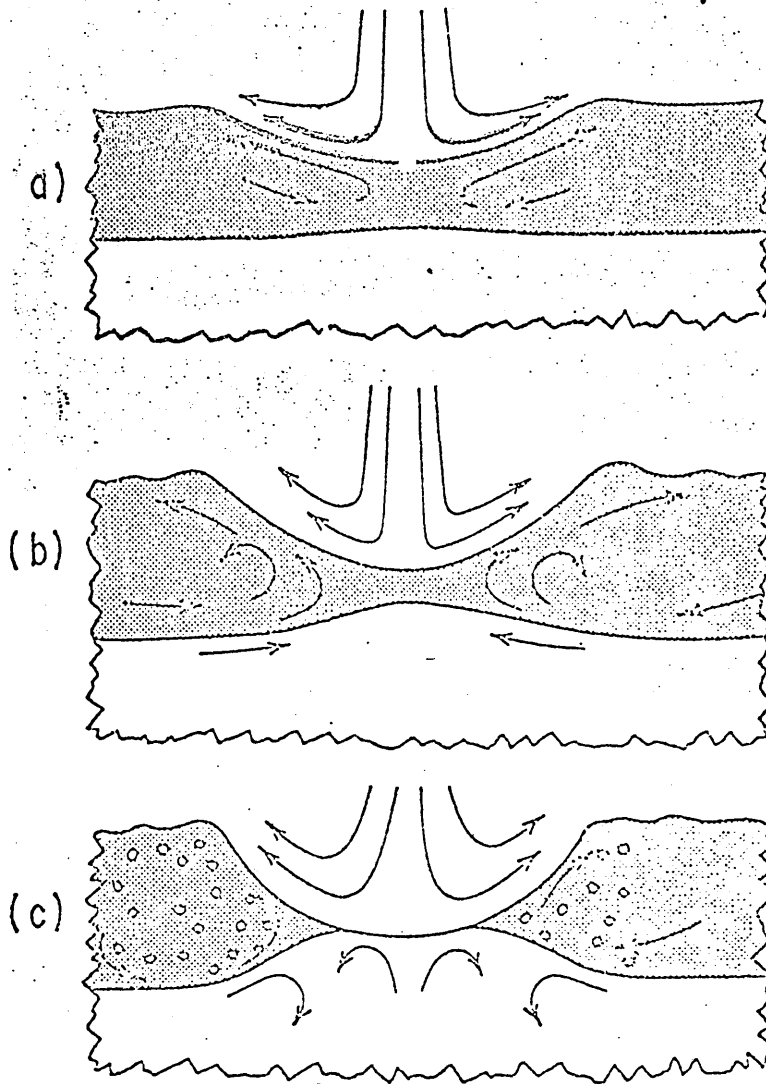
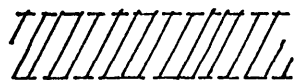
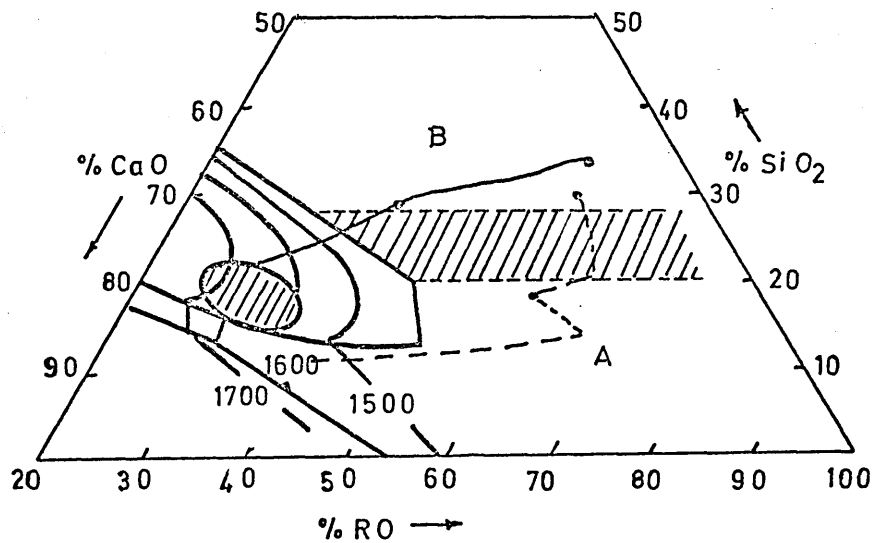
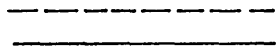


FIG. 3 THE FLOW PATTERN PRODUCED BY A GAS JET IMPINGING  
ONTO A WATER BATH COVERED BY A LAYER OF OIL [36]



GOOD SLAG PATH



SLOPPING CONDITIONS  
DRY SLAG PATH

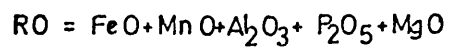


FIG.4 TYPICAL SLAG FORMATION PATHS [40]

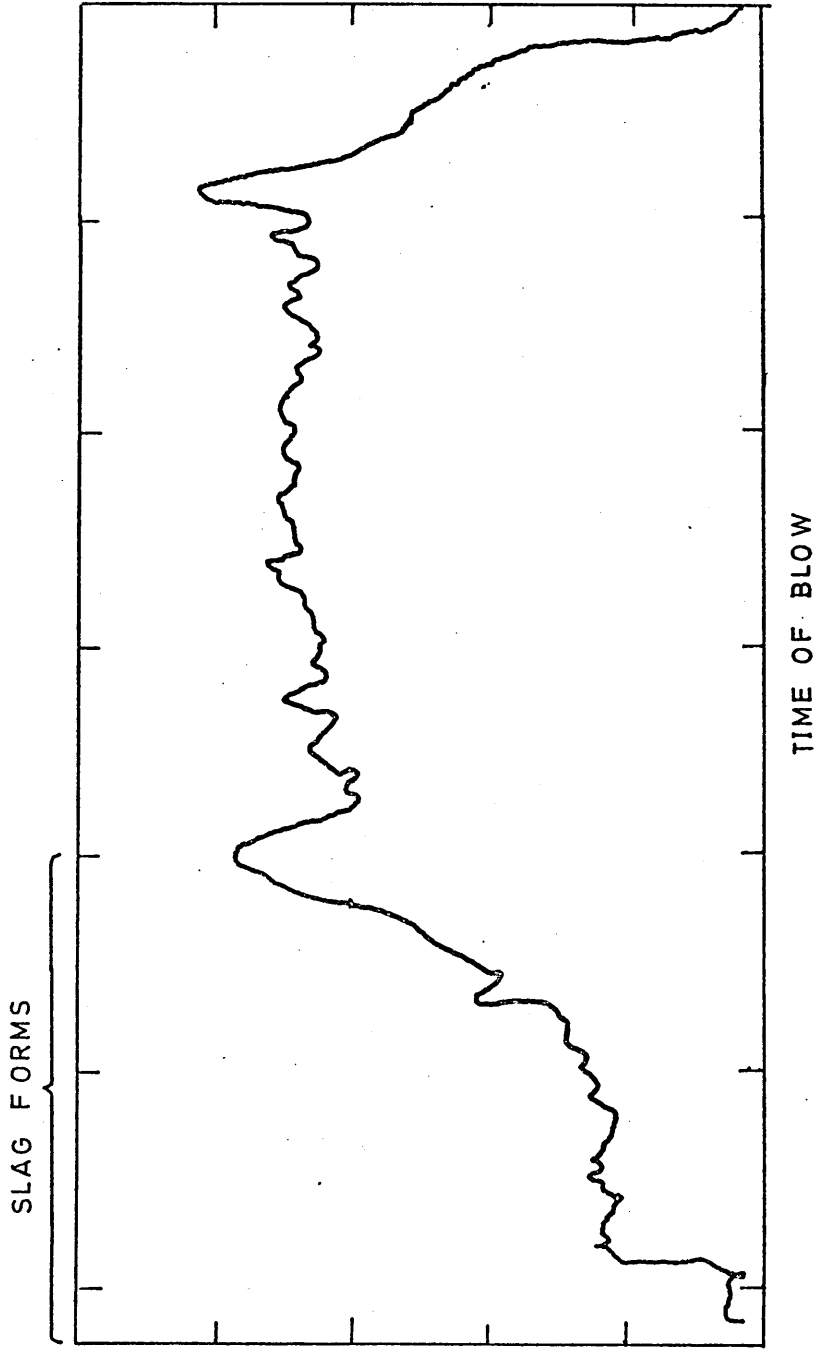
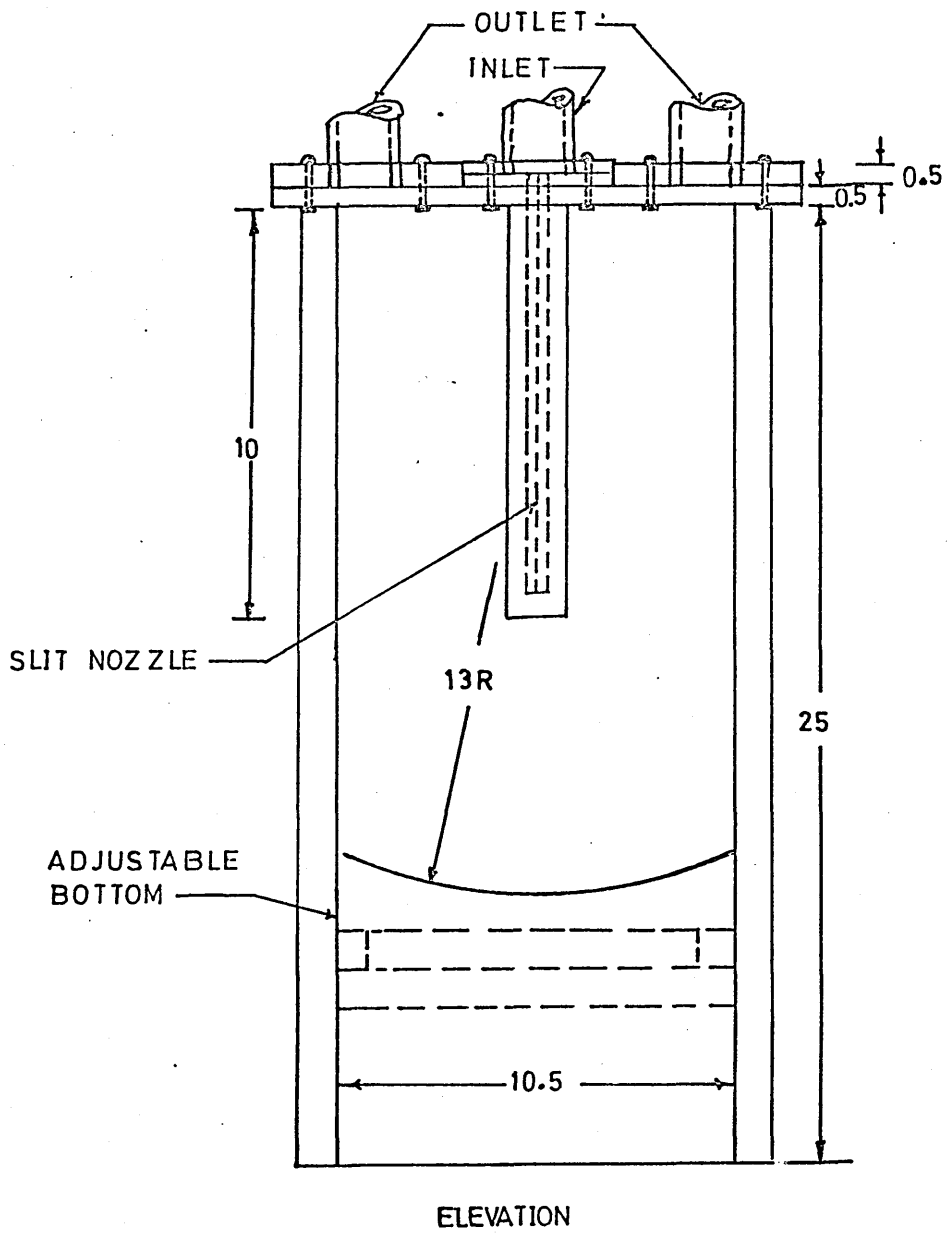
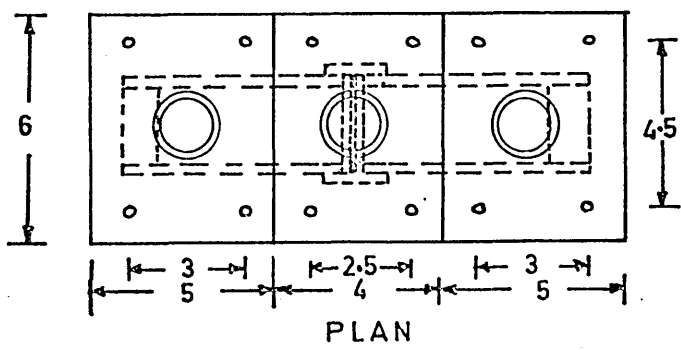


FIG.5 THE VARIATION IN DECARBURISATION RATE THROUGHOUT A TYPICAL BOS BLOW [56]



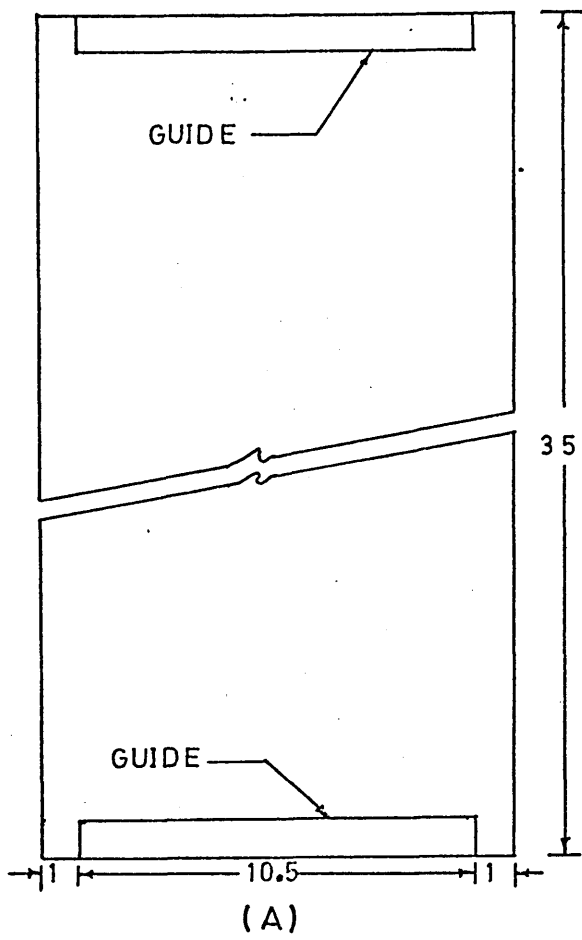
ELEVATION



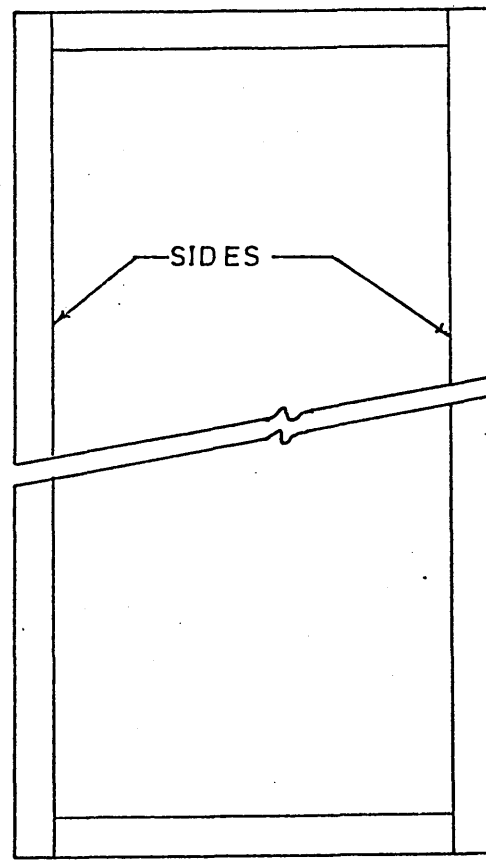
PLAN

SCALE HALF FULL SIZE DIMENSIONS IN CMS.

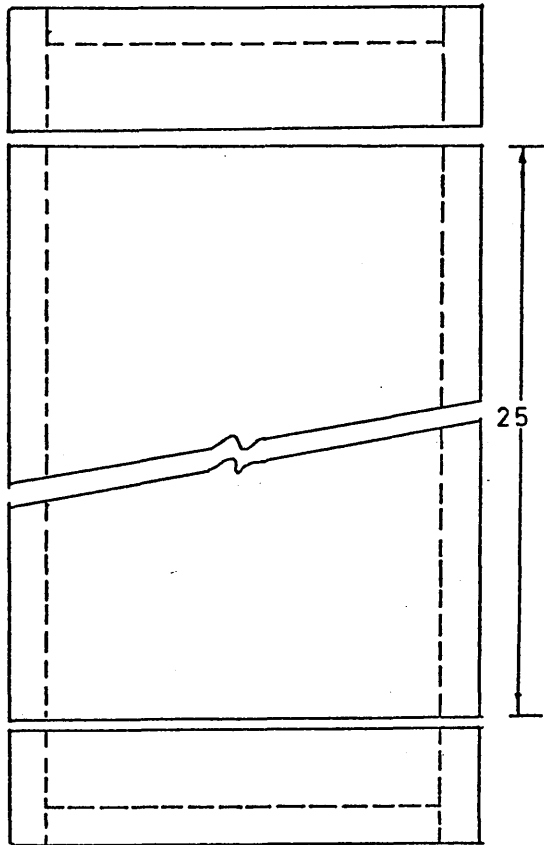
FIG.6 THE REACTOR ASSEMBLY



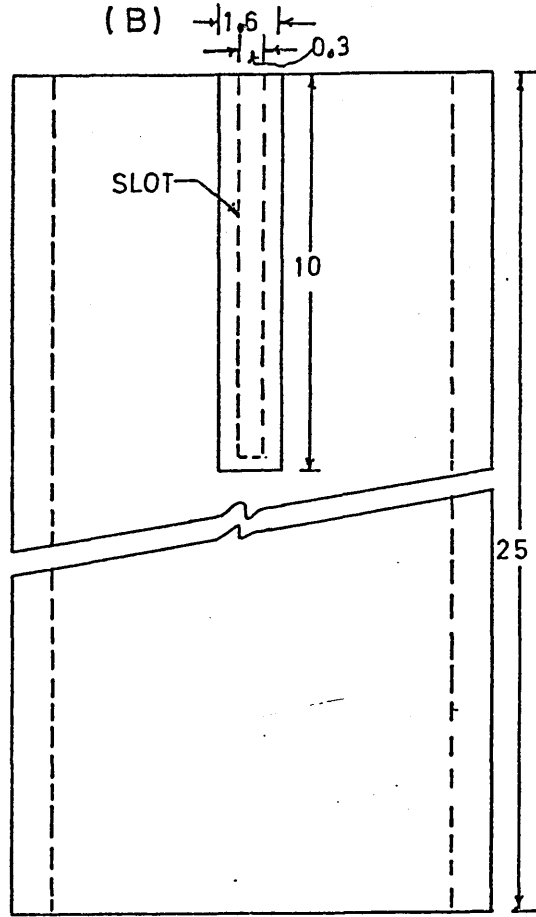
(A)



(B)



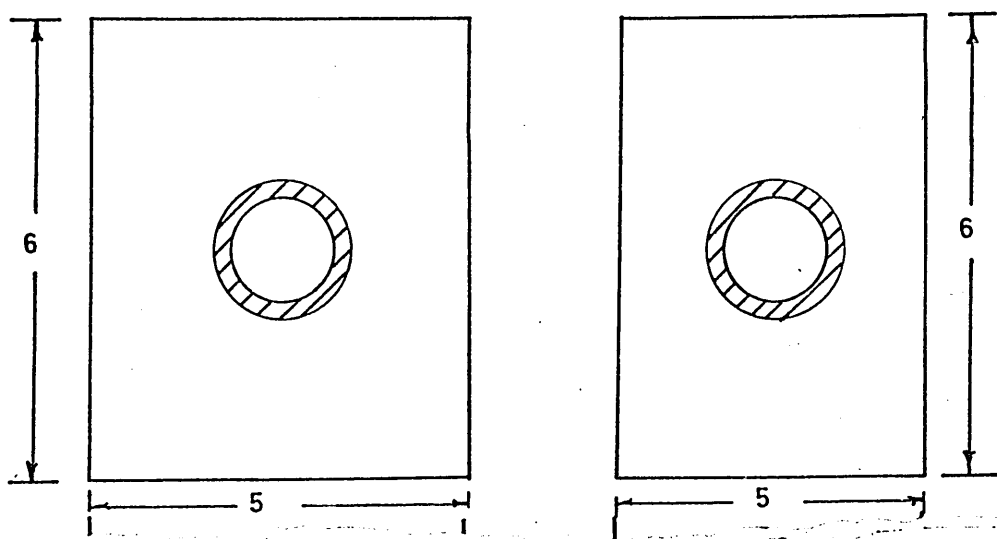
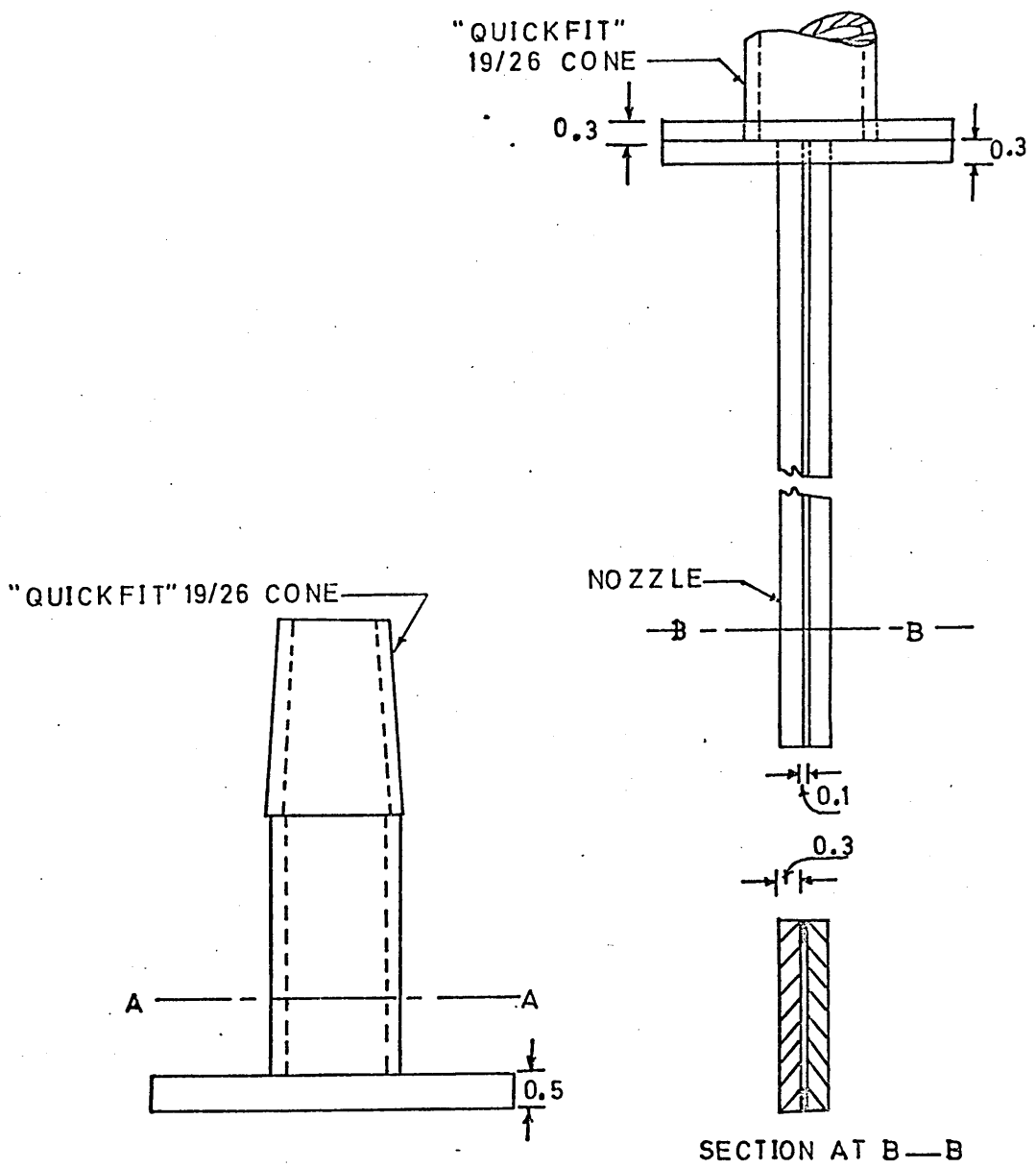
(C)



(D)

DIMENSIONS IN CMS.

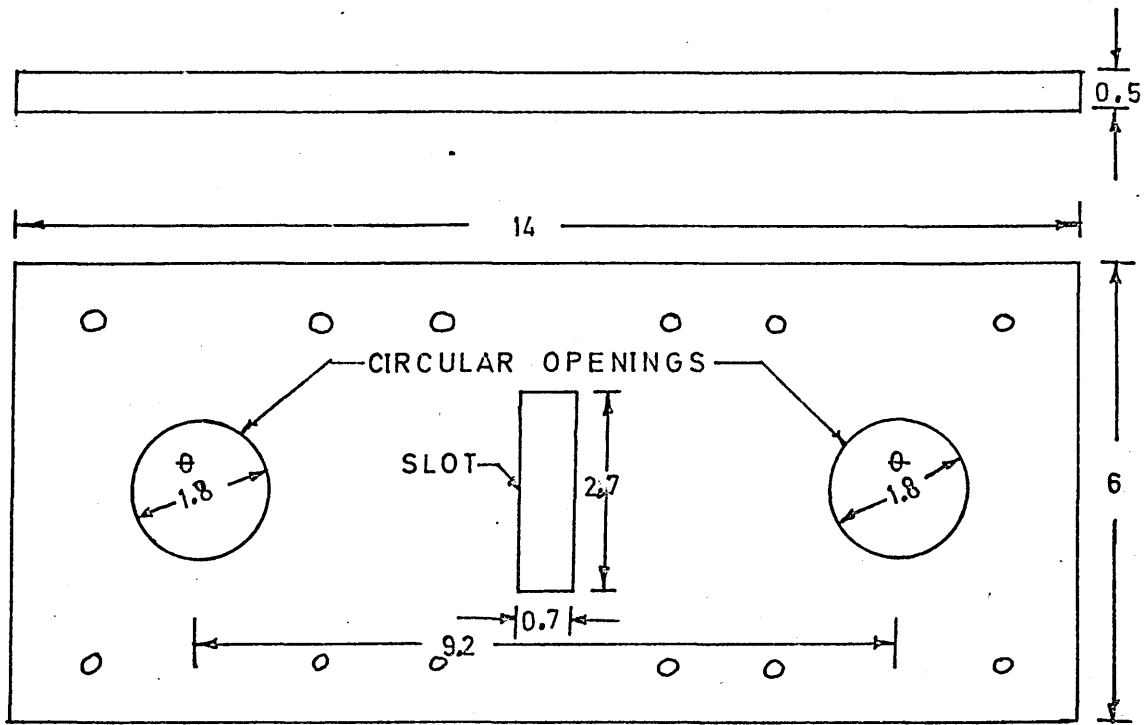
FIG. 7 THE REACTOR CONSTRUCTION



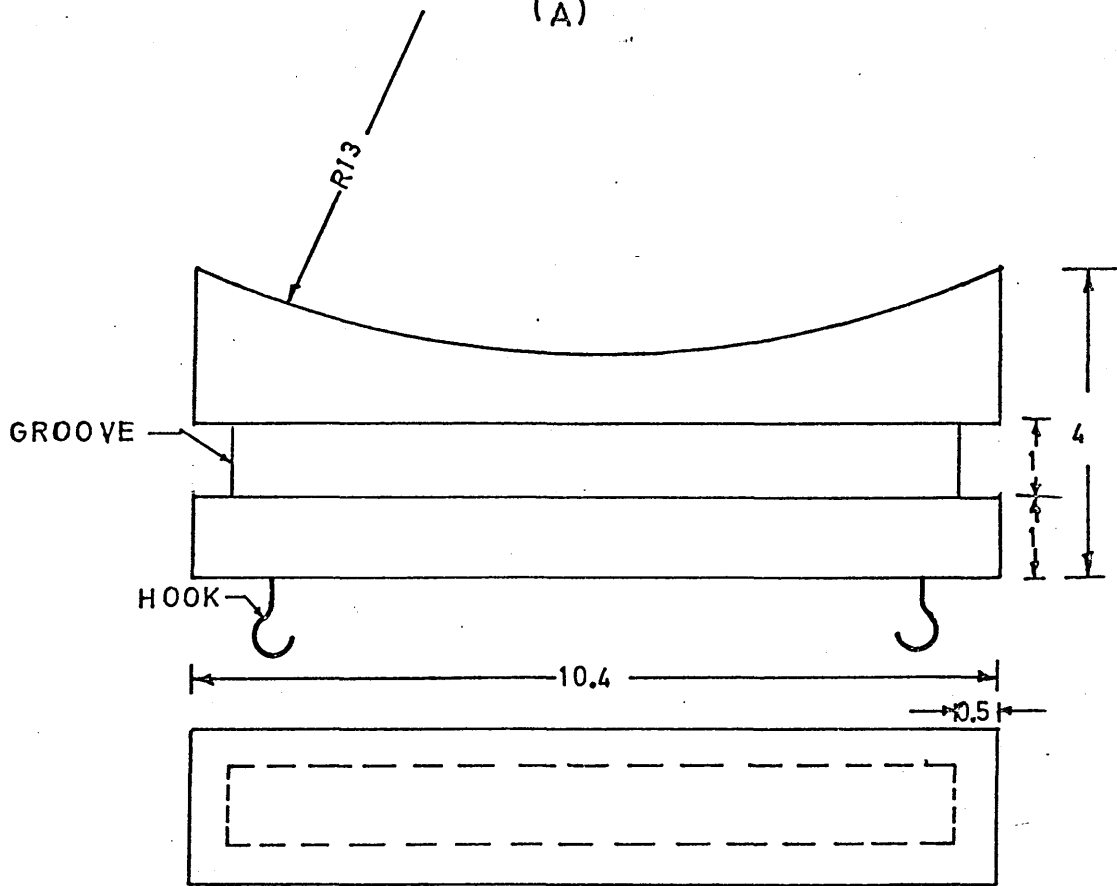
SECTION AT A—A

(A) DIMENSIONS IN CMS. (B)

FIG. 8 THE GAS OUTLET CONNECTION (A) AND THE SLIT NOZZLE ASSEMBLY (B) OF THE REACTOR



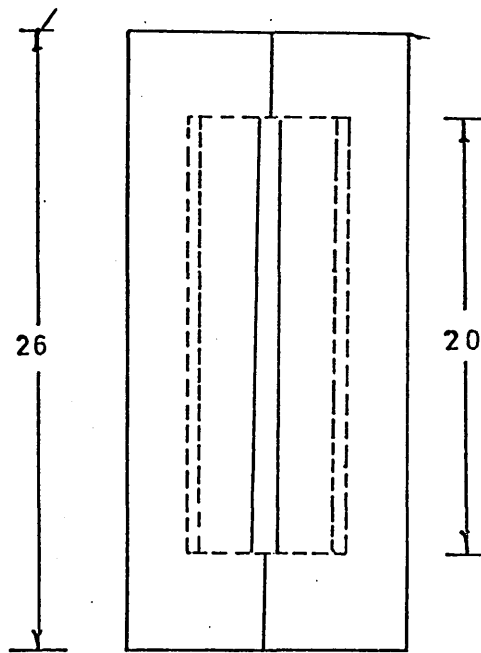
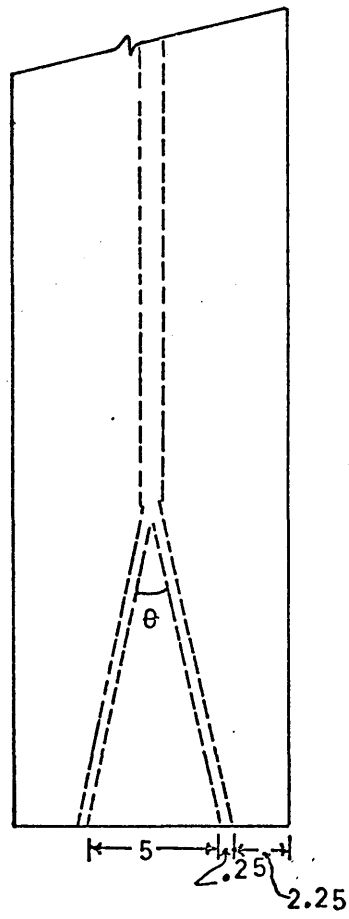
(A)



(B)

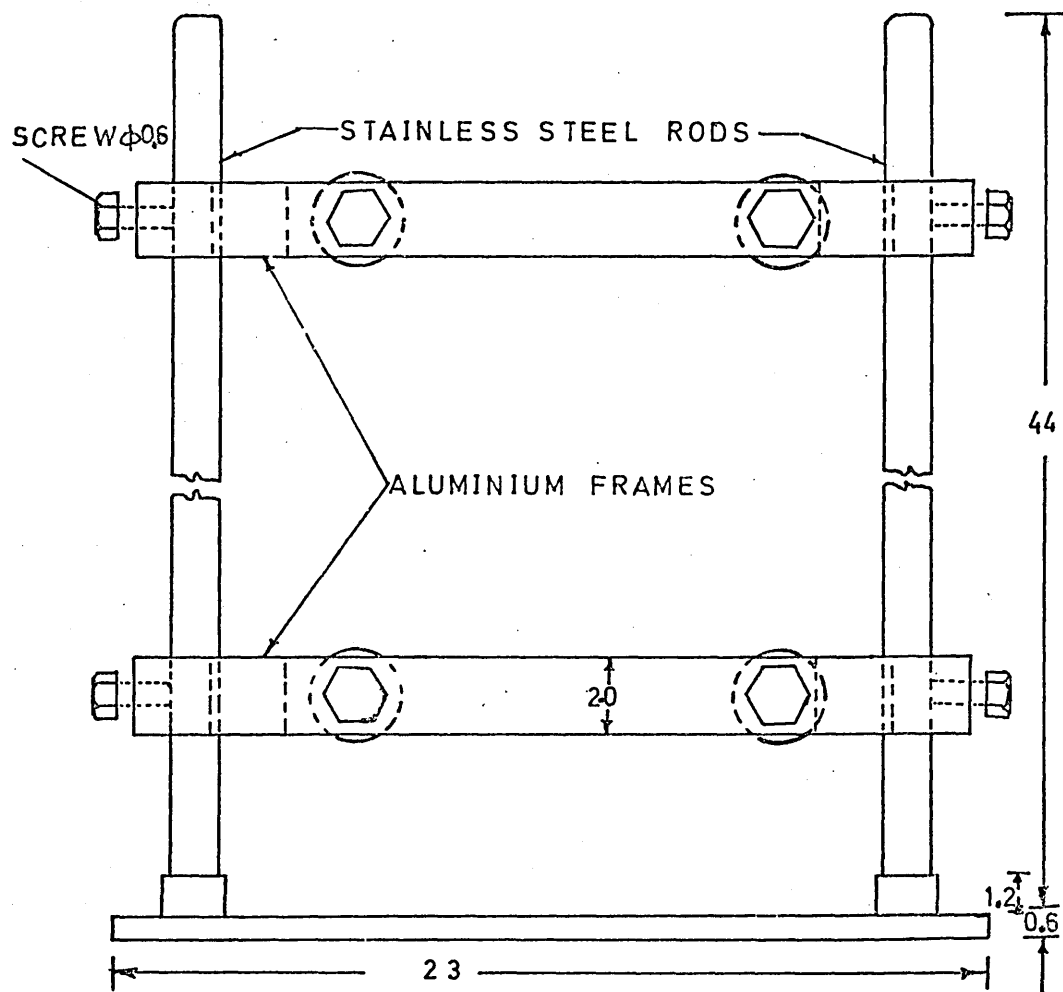
DIMENSIONS IN CMS.

FIG. 9 THE TOP COVER (A) AND BOTTOM (B) OF THE REACTOR

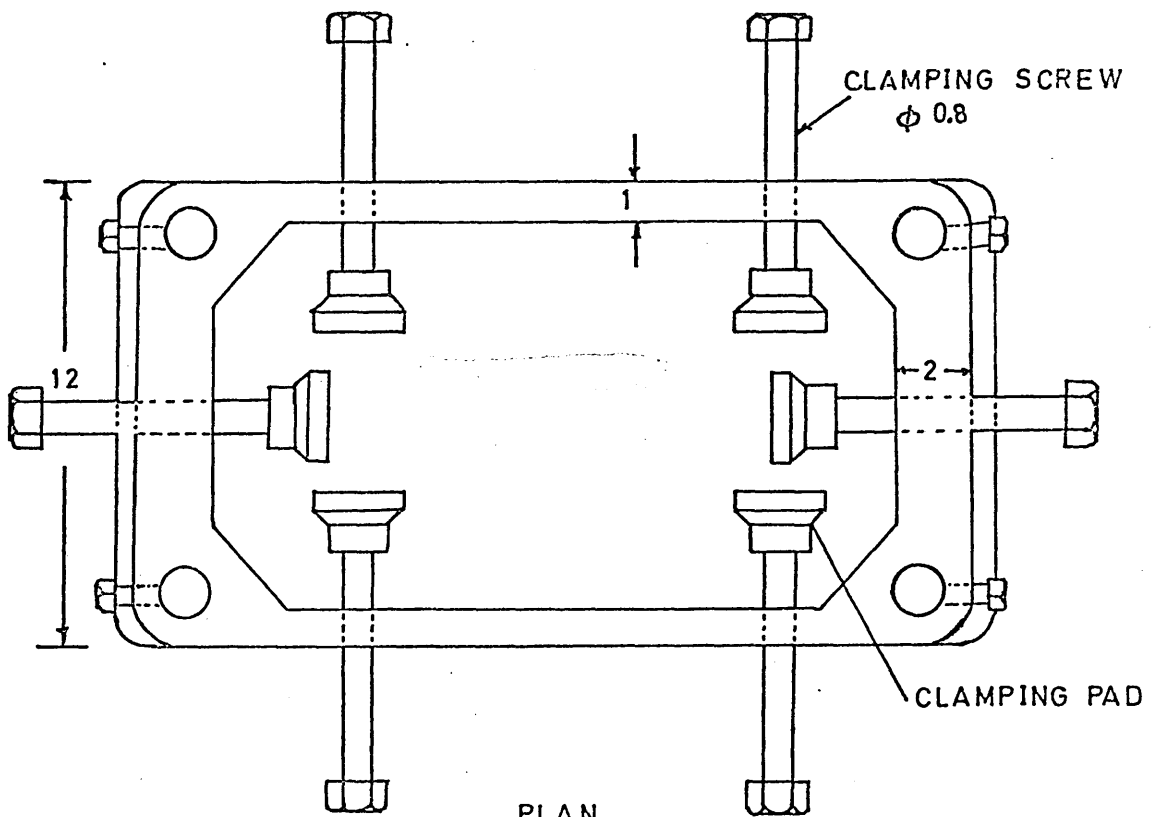


DIMENSIONS IN MMS.

FIG.10 THE TWO SLIT NOZZLE



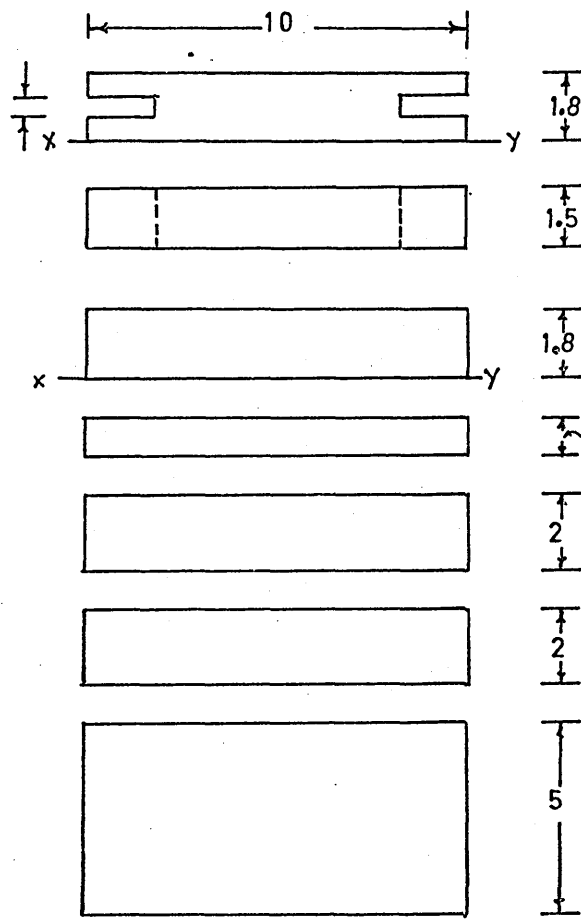
ELEVATION



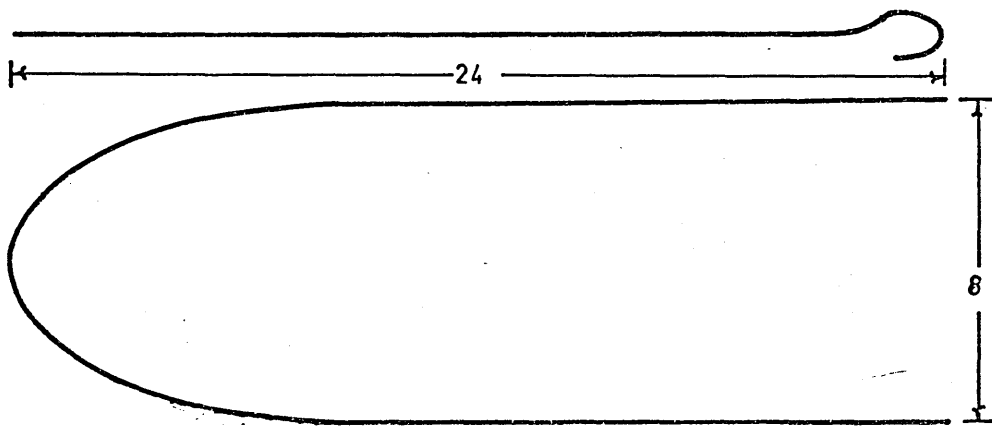
PLAN

SCALE HALF FULL SIZE DIMENSIONS IN CMS.

FIG.11 THE FRAME FOR SUPPORTING THE REACTOR



(A)



(B)

DIMENSIONS IN CMS.

FIG.12 THE PERSPEX BLOCKS (A) AND THE U SHAPED ROD (B) FOR ADJUSTING THE BOTTOM OF THE REACTOR

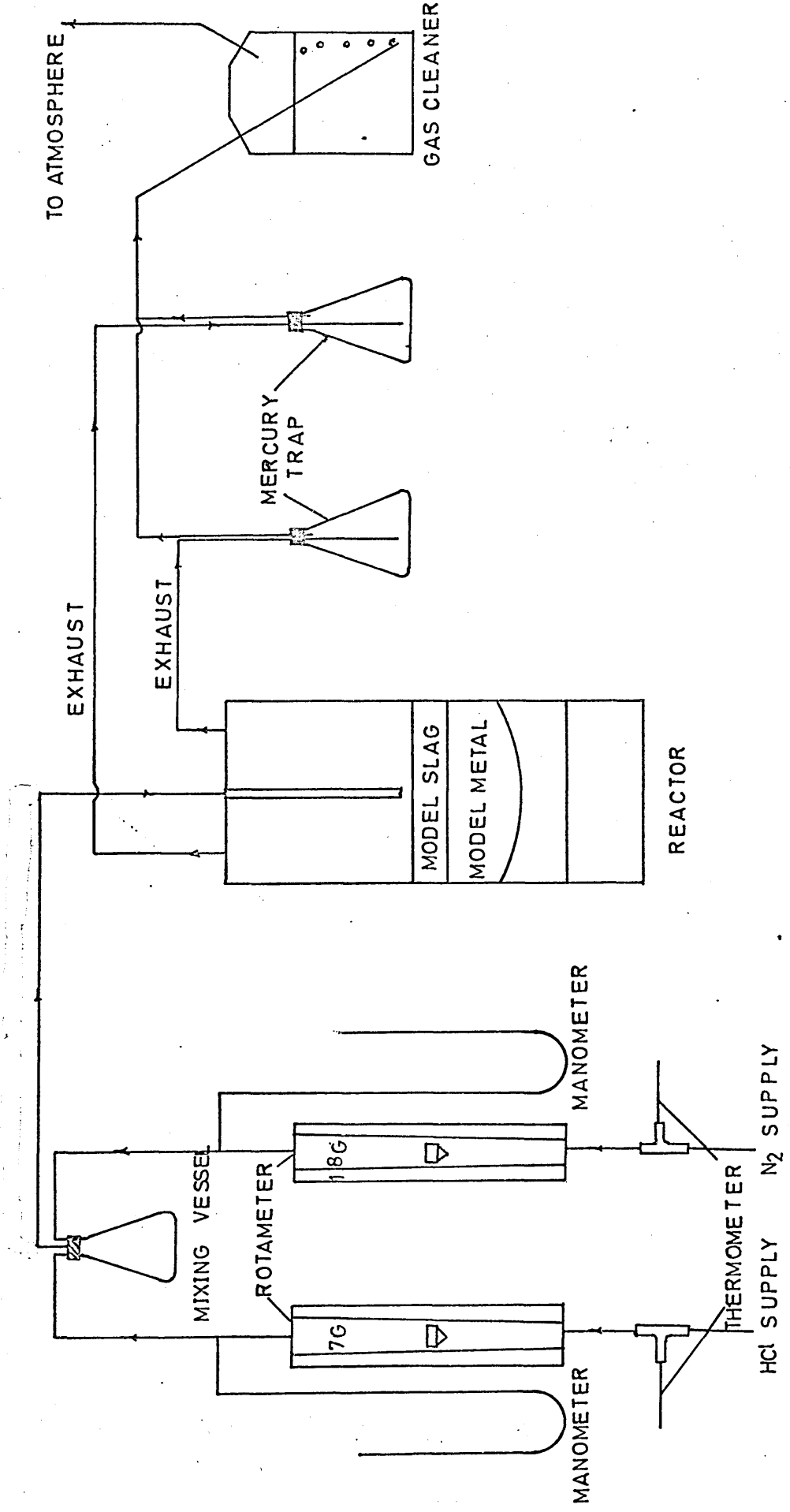
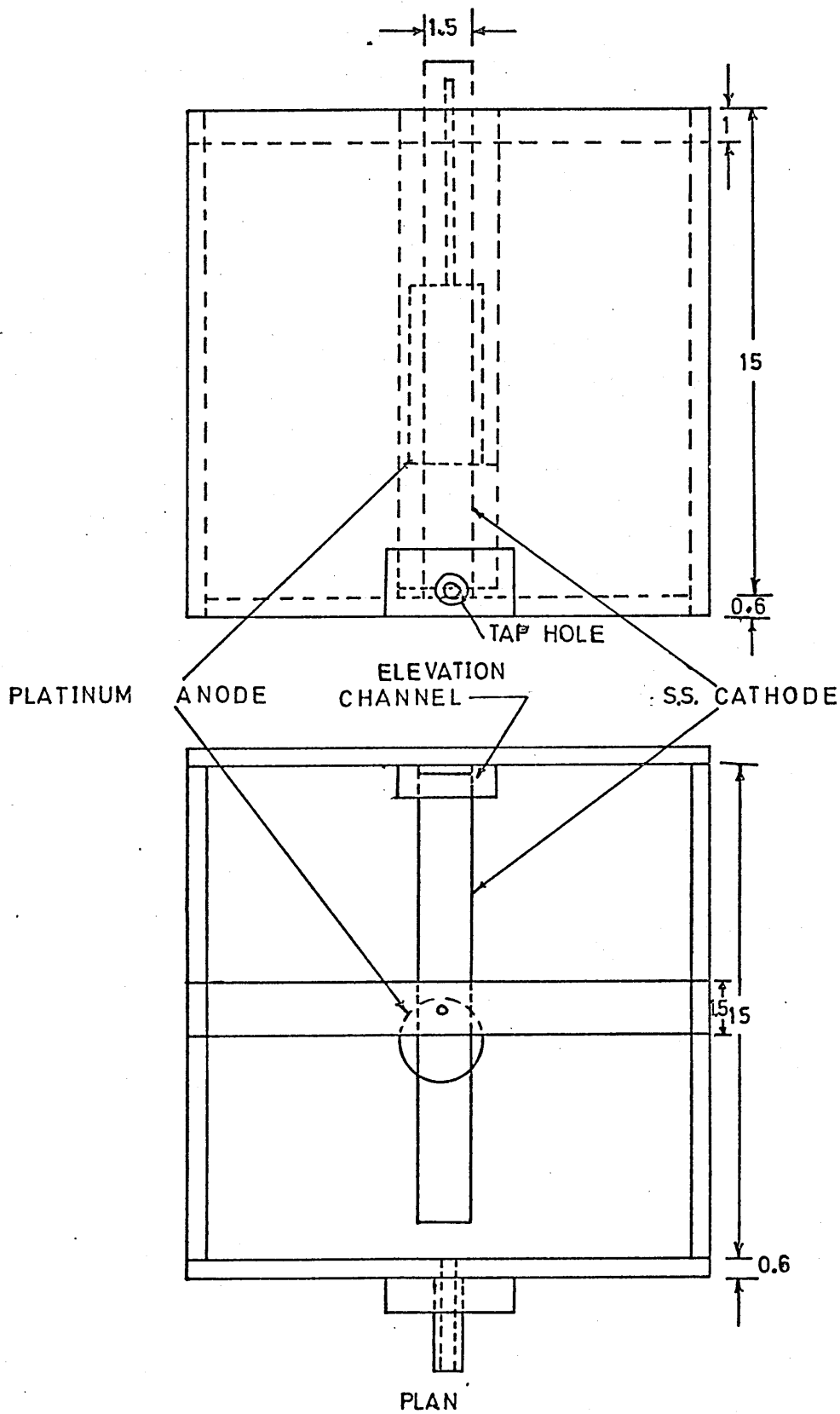


FIG.13 SCHEMATIC DIAGRAM OF THE REACTOR AND OTHER ANCILLARY EQUIPMENT



SCALE HALF FULL SIZE

DIMENSIONS IN CMS.

FIG. 14 THE AMALGAM CELL

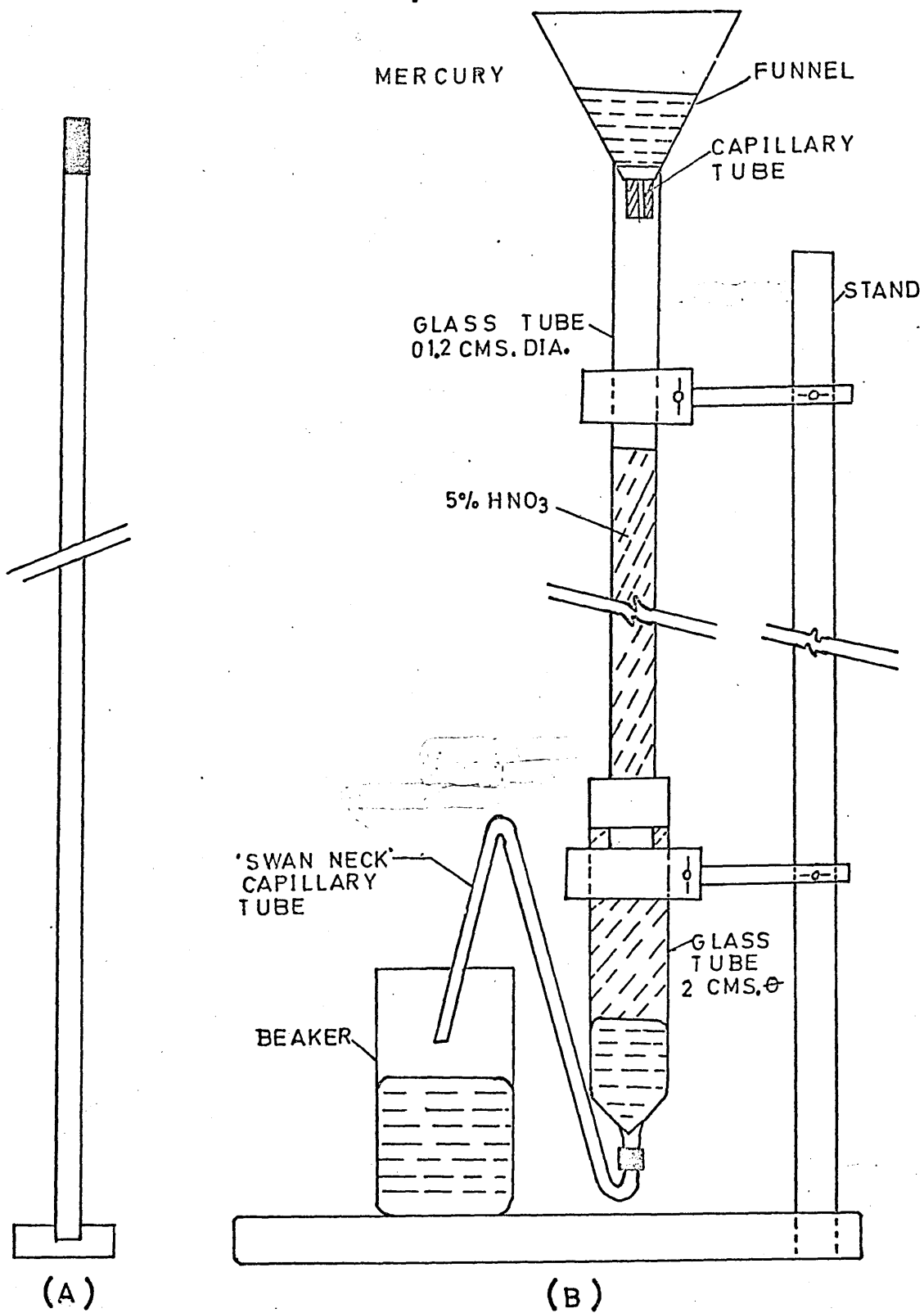


FIG. 15 (A) THE STIRRER USED IN THE AMALGAM CELL  
 (B) THE MERCURY PURIFYING UNIT

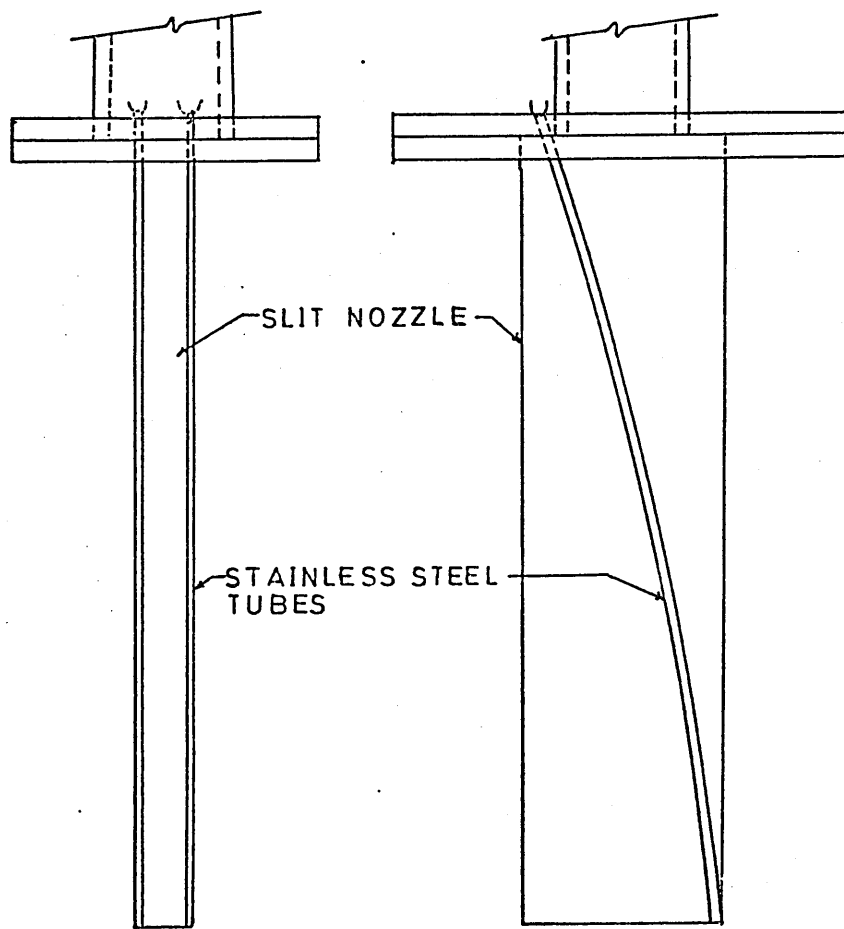


FIG. 16 THE ARRANGEMENT FOR INJECTING THE TRACER  
ADJACENT TO THE JET EXIT

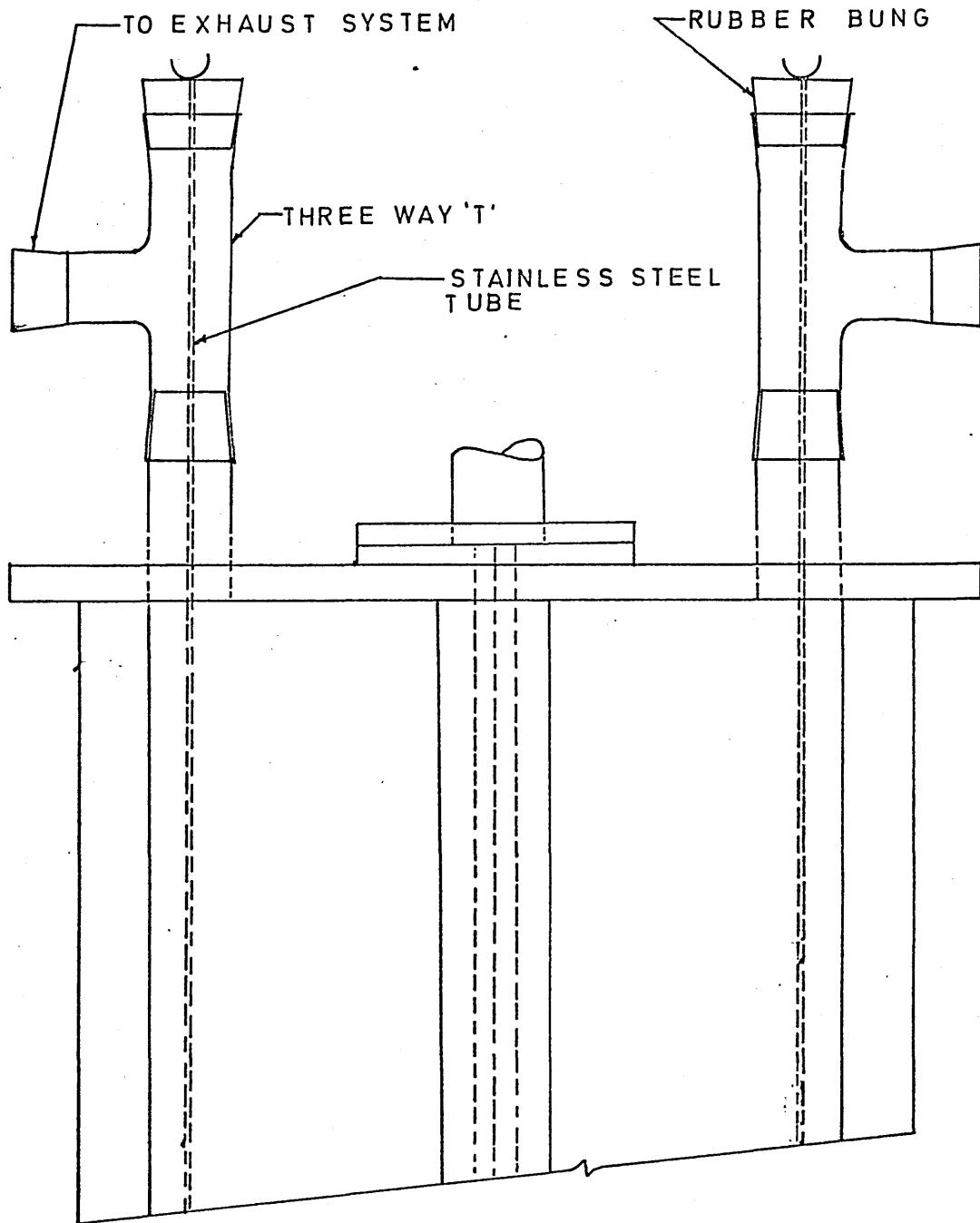


FIG. 17 THE ARRANGEMENT FOR INJECTING THE TRACER THROUGH THE OUTLETS

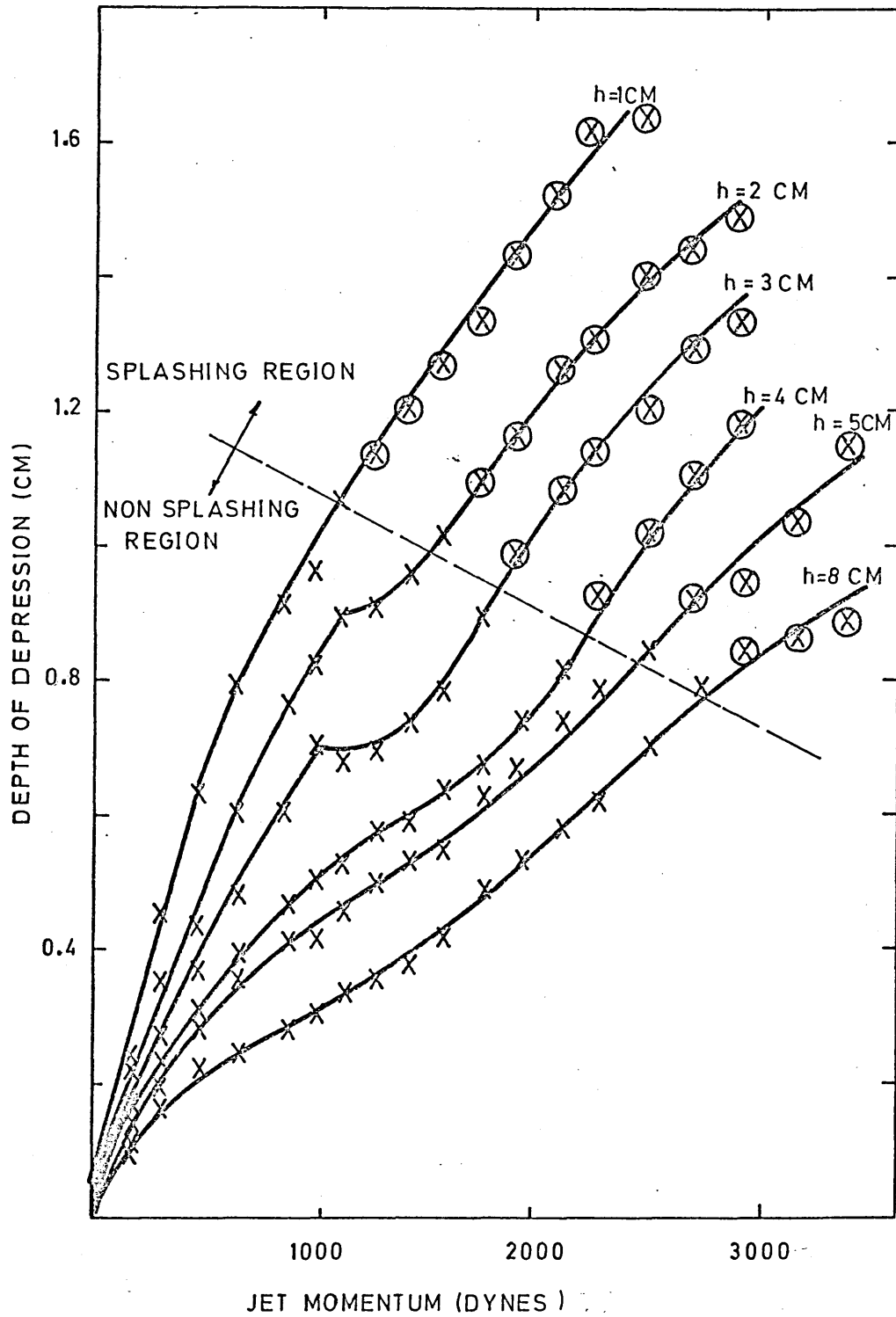


FIG. 18 THE EFFECT OF JET MOMENTUM ON THE DEPTH OF DEPRESSION IN THE NITROGEN WATER SYSTEM

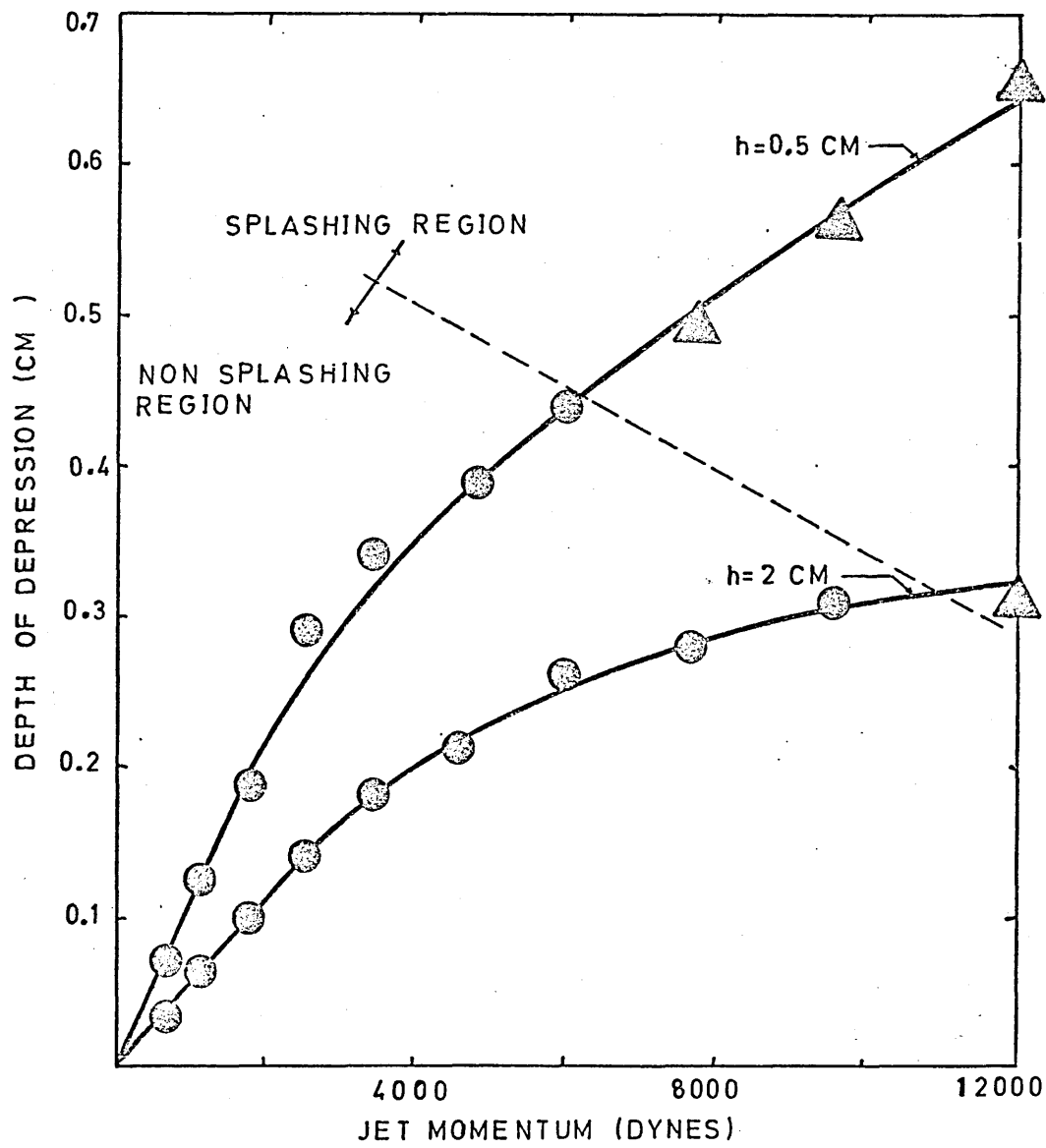


FIG. 19 THE EFFECT OF JET MOMENTUM ON THE DEPTH OF DEPRESSION IN THE NITROGEN MERCURY SYSTEM

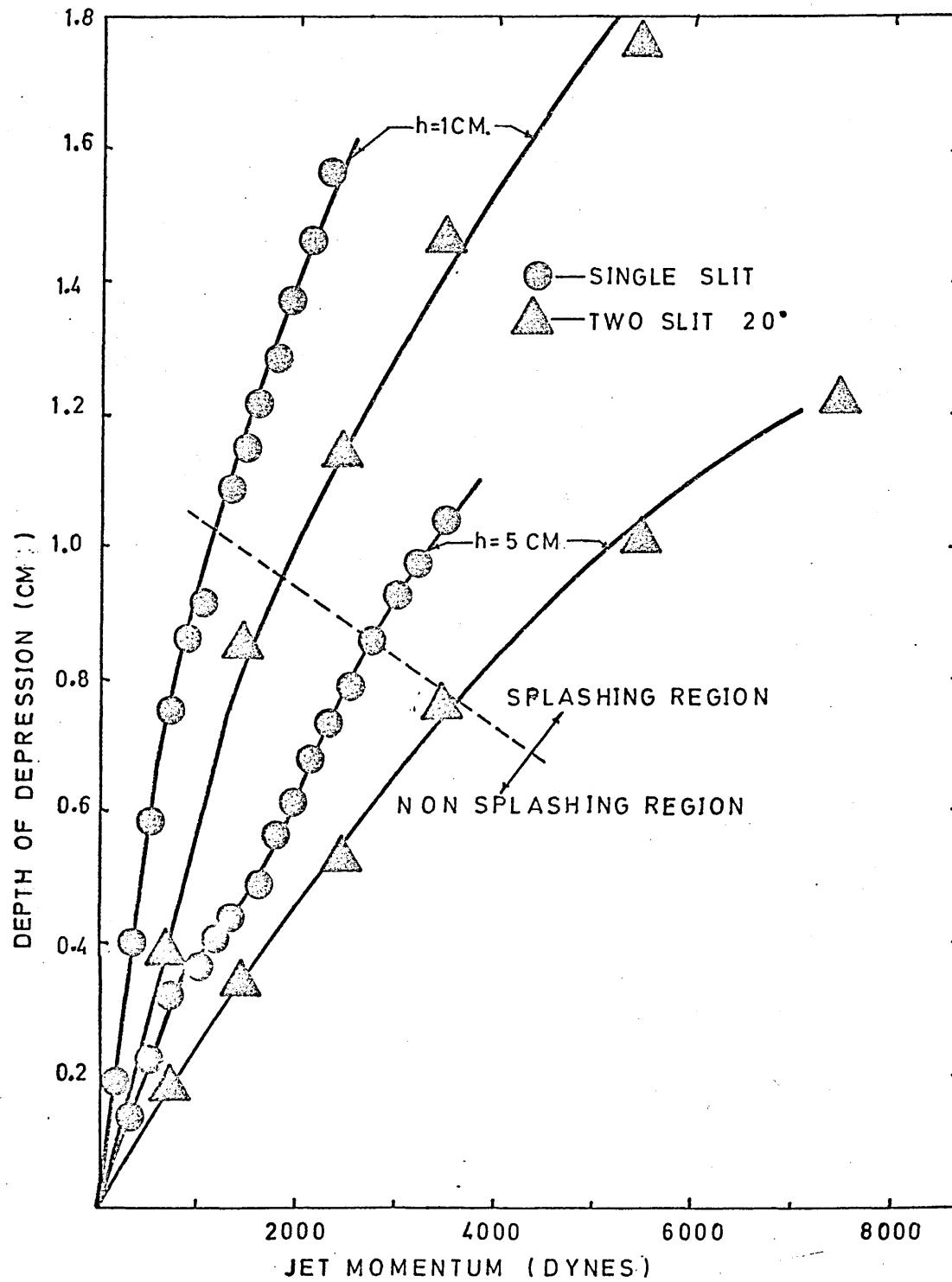


FIG. 20 THE EFFECT OF NOZZLE TYPE ON THE DEPTH OF DEPRESSION IN THE NITROGEN WATER SYSTEM

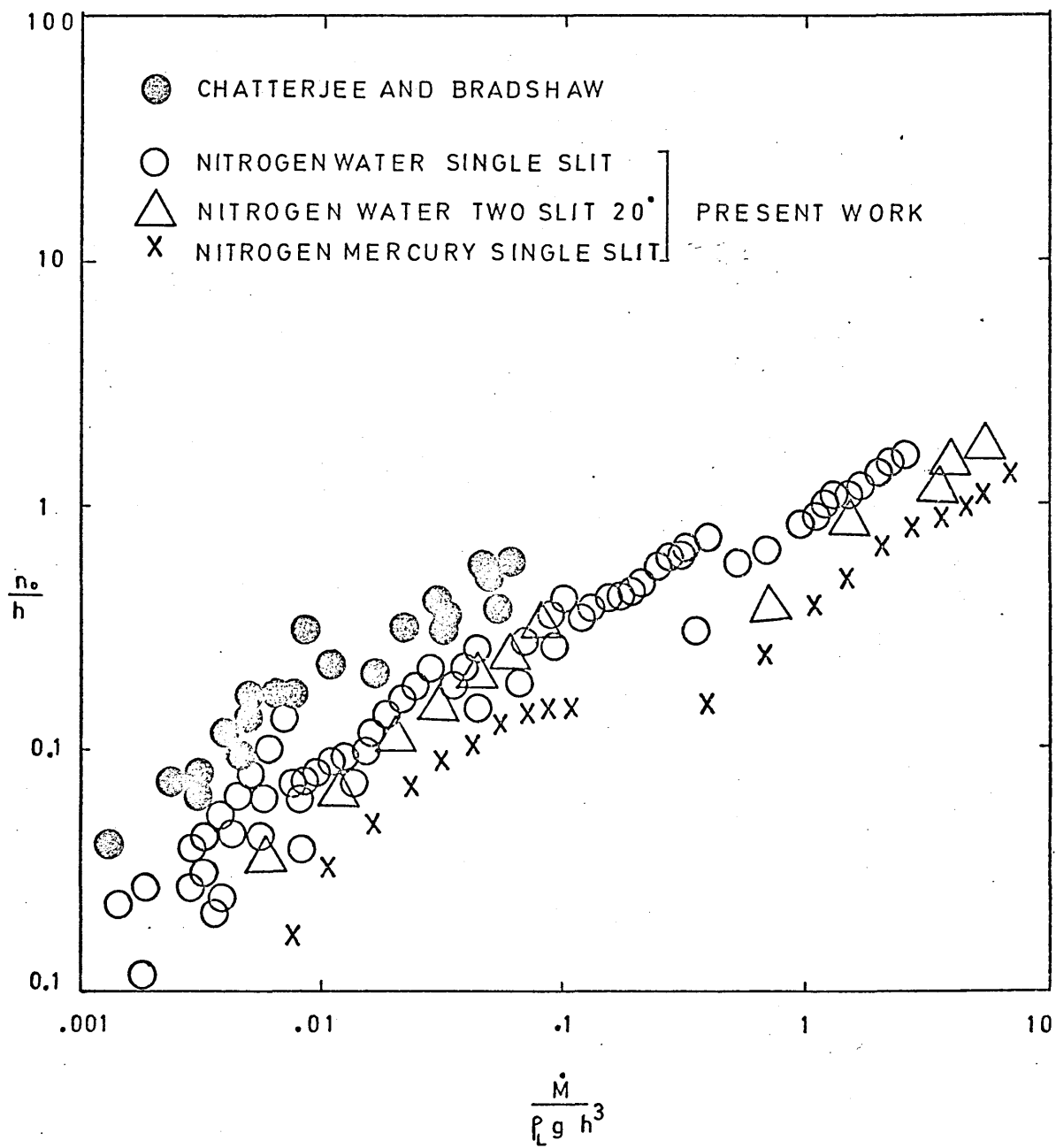


FIG 21 A PLOT OF DIMENSIONLESS JET MOMENTUM  $\left(\frac{\dot{M}}{\rho_L g h^3}\right)$   
 VERSUS DIMENSIONLESS DEPTH OF DEPRESSION  $\left(\frac{n_o}{h}\right)$

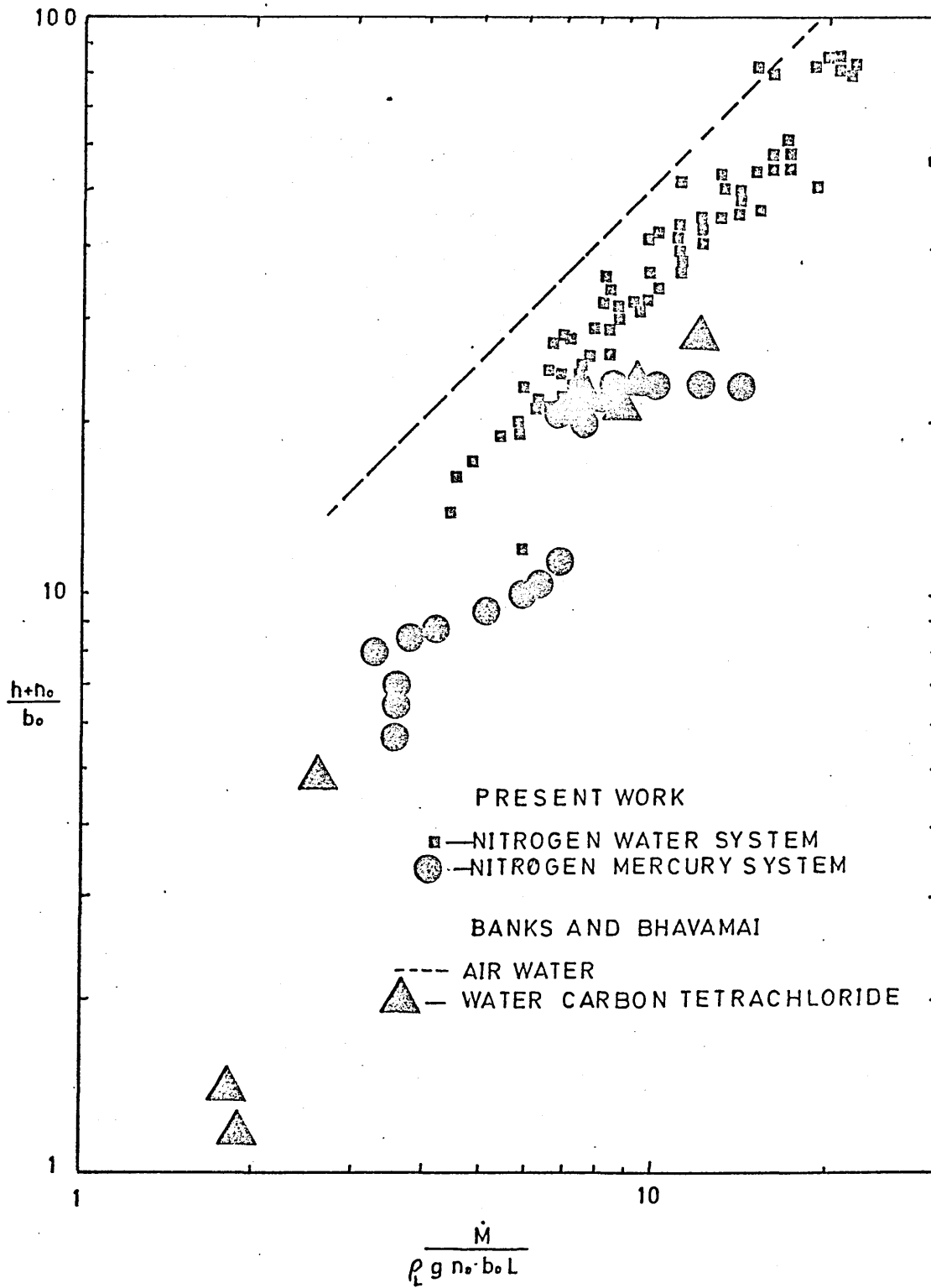


FIG. 22 A PLOT OF DIMENSIONLESS GROUPS  $\left(\frac{\dot{M}}{\rho_l g n_0 b_0 L}\right)$  VERSUS  $\left(\frac{h+n_0}{b_0}\right)$

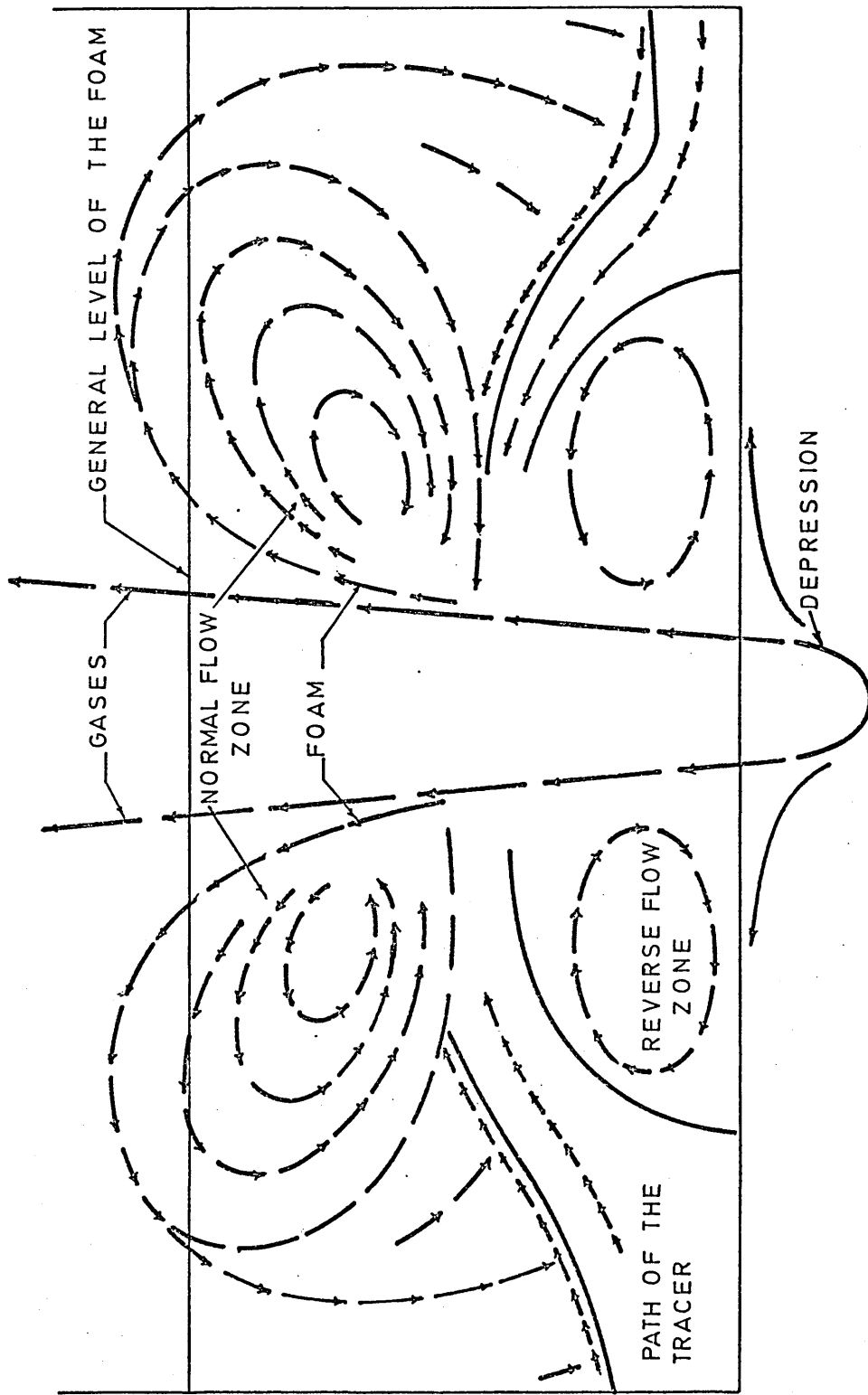
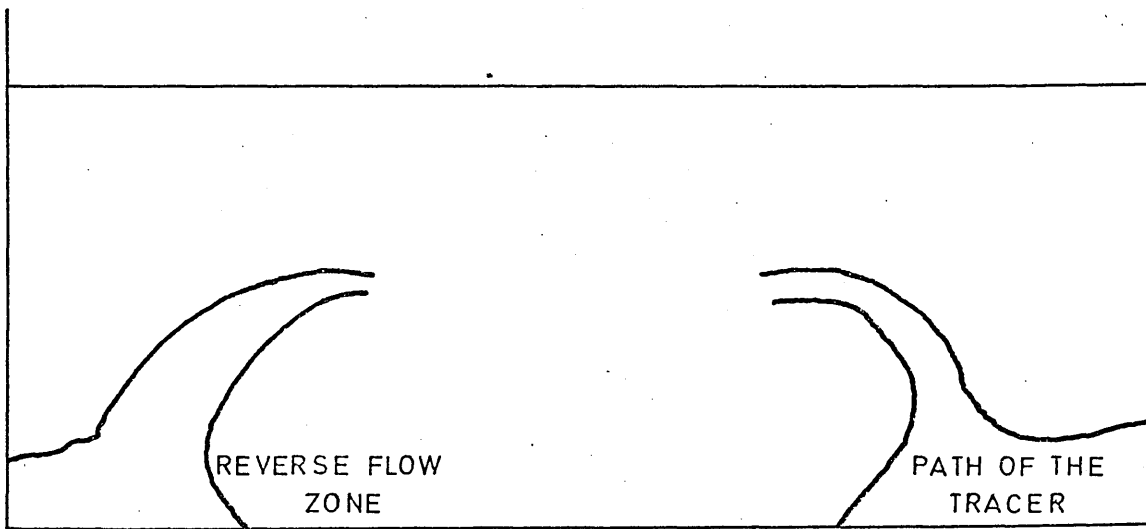
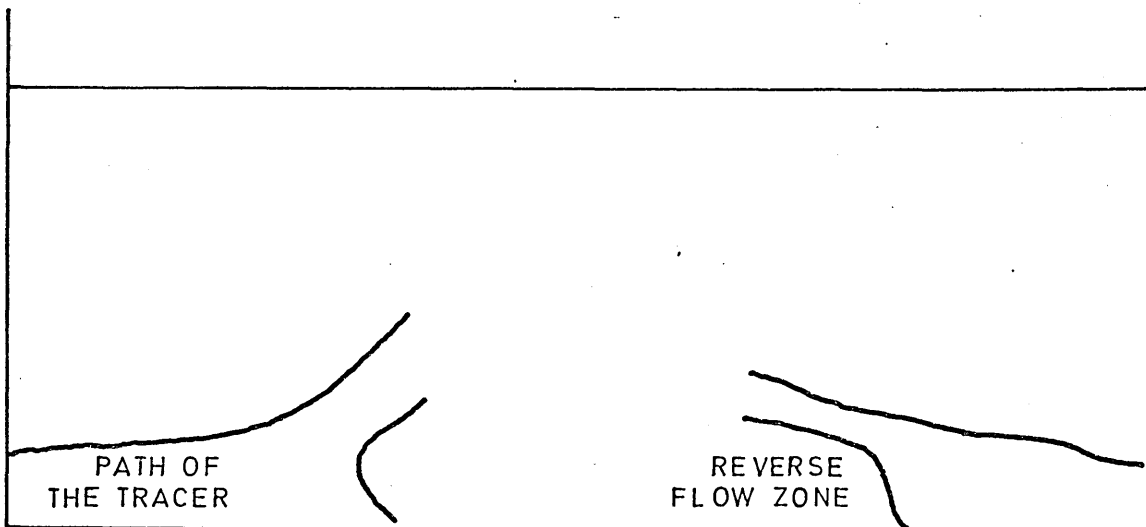


FIG. 23 A SCHEMATIC DIAGRAM OF THE STIRRING PATTERN IN THE MODEL REACTOR

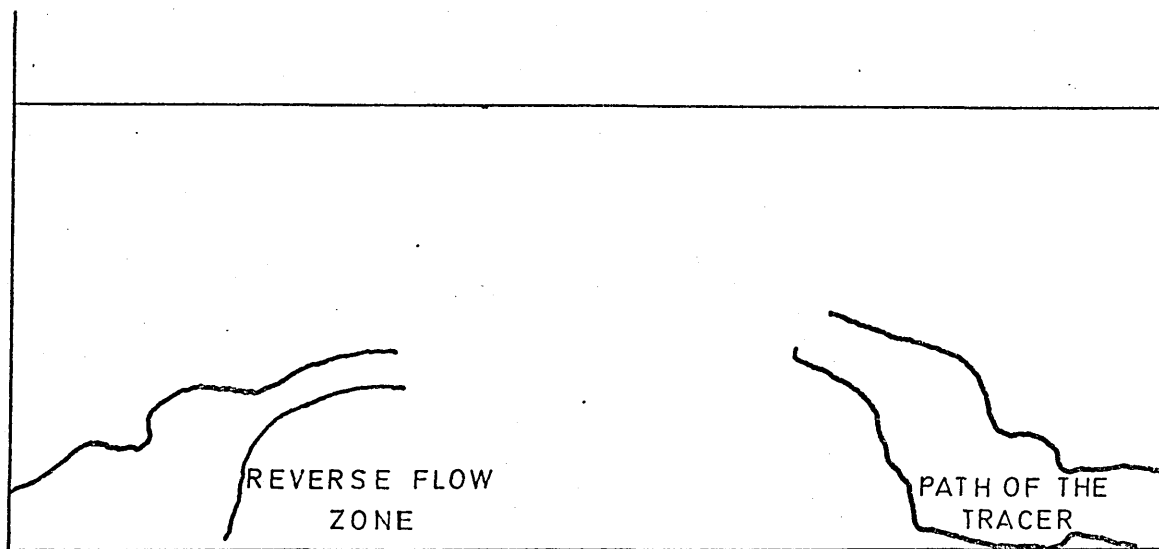


76.6 LITRES/MIN.

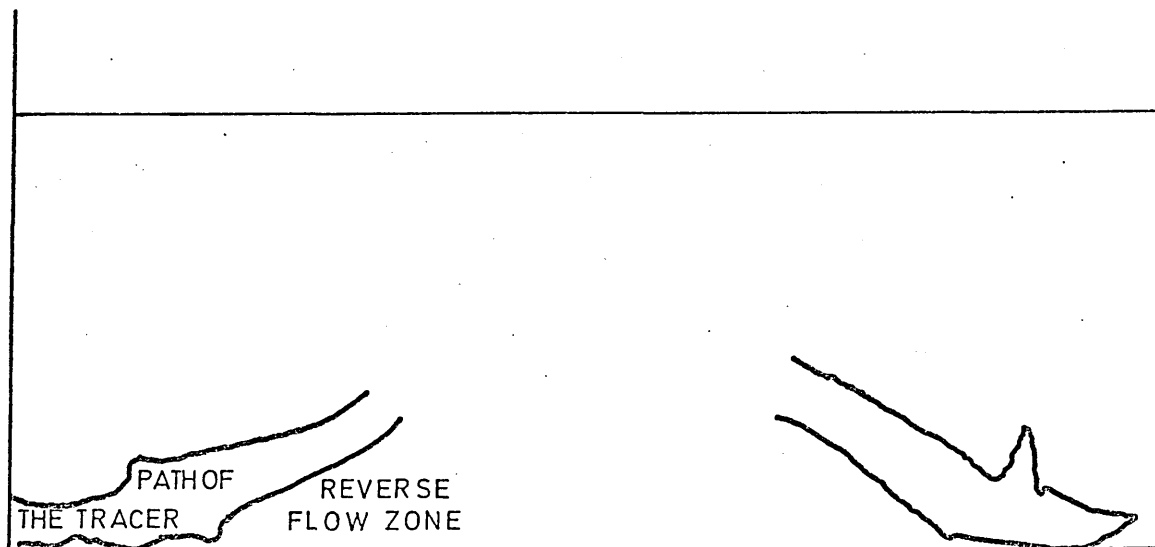


47.6 LITRES/MIN.

FIG. 24 THE EFFECT OF FLOW RATE ON THE SIZE AND SHAPE OF THE REVERSE FLOW ZONE. SINGLE SLIT NOZZLE  $h=0.2\text{CM}$ .

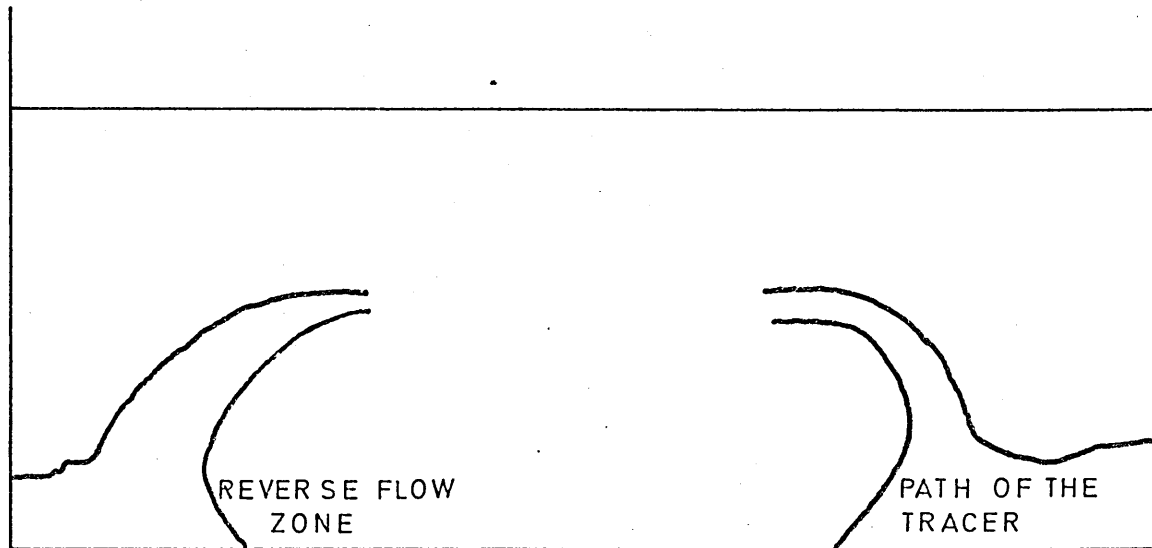


76.6 LITRES/MIN.

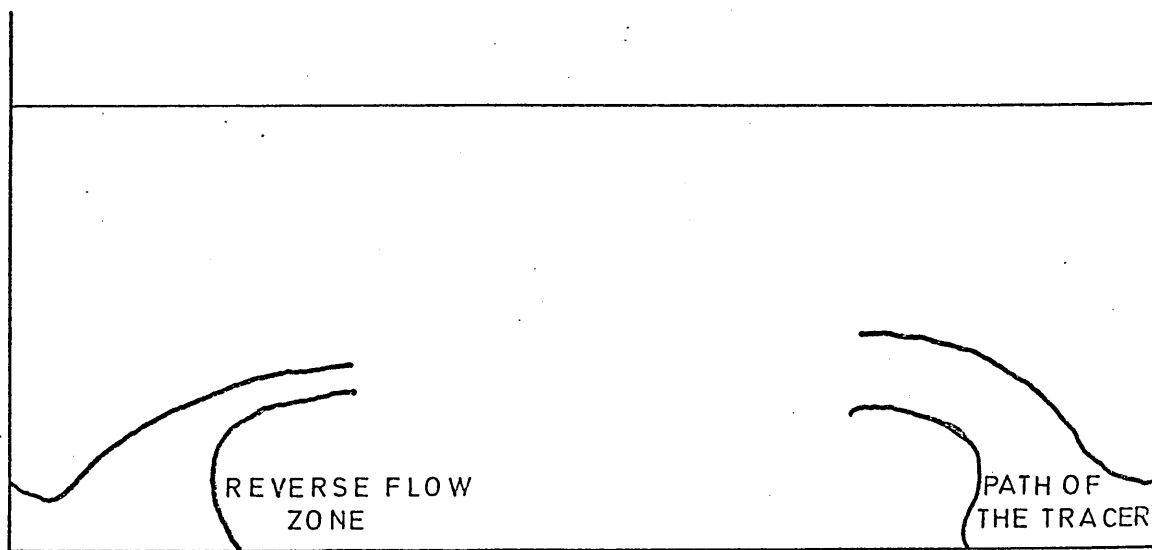


47.6 LITRES/MIN.

FIG. 2 5 THE EFFECT OF FLOW RATE ON THE SIZE AND SHAPE OF THE REVERSE FLOW ZONE. TWO SLIT NOZZLE  $h=0.2$  CM.

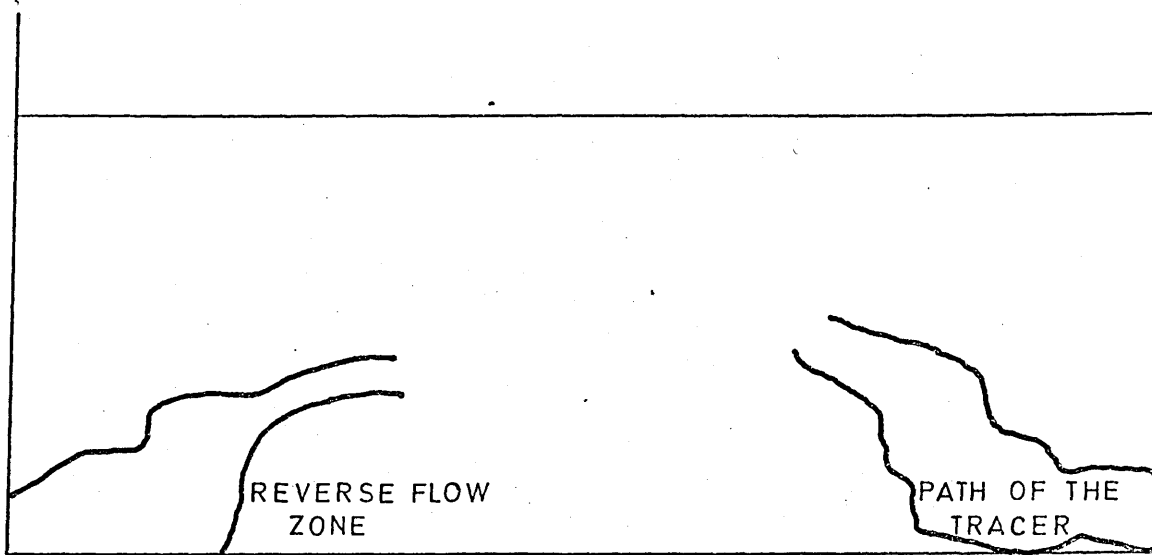


$h=0.2$  CM.

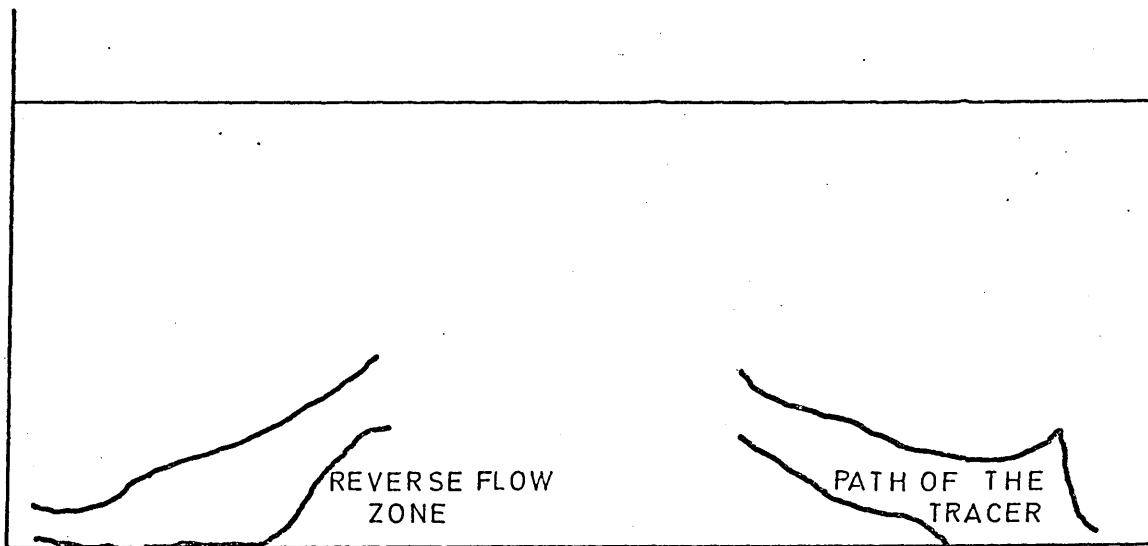


$h=1.2$  CM.

FIG. 26 THE EFFECT OF NOZZLE HEIGHT ON THE SIZE AND SHAPE OF THE REVERSE FLOW ZONE. SINGLE SLIT NOZZLE 76.6 LIT/MIN.

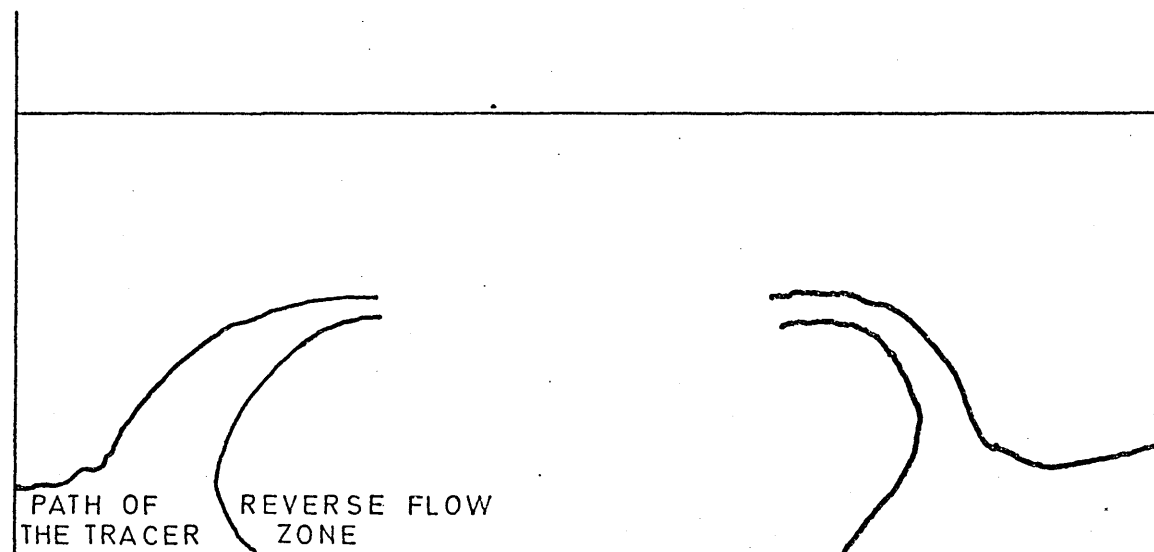


$h=0.2$  CM.

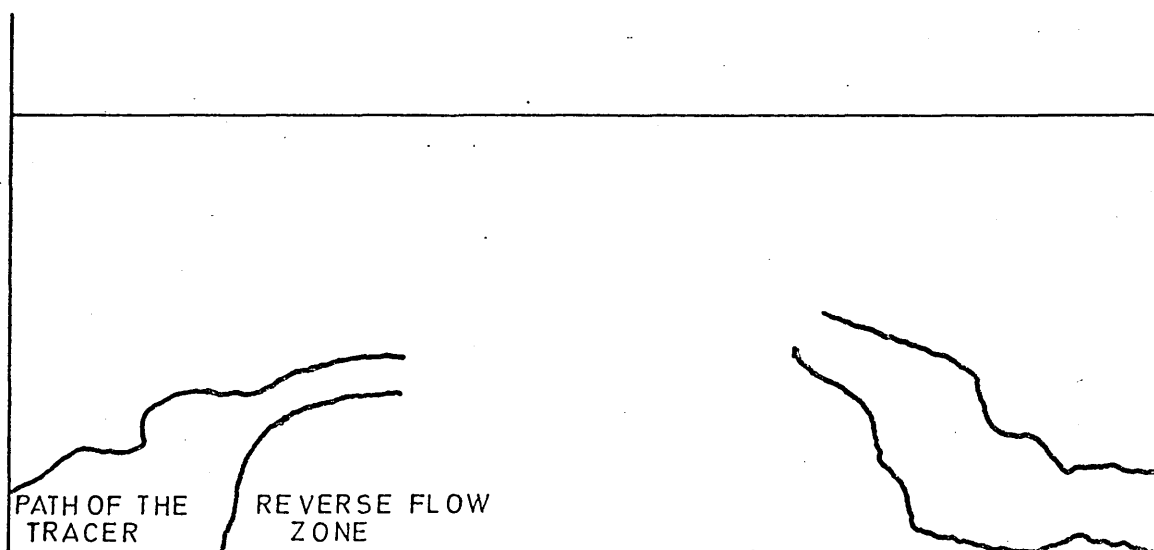


$h=0.8$  CM.

FIG 27 THE EFFECT OF NOZZLE HEIGHT ON THE SIZE AND SHAPE OF THE REVERSE FLOW ZONE. TWO SLIT NOZZLE 76.6 LIT./MIN.



SINGLE SLIT



TWO SLIT 20°

FIG. 28 THE EFFECT OF NOZZLE TYPE ON THE SIZE AND SHAPE OF THE REVERSE FLOW ZONE.  $h=0.2\text{CM}$ . 76.6 LITRES/MIN.

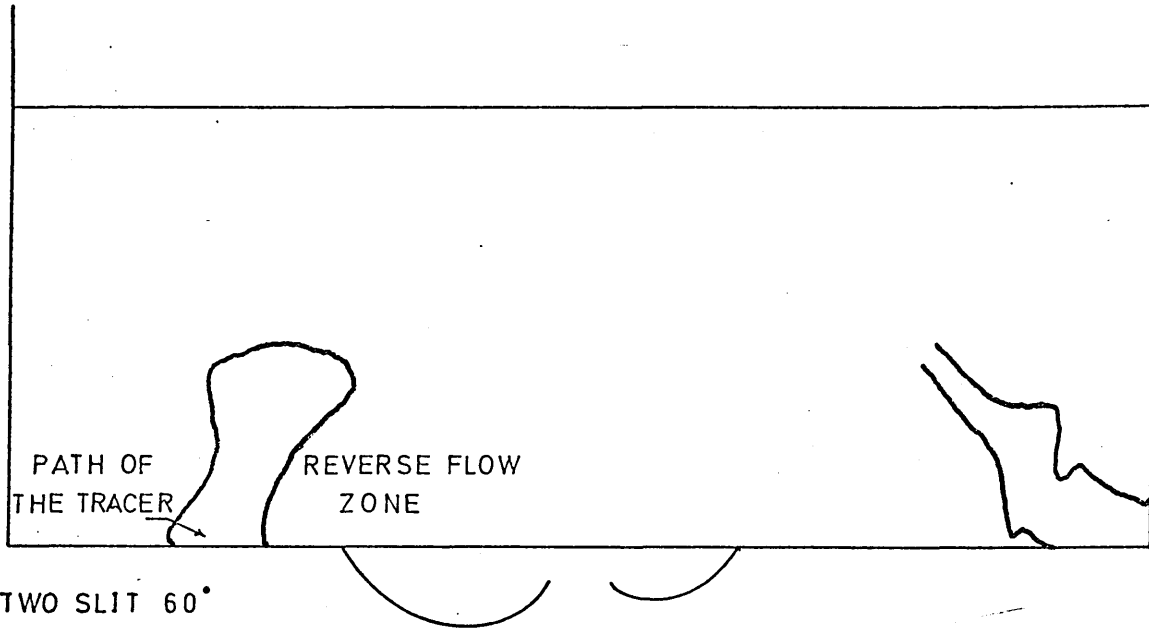
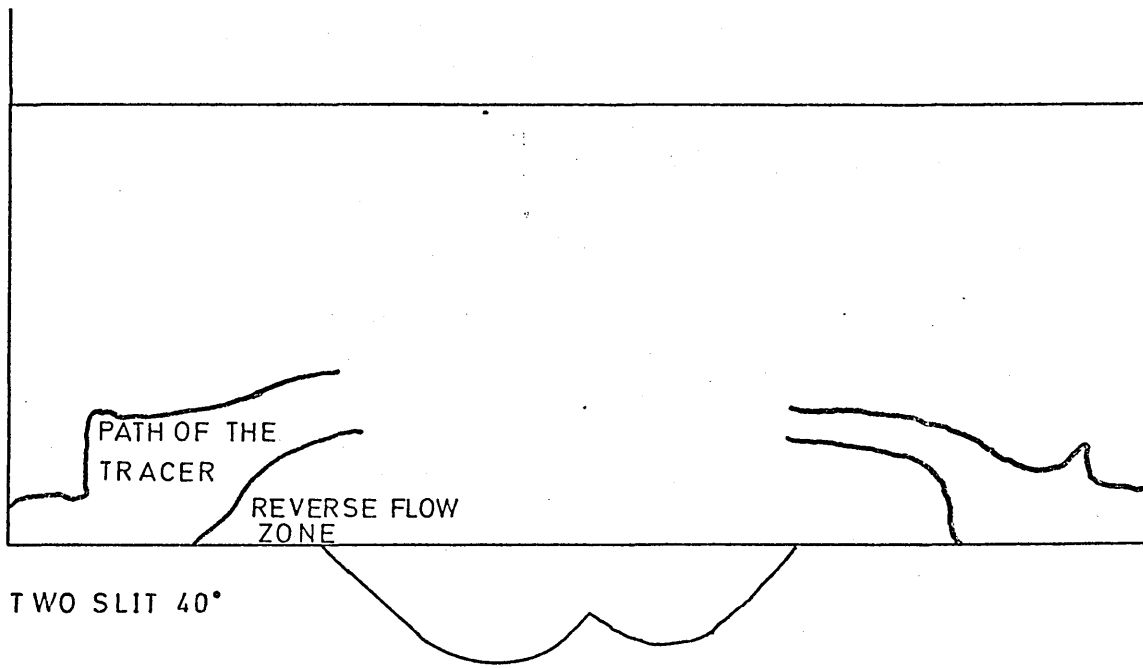
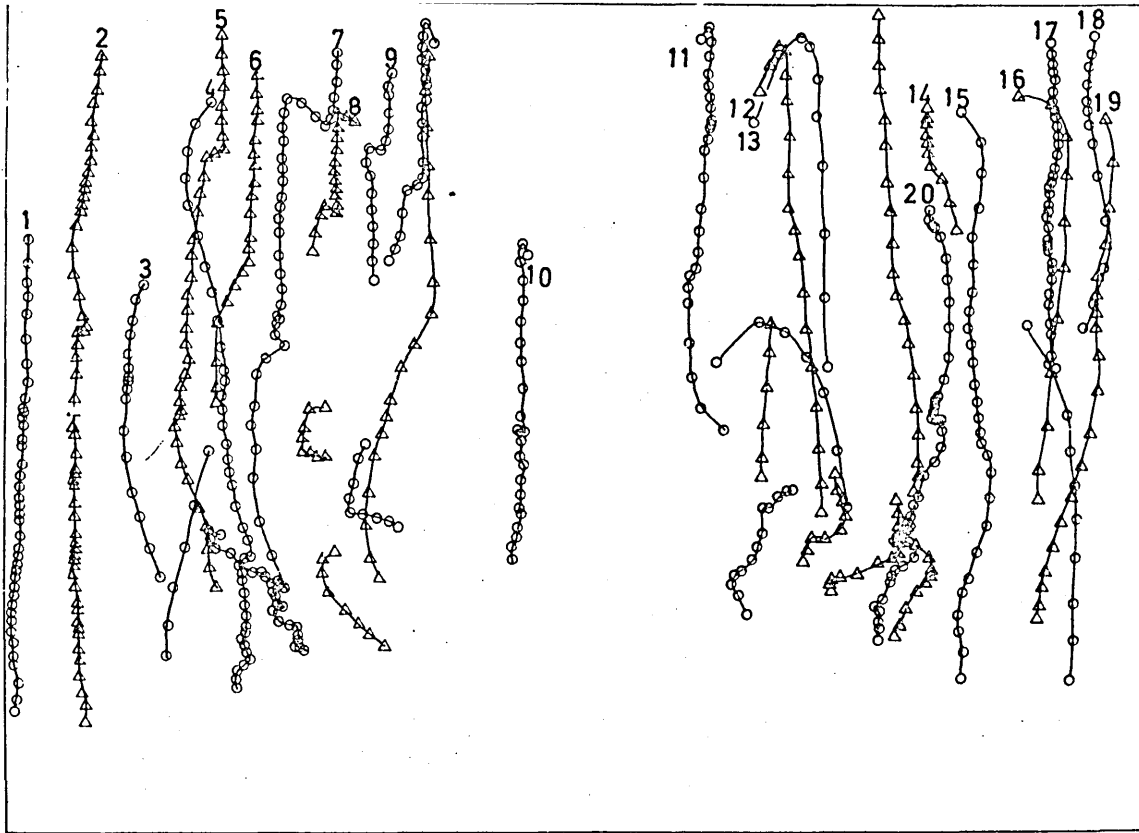
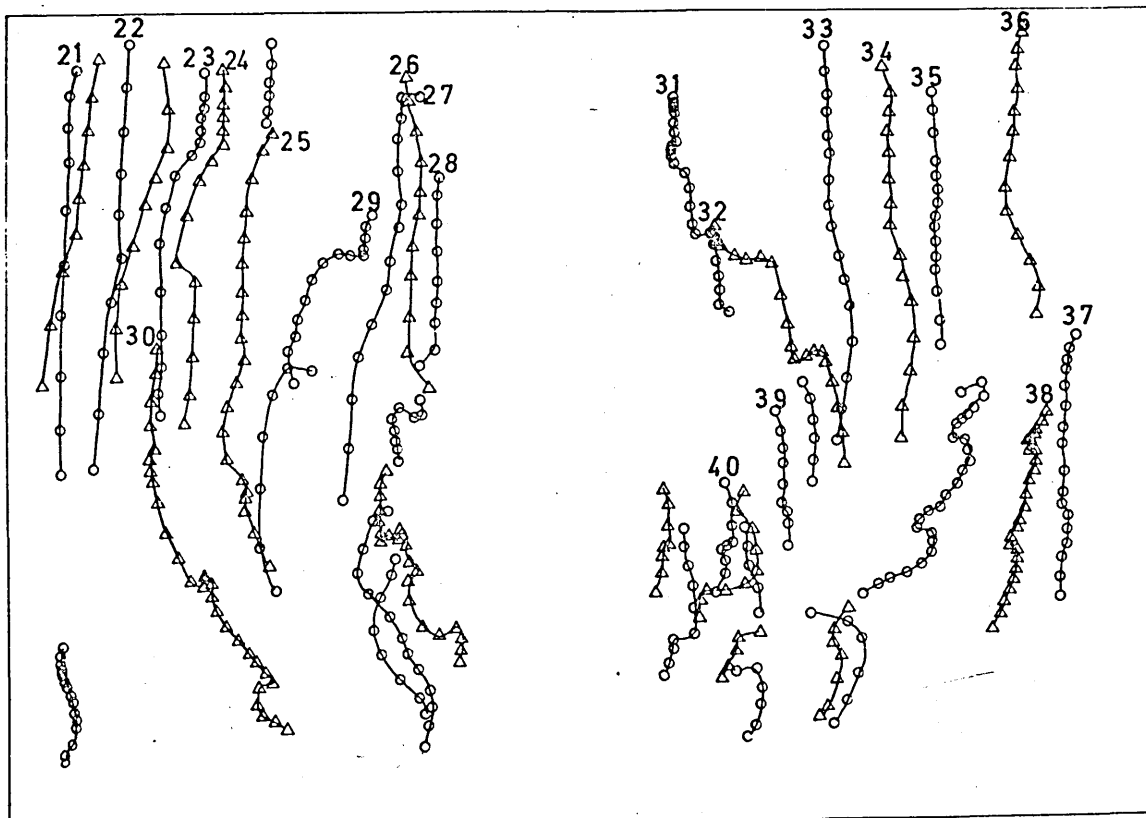


FIG. 29 THE EFFECT OF NOZZLE TYPE ON THE SIZE AND SHAPE OF THE REVERSE FLOW ZONE.  $h=0.2\text{CM}$ . 76.6 LIT./MIN.

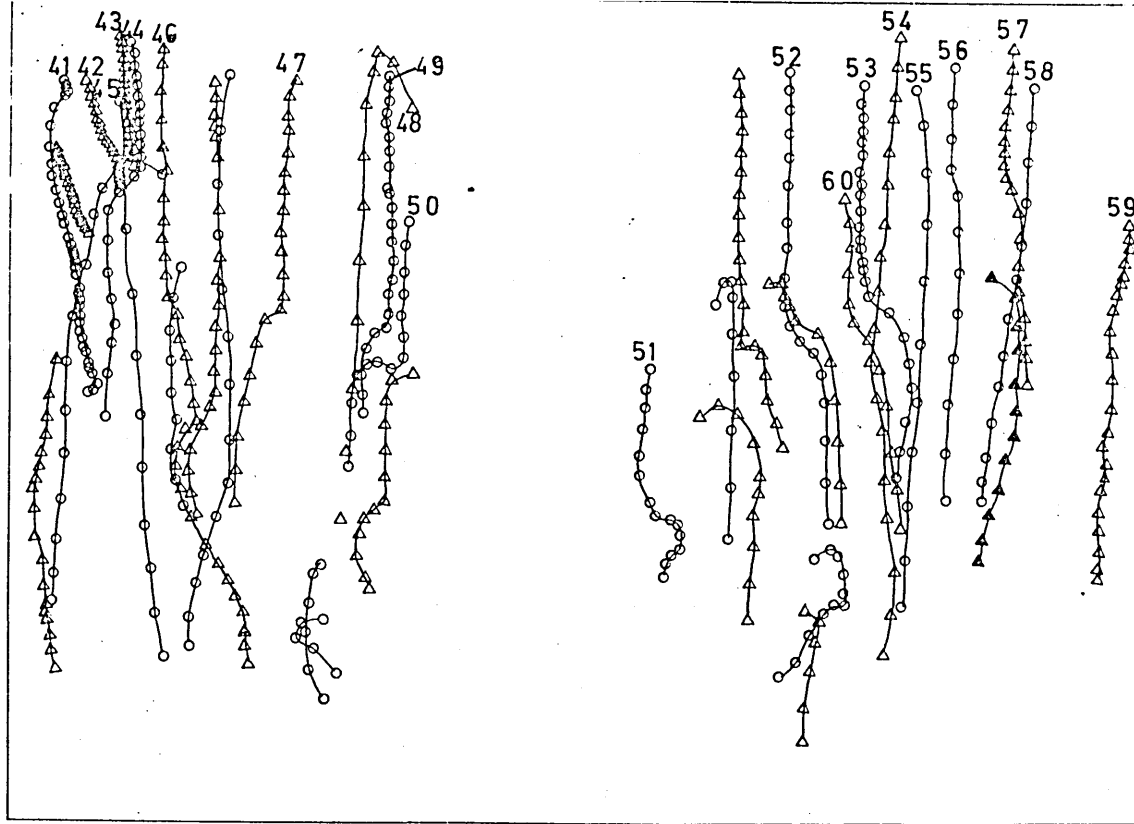


$h=0.2\text{ CM}$  76.6 LITRES/MIN SINGLE SLIT NOZZLE

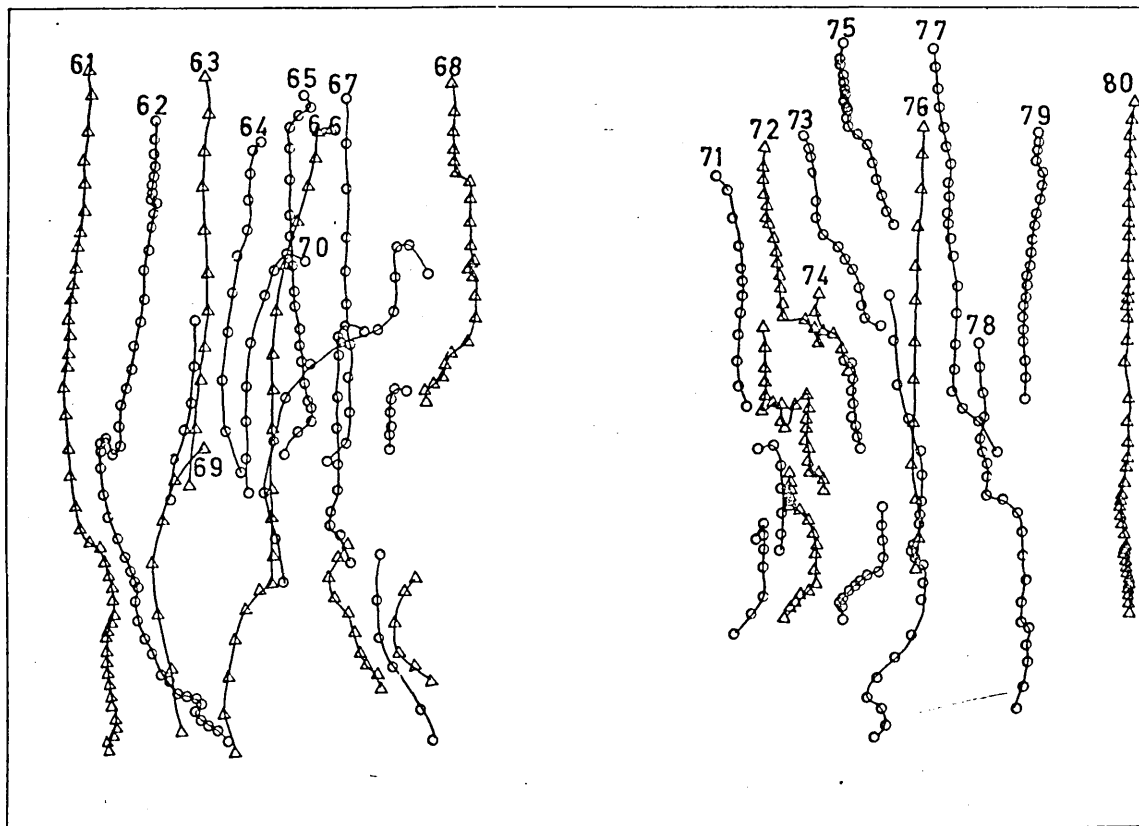


$h=0.2\text{ CM}$  47.6 LITRES/MIN SINGLE SLIT NOZZLE

FIG. 30 THE PATHS OF THE DROPLETS FALLING THROUGH THE FOAM



$h=1.2$  CM 76.6 LITRES/MIN SINGLE SLIT NOZZLE



$h=0.2$  CM 76.6 LITRES/MIN TWO SLIT  $20^\circ$  NOZZLE

FIG. 31 THE PATHS OF THE DROPLETS FALLING THROUGH THE FOAM

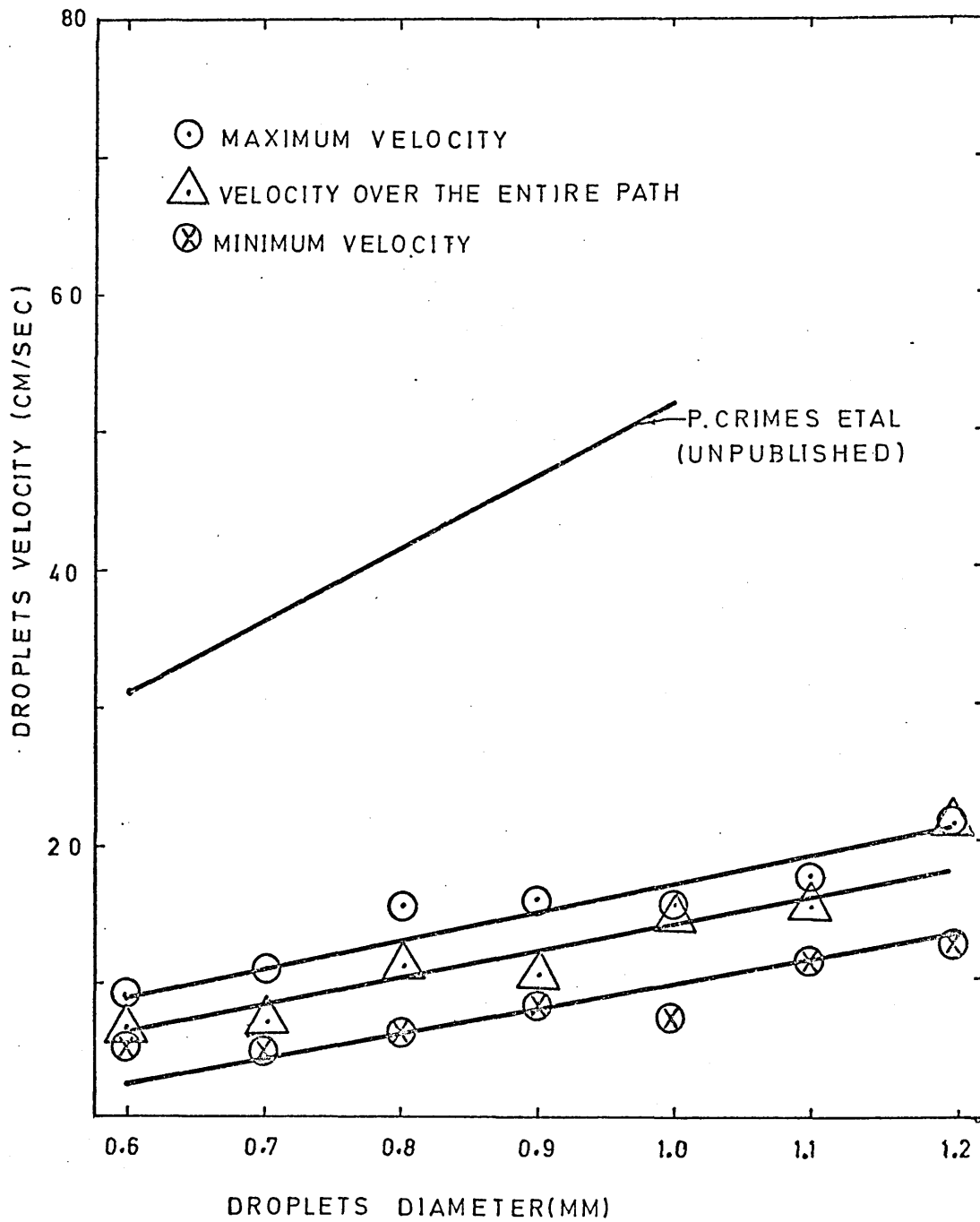
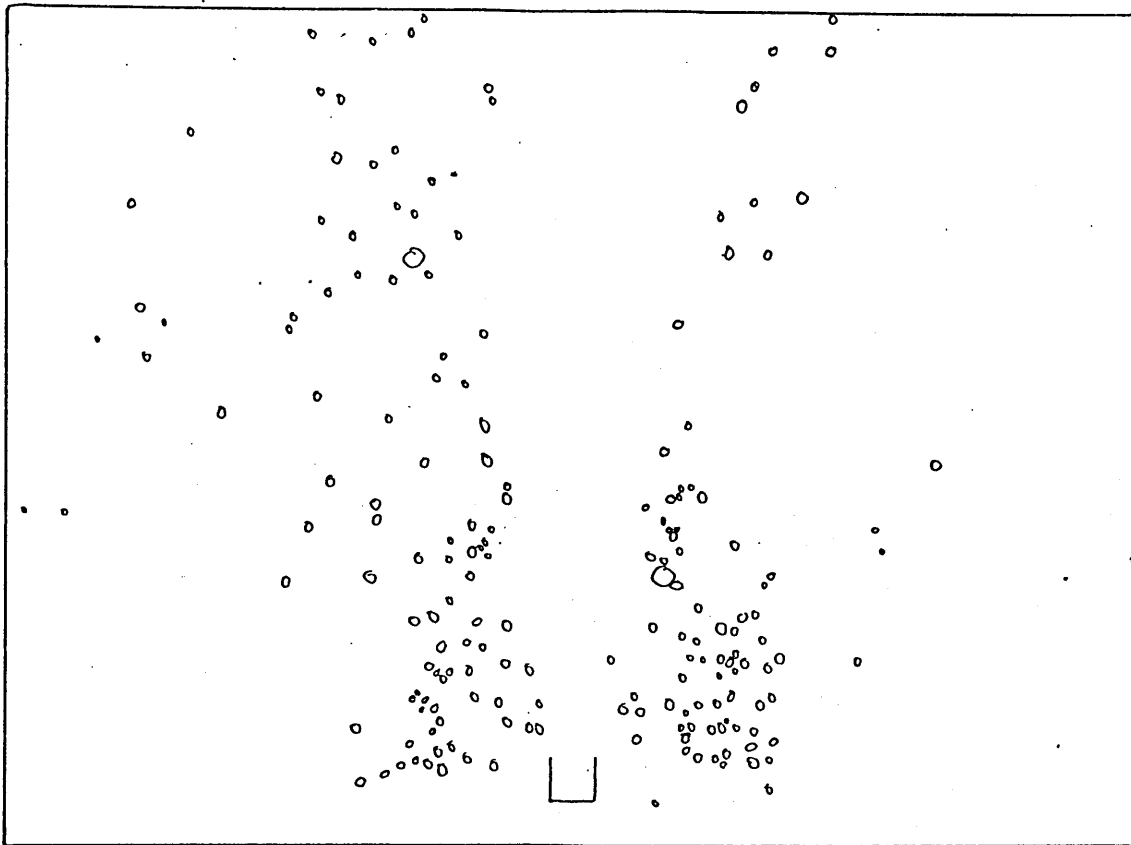


FIG. 32 THE VELOCITY OF THE DROPLETS FALLING THROUGH THE FOAM

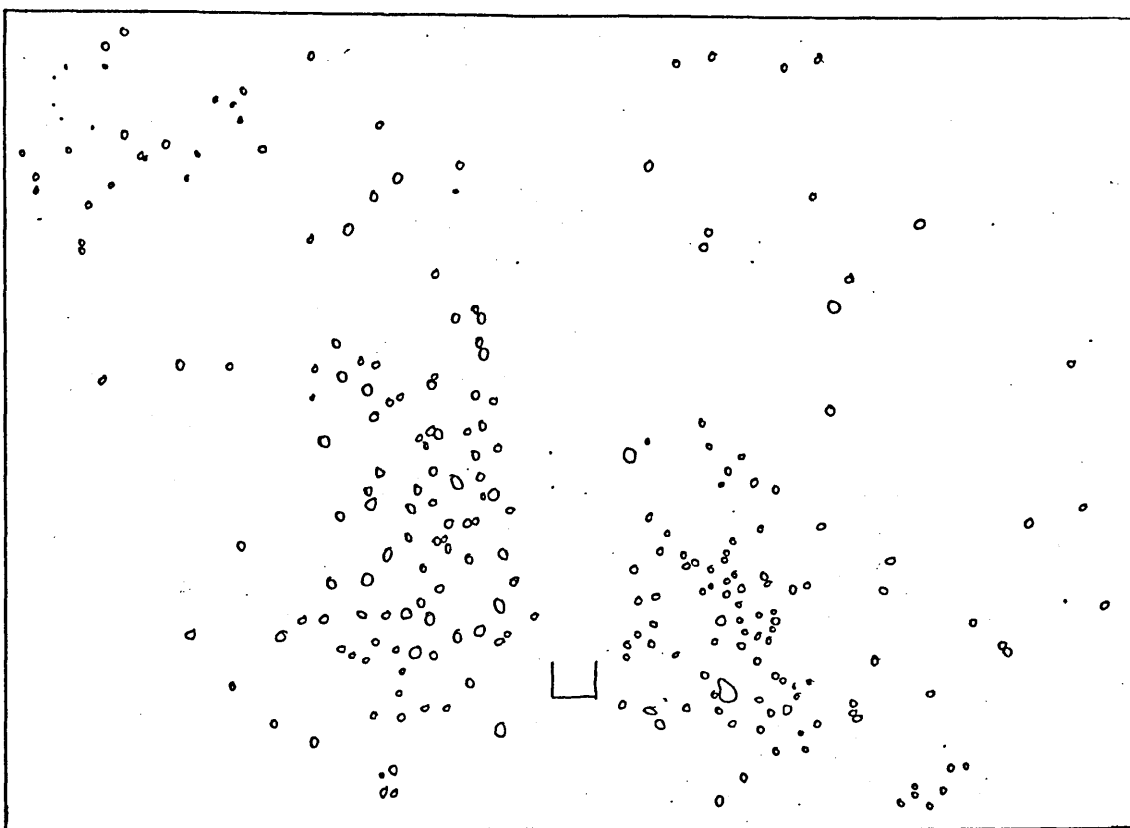


$h=0.2\text{CM.}$  76.6 LITRES/MIN SINGLE SLIT NOZZLE

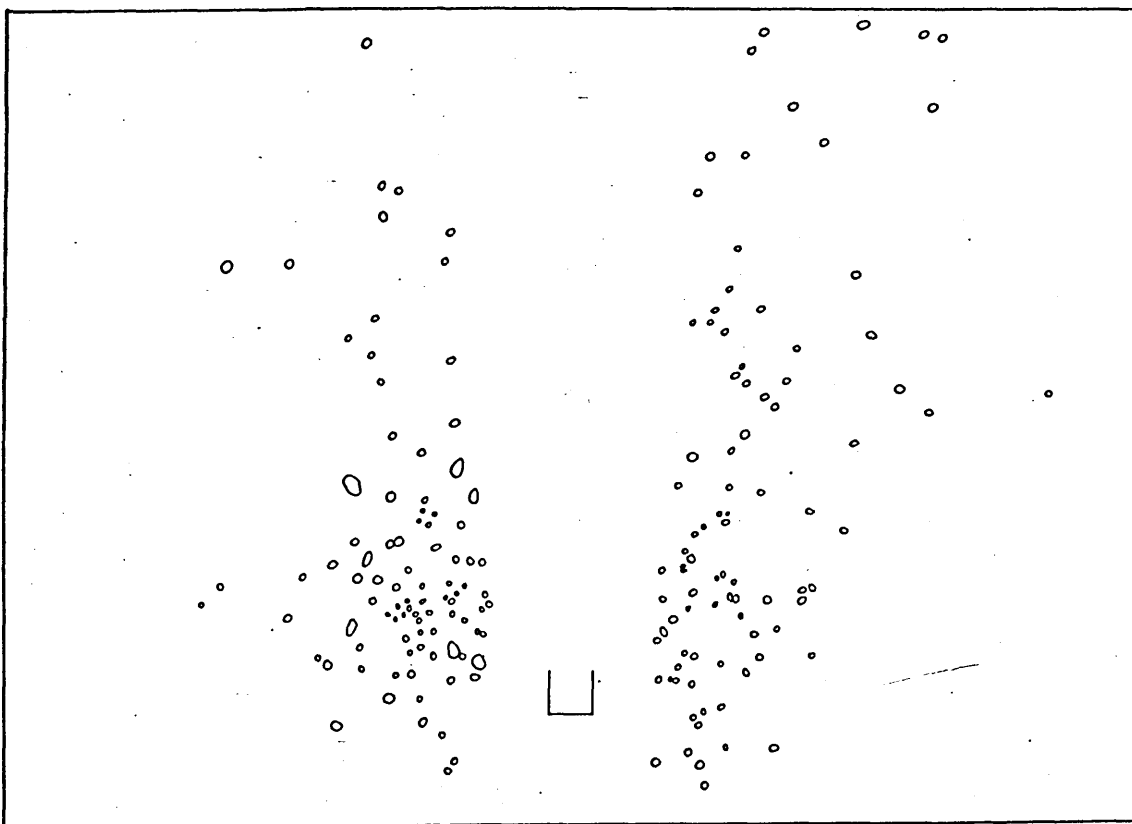


$h=0.2\text{CM.}$  47.6 LITRES/MIN SINGLE SLIT NOZZLE

FIG.33 THE DISTRIBUTION OF DROPLETS IN THE FOAM

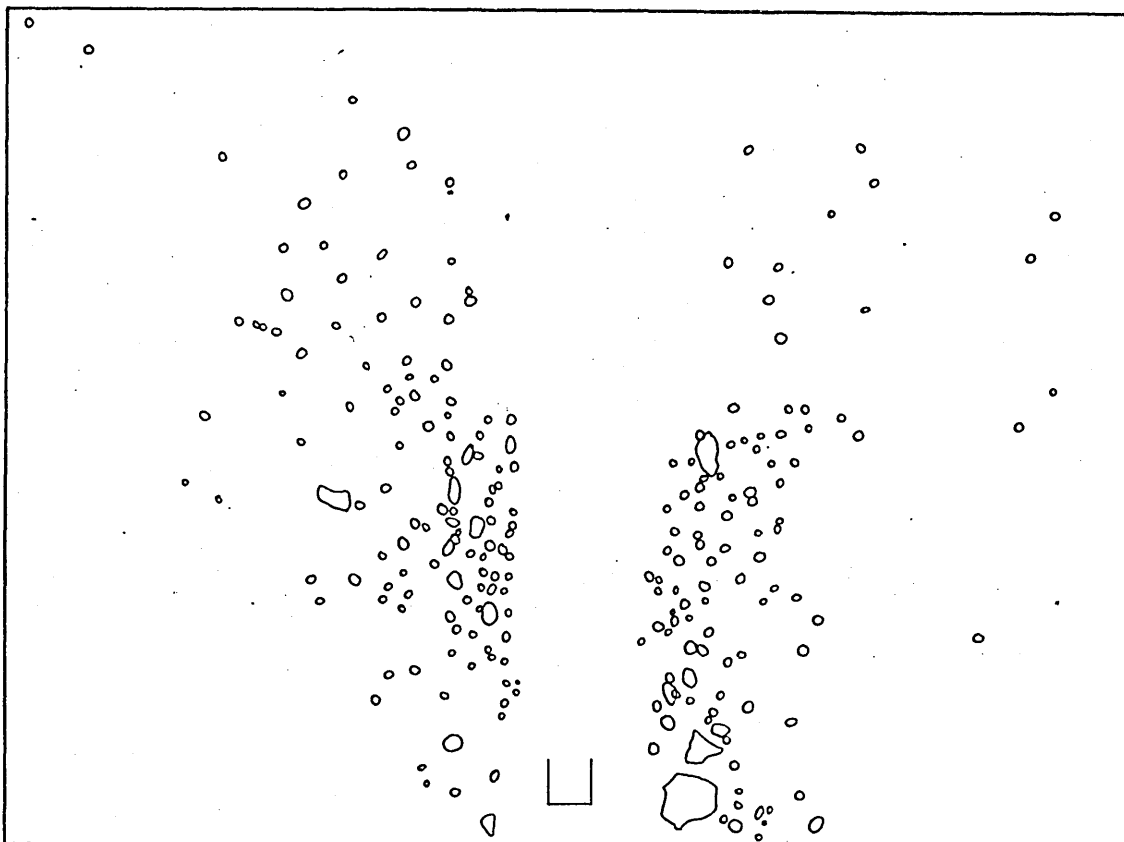


$h=1.2$  CM. 76.6 LITRES/MIN SINGLE SLIT NOZZLE

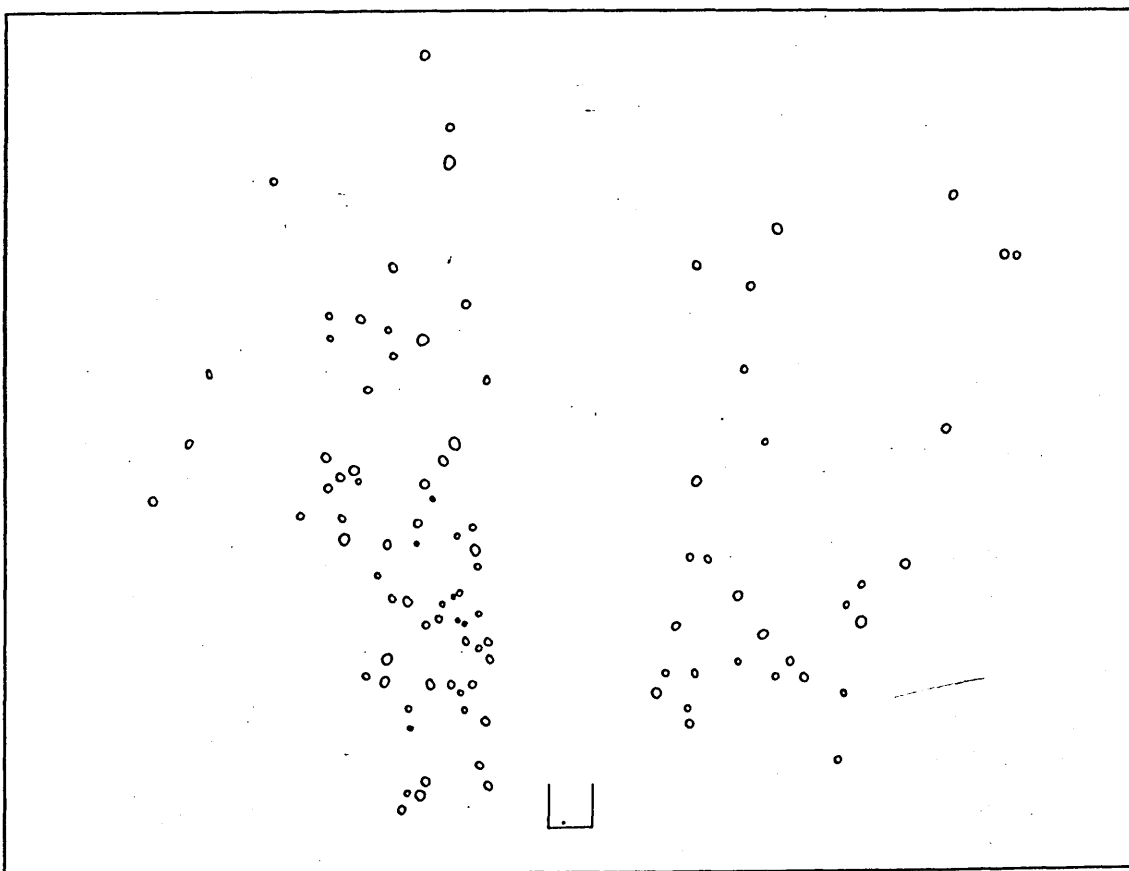


$h=0.8$  CM 76.6 LITRES/MIN TWO SLIT 20° NOZZLE

FIG.34 THE DISTRIBUTION OF DROPLETS IN THE FOAM



$h=0.2$  CM    76.6 LITRES/MIN    TWO SLIT 20° NOZZLE



$h=0.2$  CM    47.6 LITRES/MIN    TWO SLIT 20° NOZZLE

FIG. 35 THE DISTRIBUTION OF DROPLETS IN THE FOAM

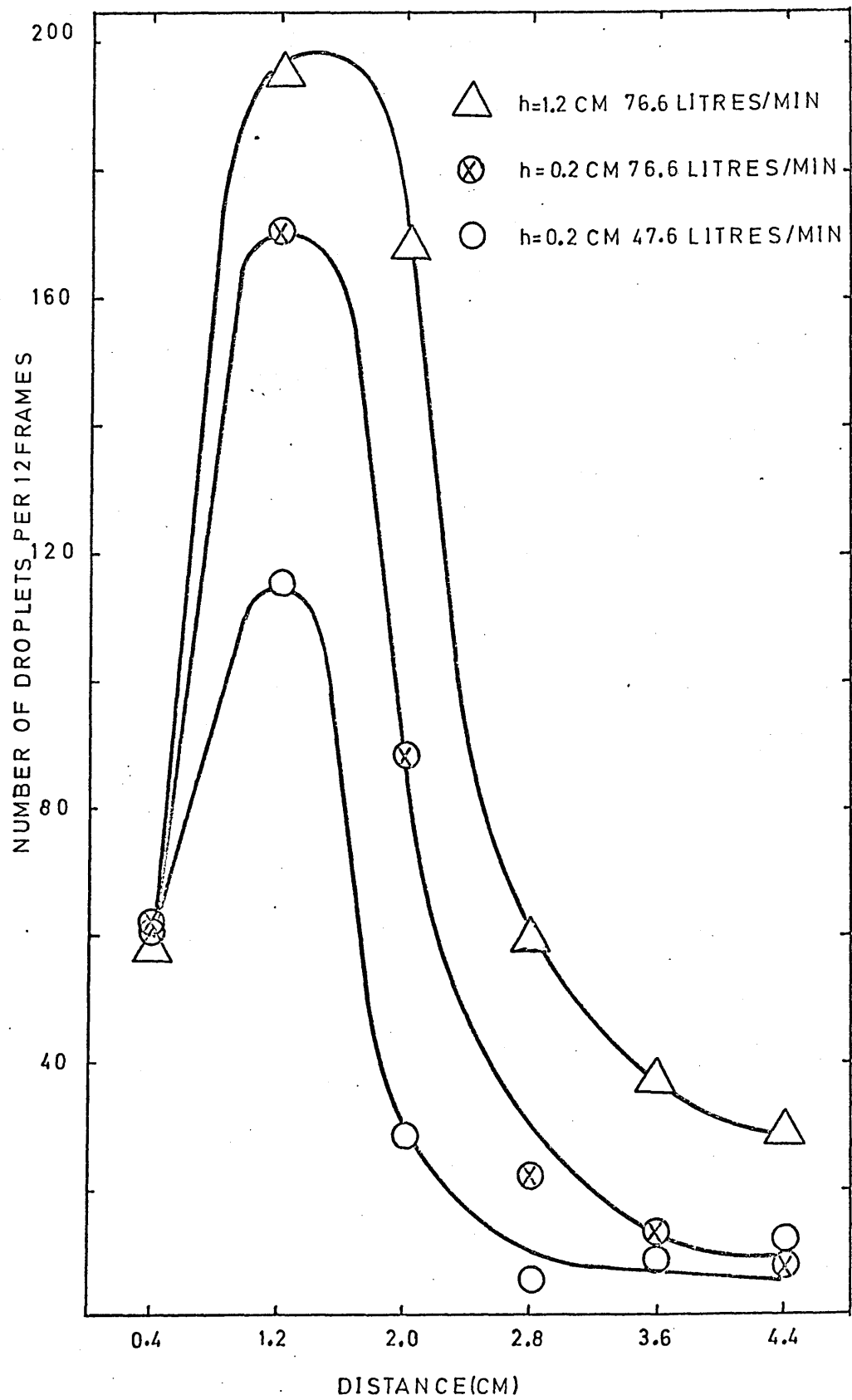


FIG. 36. THE DISTRIBUTION OF DROPLETS WITH HORIZONTAL DISTANCE FROM THE NOZZLE CENTRE LINE. SINGLE SLIT NOZZLE

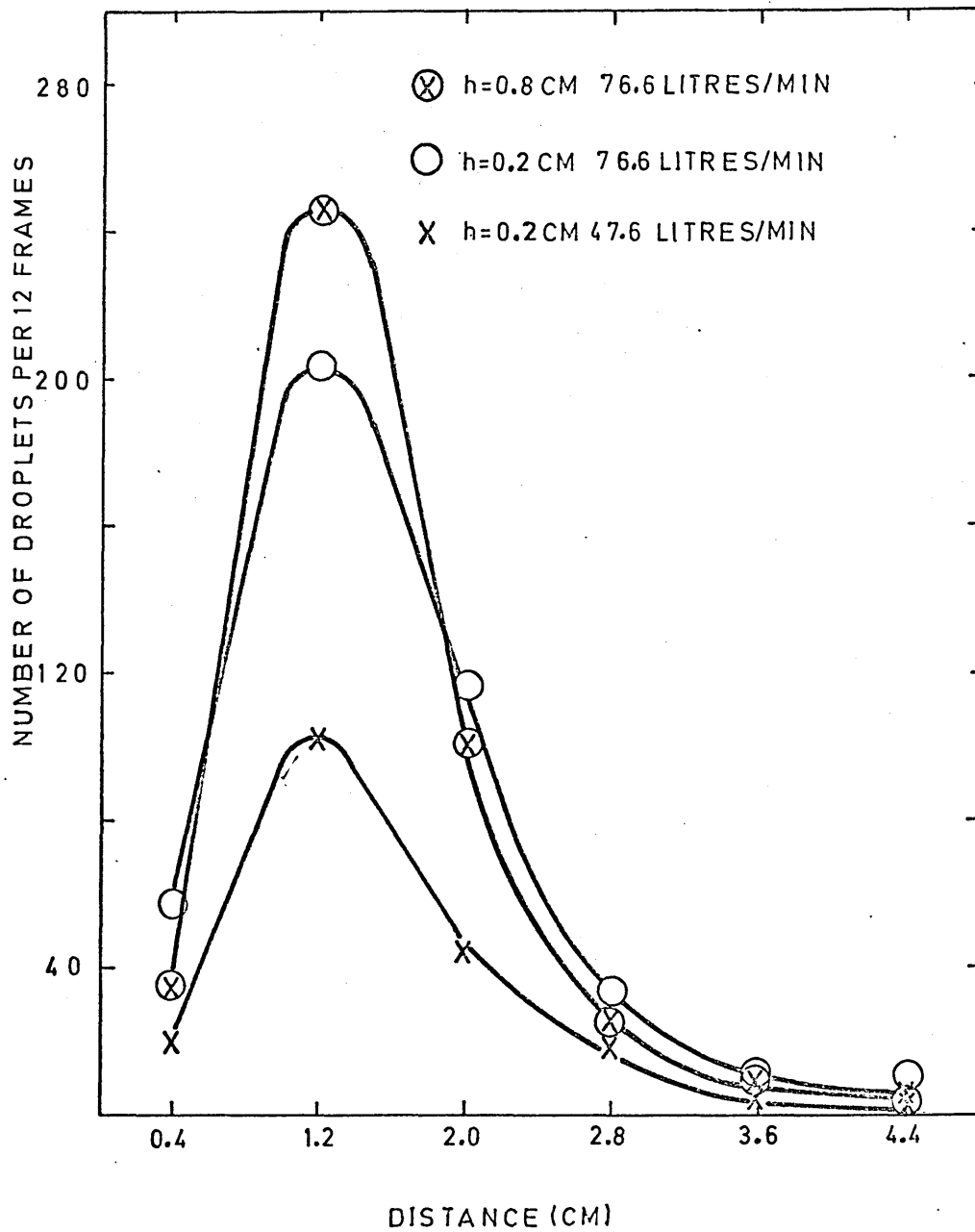


FIG. 37 THE DISTRIBUTION OF DROPLETS WITH HORIZONTAL DISTANCE FROM THE NOZZLE CENTRE LINE. TWO SLIT NOZZLE

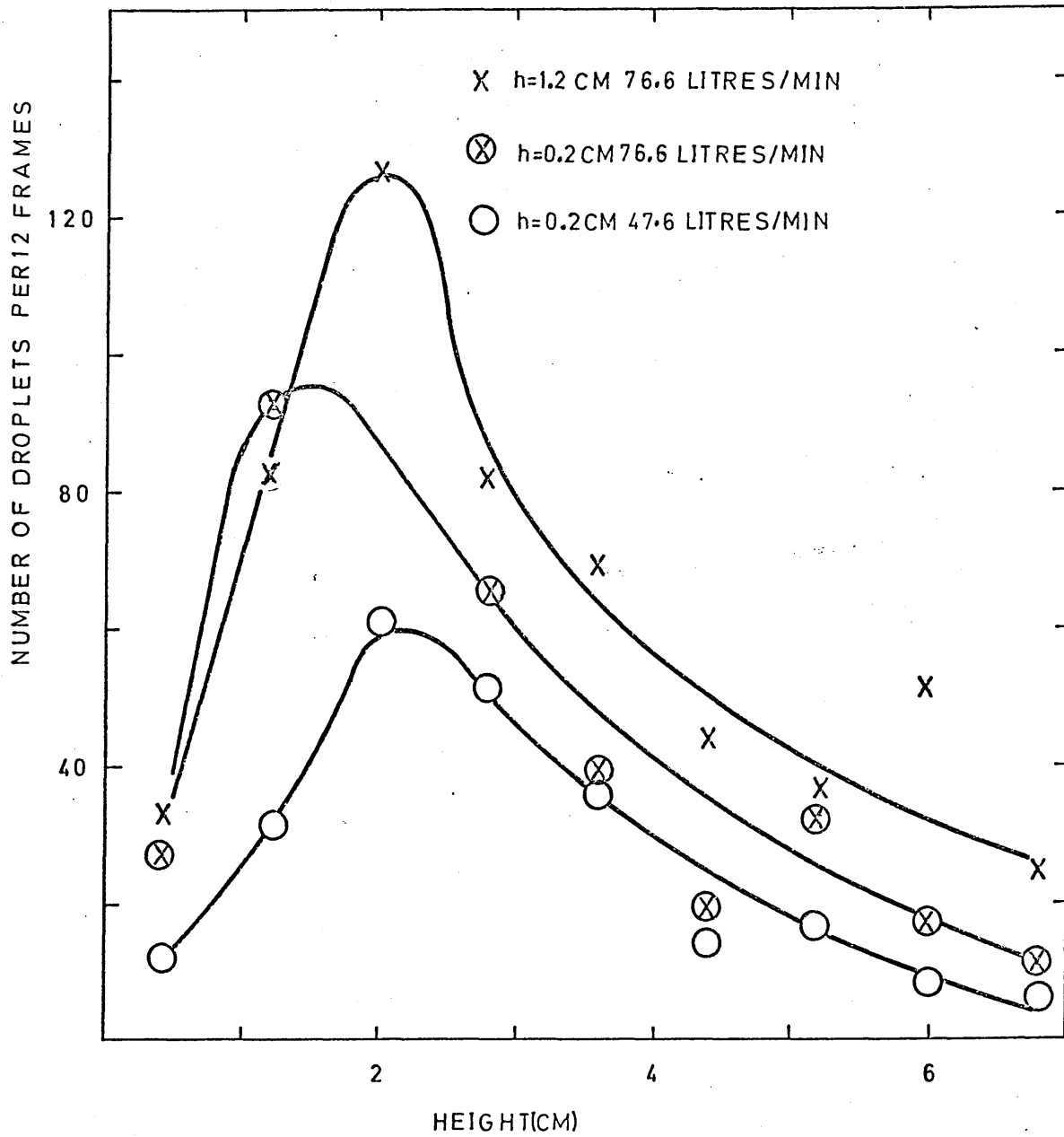


FIG 38 THE VERTICAL DISTRIBUTION OF DROPLETS FOR THE SINGLE SLIT NOZZLE

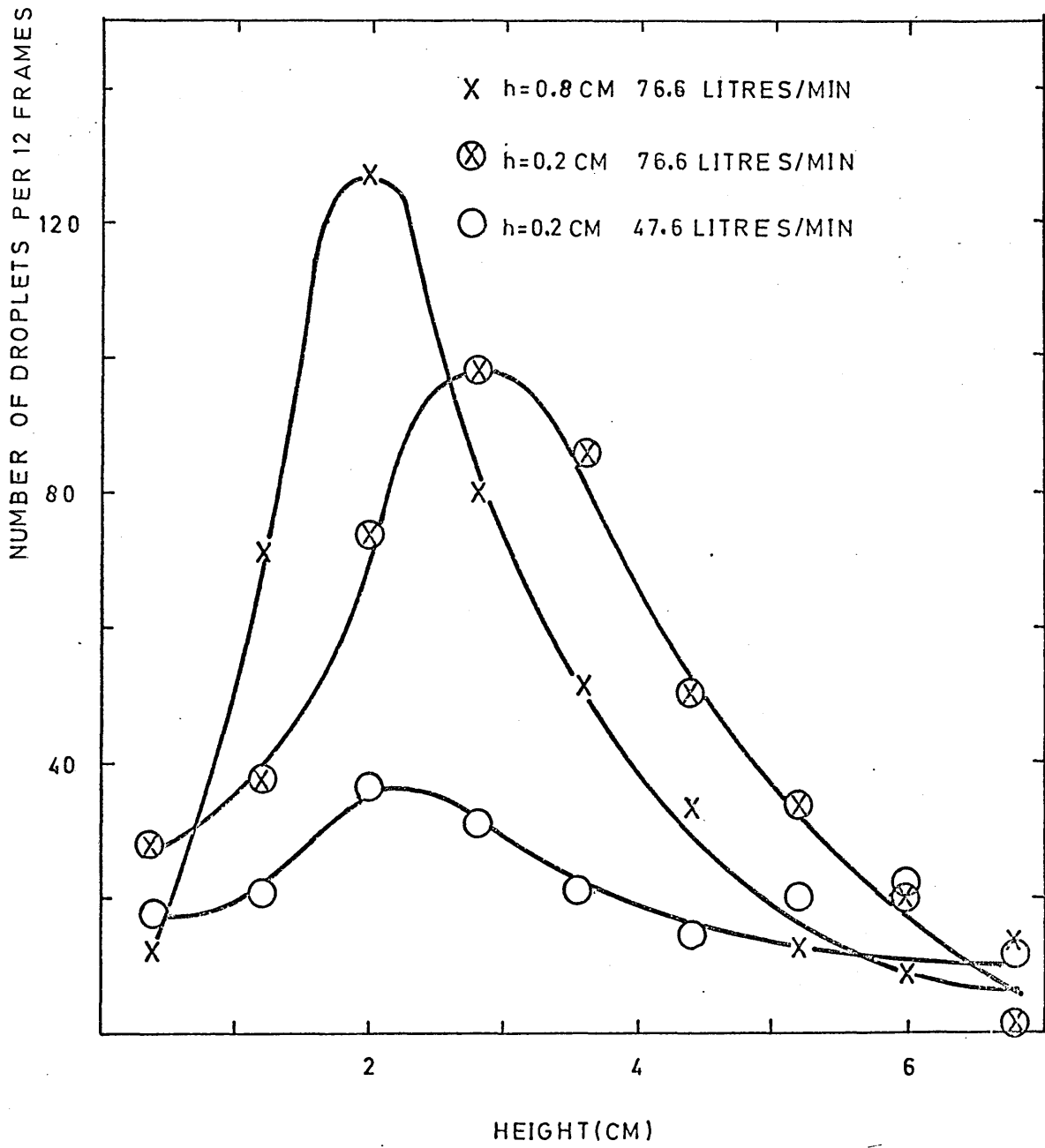


FIG. 39 THE VERTICAL DISTRIBUTION OF DROPLETS FOR THE TWO SLIT 20° NOZZLE

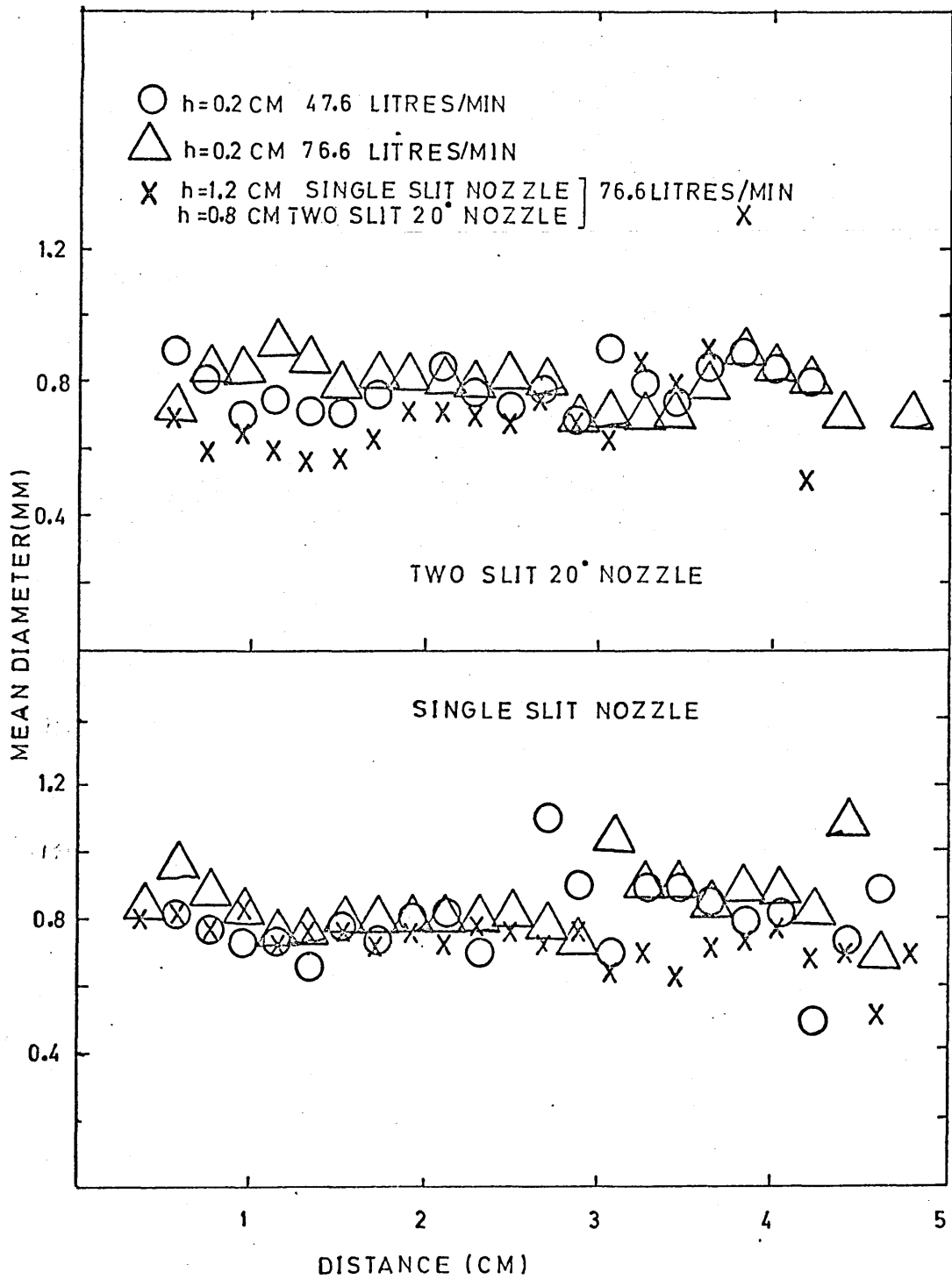


FIG 40 THE SIZE DISTRIBUTION OF DROPLETS WITH DISTANCE FROM THE NOZZLE CENTRE LINE

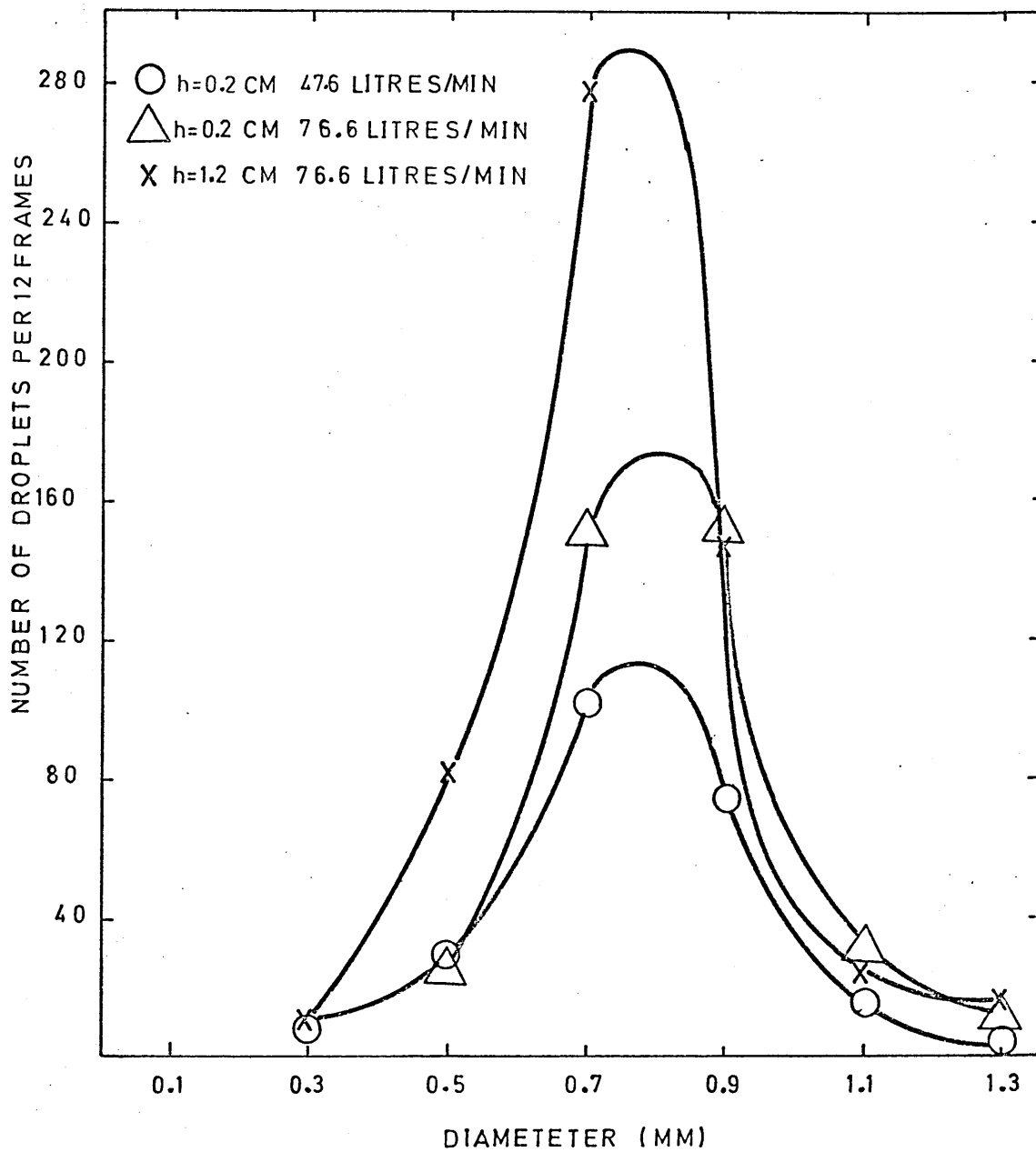


FIG. 41 THE FREQUENCY DISTRIBUTION OF DROPLETS SIZES FOR THE SINGLE SLIT NOZZLE

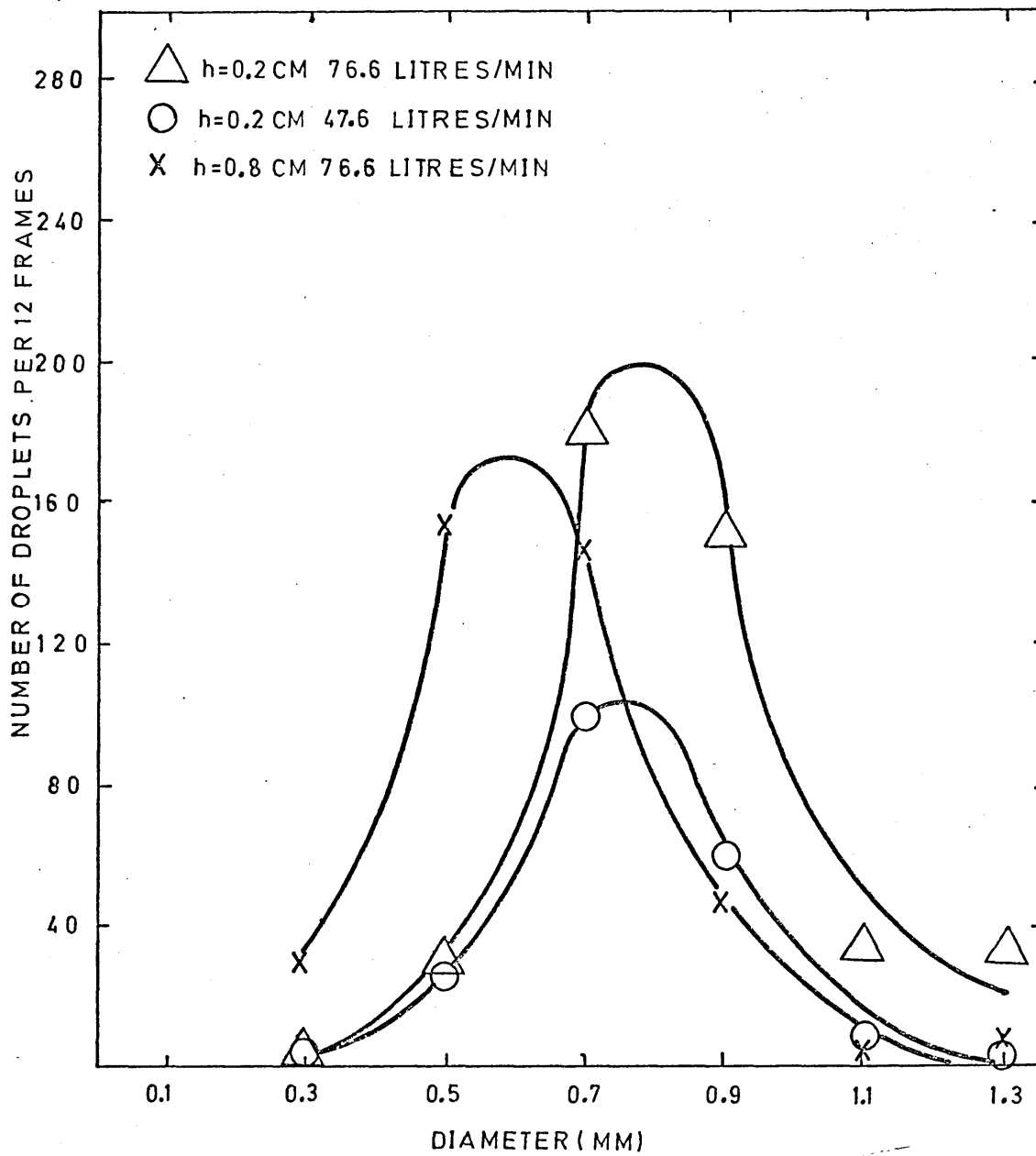


FIG. 42 THE FREQUENCY DISTRIBUTION OF DROPLETS SIZES FOR THE TWO SLIT 20° NOZZLE

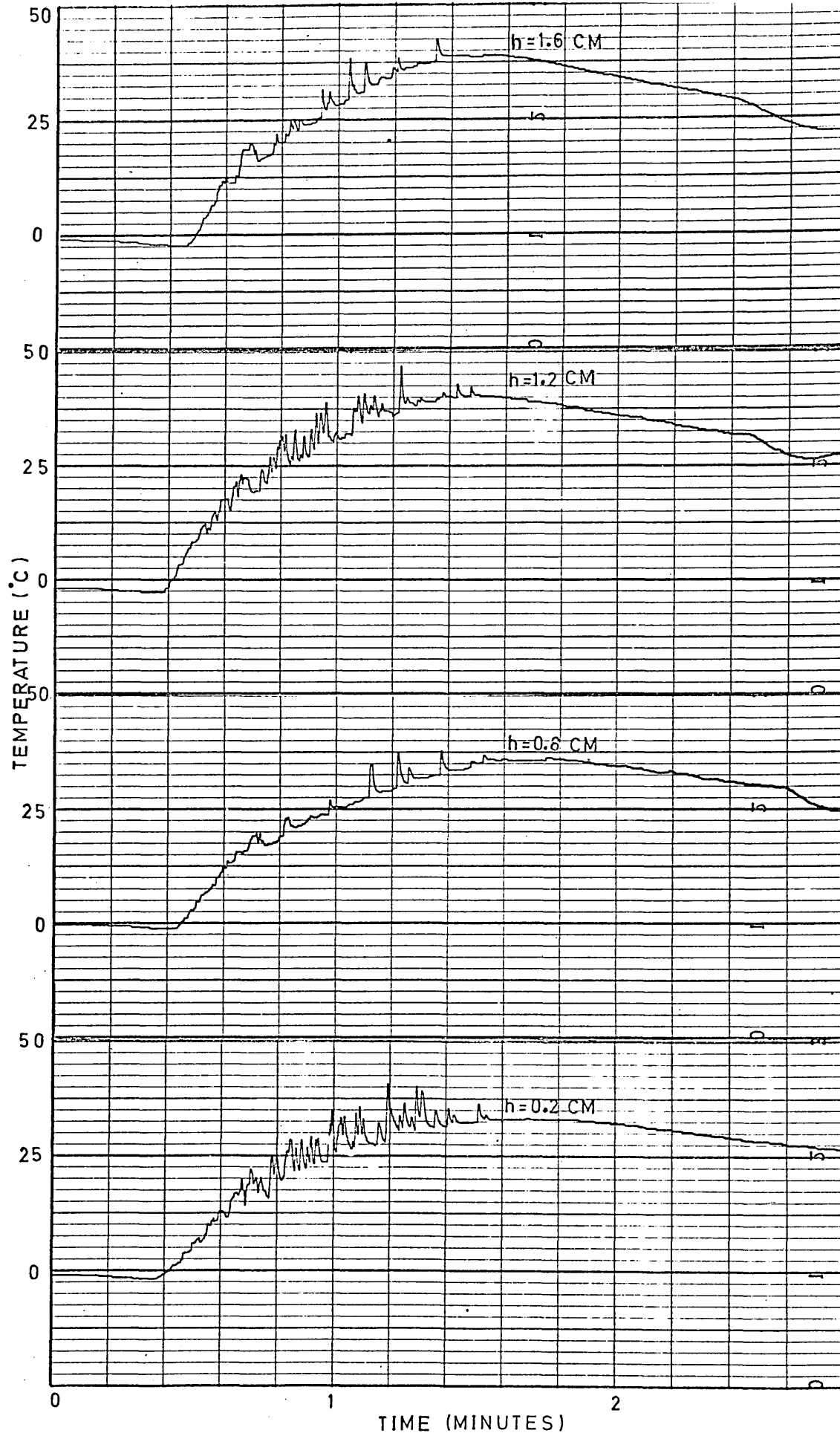


FIG.43 THE EFFECT OF NOZZLE HEIGHT ON THE TEMPERATURE OF THE MODEL FOAM. SINGLE SLIT NOZZLE, 76.6 LIT./MIN.

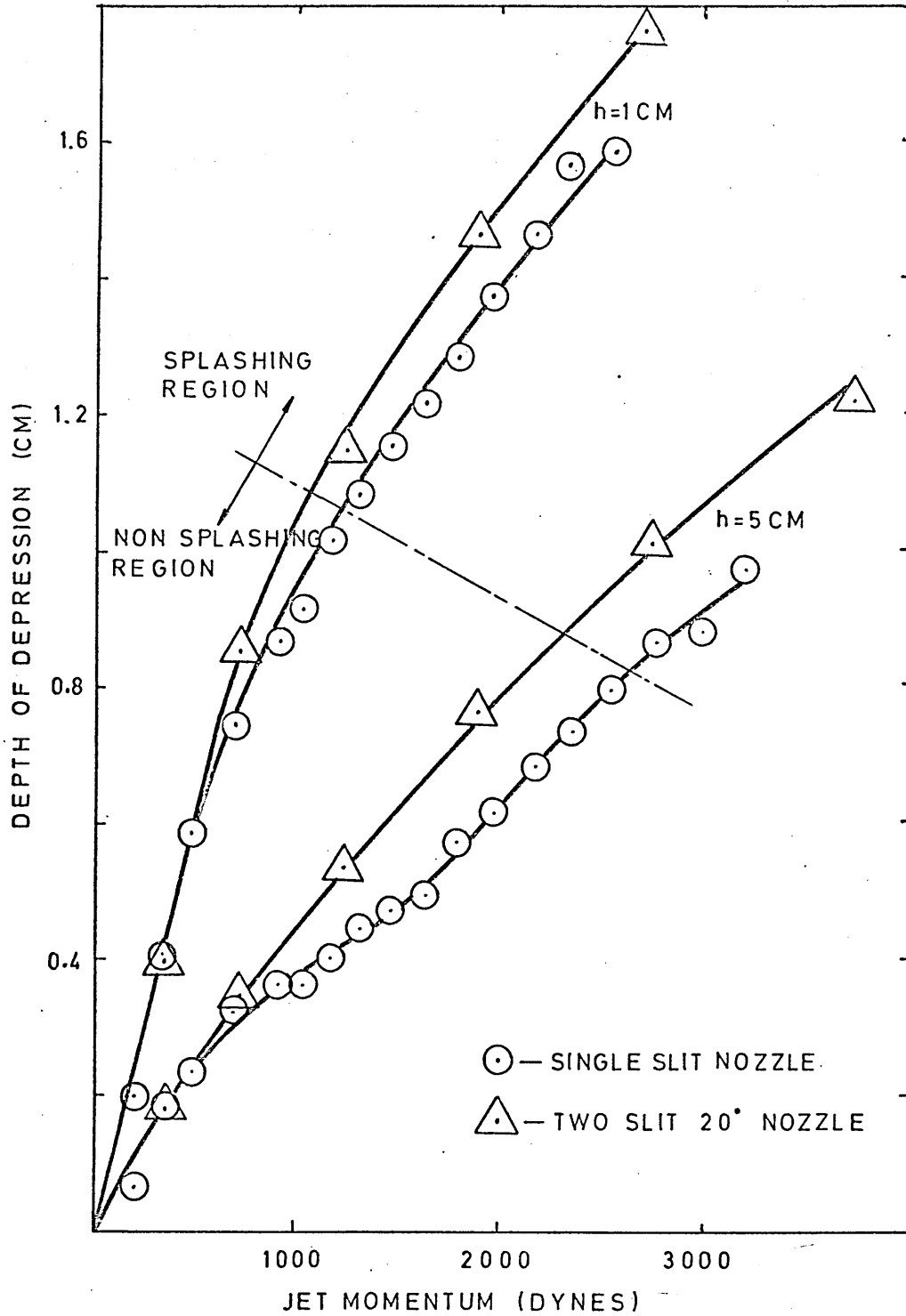


FIG. 44 THE COMPARISON BETWEEN THE SINGLE SLIT AND THE TWO SLIT NOZZLE TREATING THE LATER AS TWO SINGLE JETS

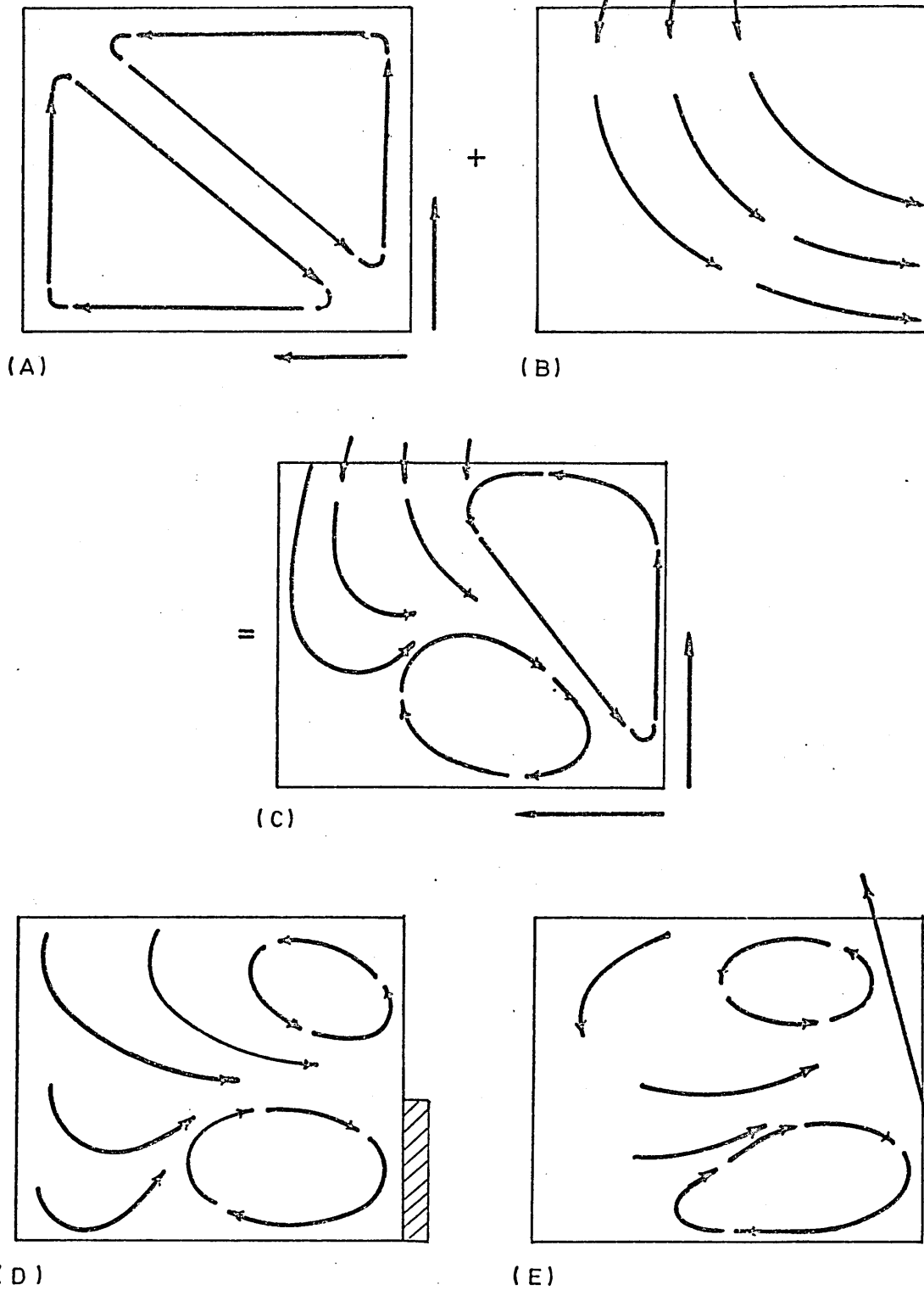


FIG.45 A SCHEMATIC DIAGRAM SHOWING ANALYSIS OF THE STIRRING PATTERN. IN THE MODEL FOAM

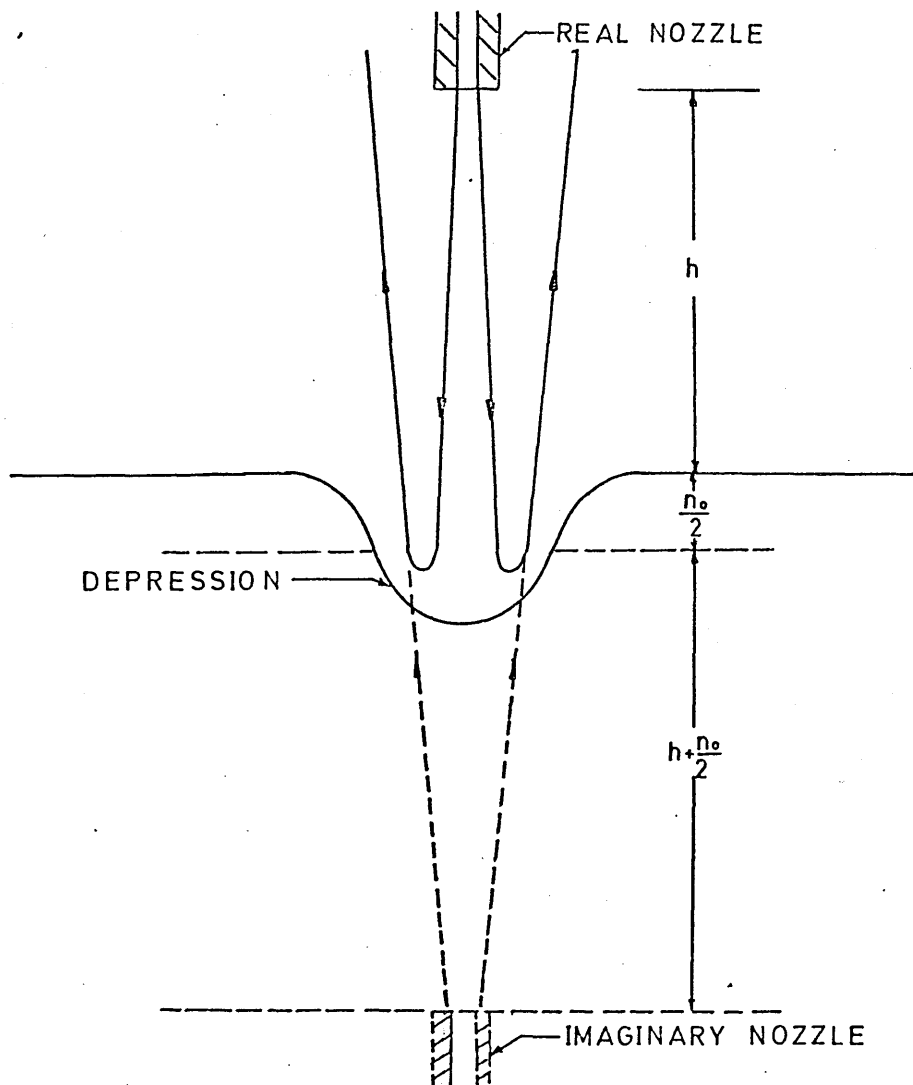


FIG.46 A SCHEMATIC DIAGRAM SHOWING THE POSITION OF THE IMAGINARY NOZZLE

- PATH OF METAL DROPLETS
- PATH OF SLAG FOAM
- BOUNDARY OF CROSS FLOW REACTION REGION

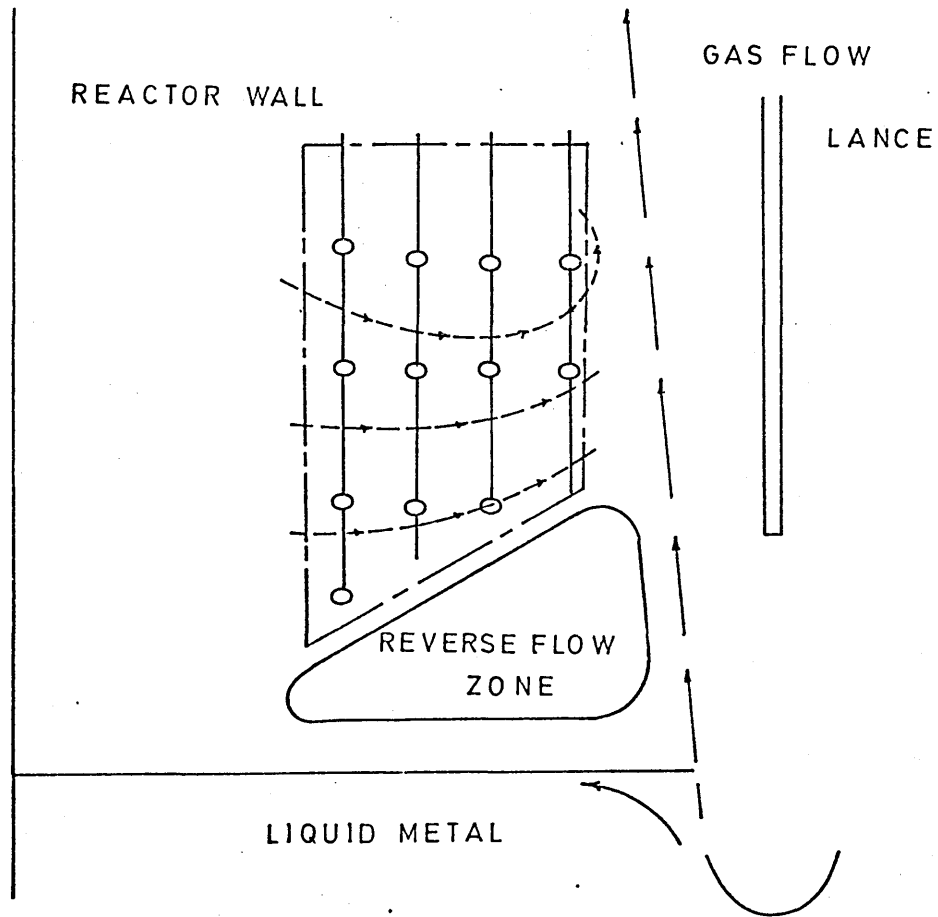


FIG.47 A SCHEMATIC DIAGRAM OF THE CROSS FLOW REACTION REGION

PLATE 1    The Slice reactor and ancillary equipment



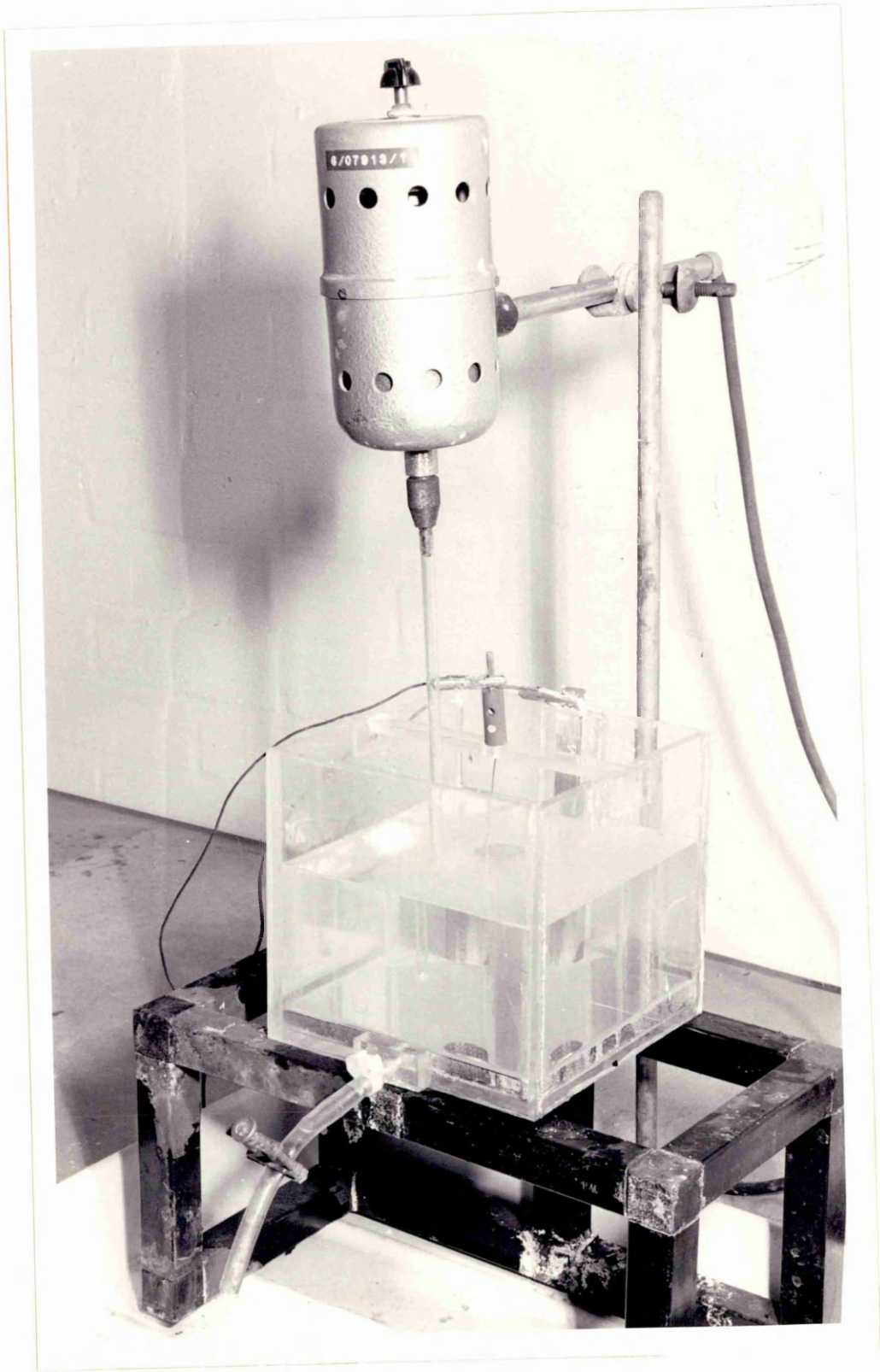


PLATE 3

A photograph of the model foam before injecting  
the tracer.

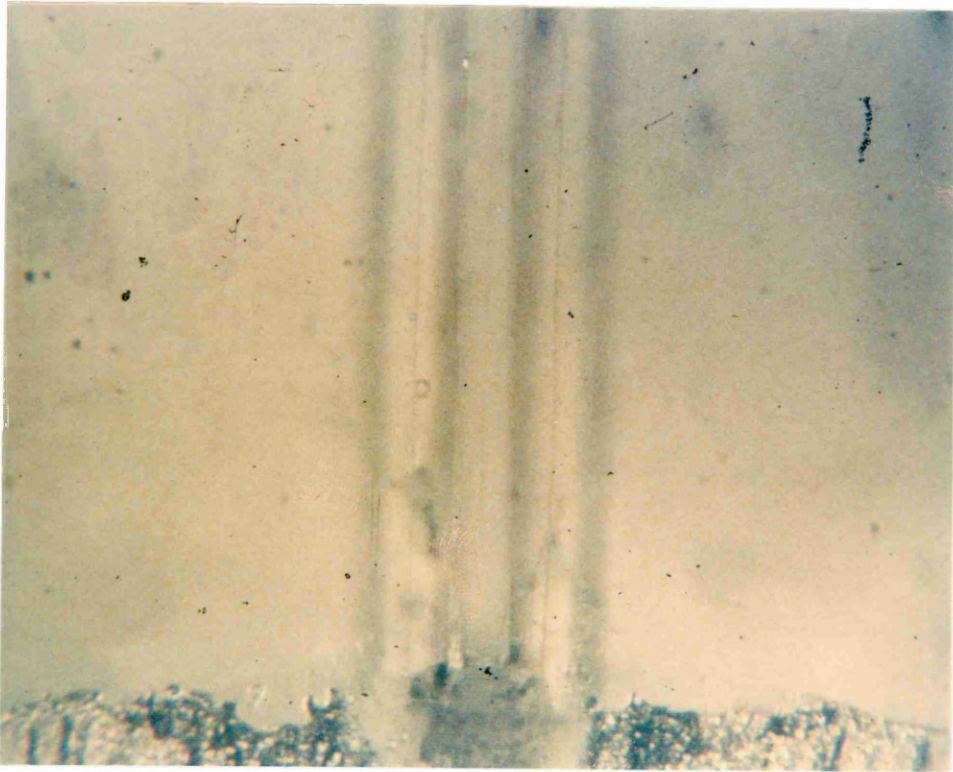


PLATE 4

The effect of jet momentum on the shape of the depression formed by the jet from the two slit nozzle at  $h = 0.8$  cm.

(a) 550 dynes

(b) 1050 dynes

(c) 2500 dynes

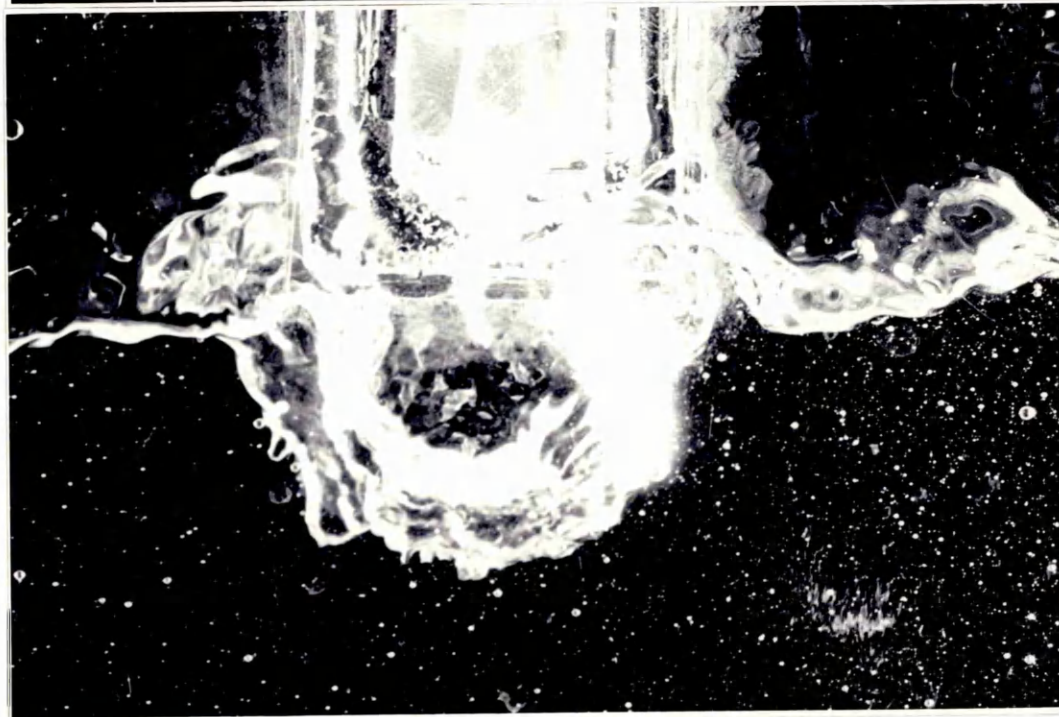
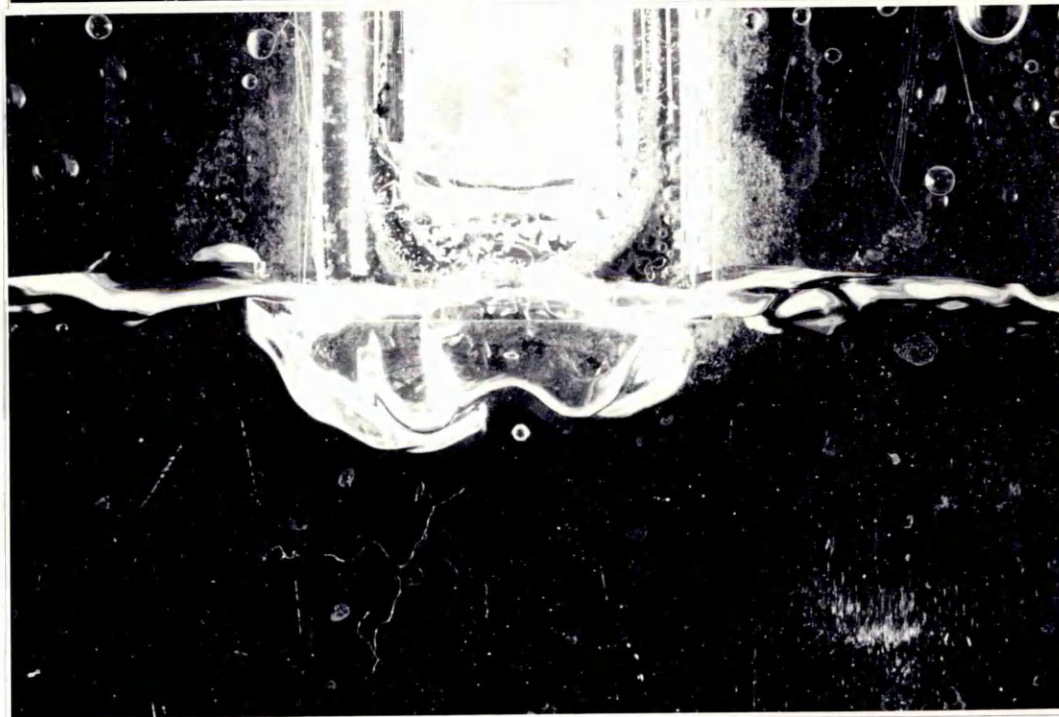
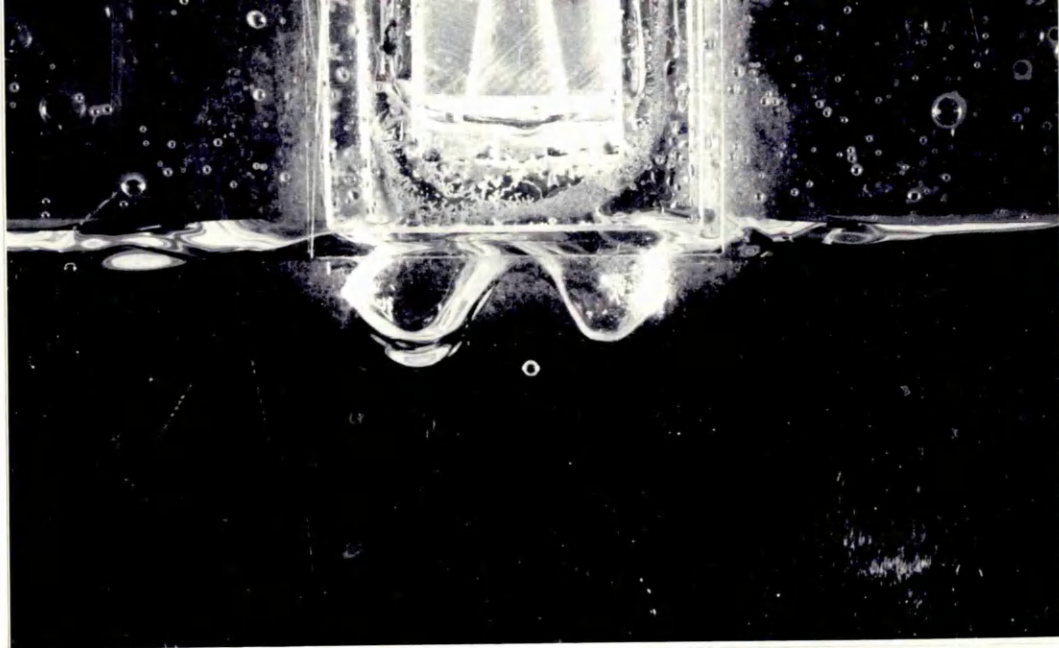


PLATE 5    The flow zones in the model foam.

(a) Using ink as the tracer

(b) Using universal indicator as the tracer

PLATE 6 Photographs showing the way mixing proceeds

(a) Ink just arrived outside the tip of the nozzle

(b) Ink starts spreading from top

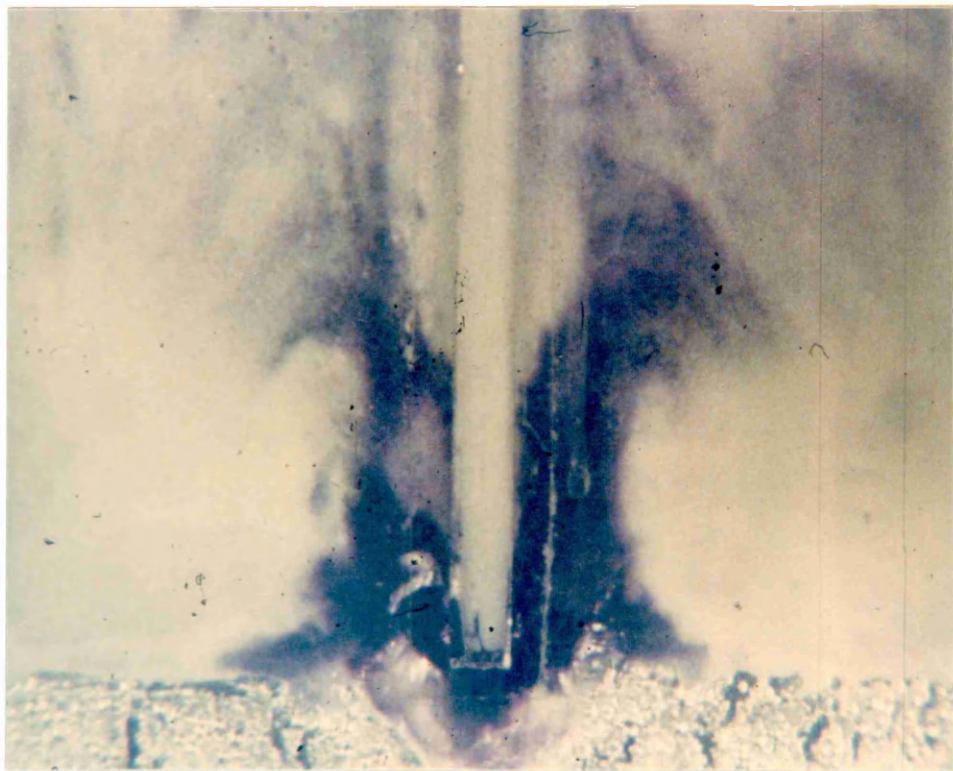
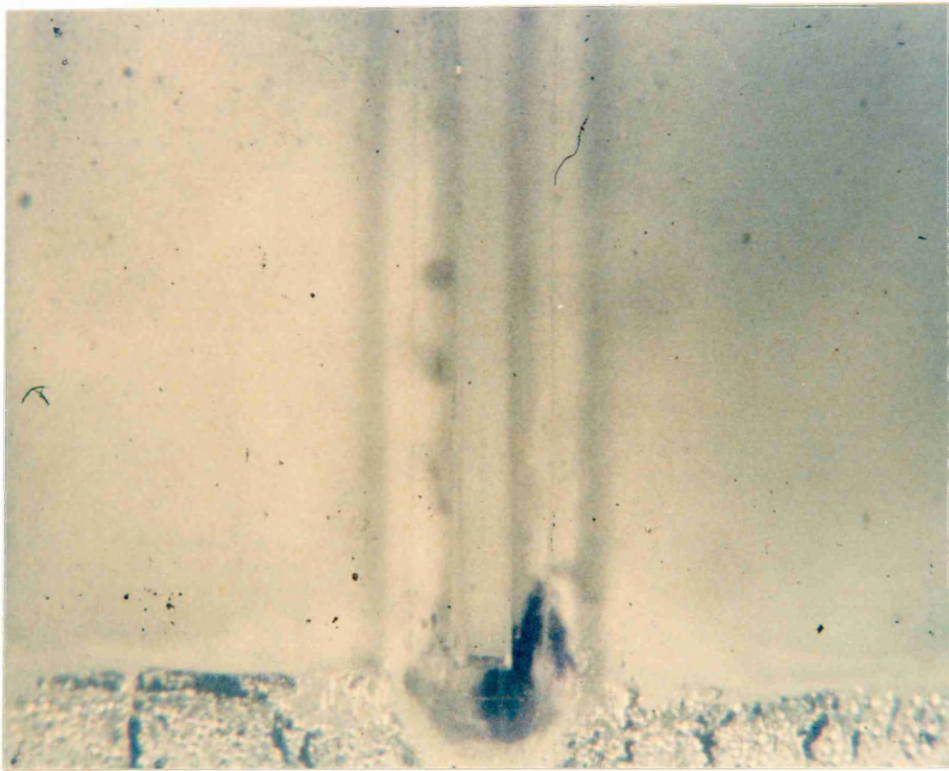


PLATE 7 Photographs showing the way mixing proceeds.

(a) Ink not mixed in the lower portions

(b) Complete mixing

